NASA CONTRACTOR REPORT 152247

LOW SPEED WIND TUNNEL TEST OF GROUND PROXIMITY AND DECK EDGE EFFECTS ON A LIFT CRUISE FAN V/STOL CONFIGURATION

BY V. R. STEWART

Prepared under contract NAS2-9882 by

ROCKWELL INTERNATIONAL CORPORATION
Columbus, Ohio
for

NASA

AMES RESEARCH CENTER
NATIONAL AERONAUTICS AND SPACE ADMINISTRATION

UNCLASSIFIED

SECURITY CLASSIFICATION OF THIS PAGE *(When Data Entered)*

REPORT DOCUMENTATION PAGE		READ INSTRUCTIONS BEFORE COMPLETING FORM
1. REPORT NUMBER CR 152247	2. GOVT ACCESSION NO.	3 RECIPIENT'S CATALOG NUMBER
4. TITLE *(and Subtitle)* Low Speed Wind Tunnel Test of Ground Proximity and Deck Edge Effects on a Lift Cruise Fan V/STOL Configuration		5 TYPE OF REPORT & PERIOD COVERED Contractor Report March 1978 - February 1979
		6. PERFORMING ORG. REPORT NUMBER NR79H-12
7. AUTHOR(s) V. R. Stewart		8. CONTRACT OR GRANT NUMBER(s) NAS2-9882
9. PERFORMING ORGANIZATION NAME AND ADDRESS Rockwell International Corporation 4300 E. Fifth Avenue, P.O. Box 1259 Columbus, OH 43216		10. PROGRAM ELEMENT, PROJECT, TASK AREA & WORK UNIT NUMBERS
11. CONTROLLING OFFICE NAME AND ADDRESS NASA, Ames Research Center Moffett Field, CA 94035		12. REPORT DATE February 1979 13. NUMBER OF PAGES 109
14. MONITORING AGENCY NAME & ADDRESS*(if different from Controlling Office)*		15. SECURITY CLASS. *(of this report)* None 15a. DECLASSIFICATION/DOWNGRADING SCHEDULE

16. DISTRIBUTION STATEMENT *(of this Report)*

Unlimited

17. DISTRIBUTION STATEMENT *(of the abstract entered in Block 20, if different from Report)*

18. SUPPLEMENTARY NOTES

A. Compilation of all Basic Data appears in CR 152248

19. KEY WORDS *(Continue on reverse side if necessary and identify by block number)*

V/STOL
Lift Cruise Fans
Ground Effects
Deck Edge
Wind Tunnel Test

20. ABSTRACT *(Continue on reverse side if necessary and identify by block number)*

Results are presented of a wind tunnel test to determine the characteristics of a lift cruise fan V/STOL multi-mission configuration in the near proximity to the edge of a small flat surface representation of a ship deck. Tests were conducted at both static and forward speed test conditions. The primary concern of the study was to determine if the location of the deck edge induced significant force or moment changes on the airplane. The model tested was a four-fan configuration with modifications to represent a three-fan configuration. The model was approximately a 0.12 scale multimission configuration.

DD FORM 1 JAN 73 1473 EDITION OF 1 NOV 65 IS OBSOLETE

UNCLASSIFIED

SECURITY CLASSIFICATION OF THIS PAGE *(When Data Entered)*

NASA CONTRACTOR REPORT 152247

LOW SPEED WIND TUNNEL TEST OF GROUND PROXIMITY AND DECK EDGE EFFECTS ON A LIFT CRUISE FAN V/STOL CONFIGURATION

BY V. R. STEWART

MAY 1979

Prepared under contract NAS2-9882 by

ROCKWELL INTERNATIONAL CORPORATION
Columbus, Ohio
for

NASA

AMES RESEARCH CENTER
NATIONAL AERONAUTICS AND SPACE ADMINISTRATION

CONTENTS

LIST OF ILLUSTRATIONS

LIST OF TABLES

LOW SPEED WIND TUNNEL TEST OF GROUND PROXIMITY AND DECK EDGE EFFECTS ON A LIFT CRUISE FAN V/STOL CONFIGURATION

By Vearl R. Stewart
Rockwell International
Columbus Aircraft Division

SUMMARY

Results are presented of a wind tunnel test to determine the characteristics of a lift cruise fan V/STOL multi-mission configuration in the near proximity to the edge of a small flat surface representation of a ship deck. Tests were conducted at both static and forward speed test conditions. The primary concern of the study was to determine if the location of the deck edge induced significant force or moment changes on the airplane. The model (0.12 scale) tested was a four fan configuration with modifications to represent a three fan configuration.

Analysis of data has shown that the deck edge effects are in general less critical in terms of differences from free air than a full deck (in ground effect) configuration. The one exception to this is when the aft edge of the deck is located under the center of gravity. This condition, representative of an approach from the rear, shows a significant lift loss. Induced moments are generally small compared to the single axis control power requirements of reference (1), but will likely add to the pilot work load.

INTRODUCTION

Although many studies (references 2-4) have investigated free air and ground effects on lift cruise fan V/STOL aircraft, the studies have not addressed V/STOL operations from relatively small ships having small landing decks. Here, part of the airplane may be over the deck, while part of the airplane may be operating in free air or at a different height due to deck level variations relative to the landing deck. For example, the deck forward edge will briefly be under the mid-part of the airplane during STOL takeoff and the rear edge will be under the airplane during STOL landing. The smaller carriers may result in a partial wing overhang during the STOL deck runs. In contrast, during VTOL operations, any part of the aircraft may overhang the deck. This study was done to investigate these effects.

The effects of the partial decks were investigated both statically and at forward speed for a V/STOL configuration with four lift cruise fans. A limited amount of data were also obtained with a three-fan configuration

for comparison purposes. The present report includes both full and partial deck effects.

This report presents the summarized results of the model tests. Also, some of the data were extrapolated to a representative full scale airplane for comparison purposes. The basic data from the LaRC V/STOL Wind Tunnel Test are presented in Appendix A. The static test data are presented in Appendix B, and the fan calibration data are in Appendix C. Appendices A, B, and C are published in Volume II (NASA CR 152248).

The deck model fabricated for this test was designed to generate as little turbulence as possible. It is recognized that the superstructure associated with small ships will generate considerable turbulence and cross-flows. The ship could not be modeled for obvious reasons, such as tunnel size. In addition, the variations of speed associated with STOL operation are much greater than ship wind-over-deck speeds. The turbulence is considered a significant item in V/STOL operations around small ships and will require a separate investigation to determine the effect of turbulence on the airplane and, perhaps more important to the overall problem, the effect of the airplane power on the turbulence generated by the ship.

SYMBOLS

Total Forces

L	lift	newtons (pounds)
D	drag	newtons (pounds)
M	pitching moment	newton-meters (foot-pounds)
RM	rolling moment	newton-meters (foot-pounds)
T	thrust	newtons (pounds)
TL	thrust, left hand side	newtons (pounds)
TR	thrust, right hand side	newtons (pounds)

Thrust Induced Aerodynamic Forces (Power ON - Power OFF)

ΔL	lift	newtons (pounds)
ΔD	drag	newtons (pounds)
ΔM	pitching moment	newton-meters (foot-pounds)
ΔRM	rolling moment	newton-meters (foot-pounds)

Total Coefficients (Stability Axis)

CL, C_L	lift coefficient, L/qS
CD, C_D	drag coefficient, D/qS
CM, C_M	pitching moment coefficient, M/qS$\bar{c}$
CRM, C_{RM}	rolling moment coefficient, RM/qS

Thrust Coefficients

C_T	thrust coefficient T/qS
ΔC_{L_T}	lift coefficient due to thrust
ΔC_{D_T}	drag coefficient due to thrust
ΔC_{M_T}	pitching moment coefficient due to thrust
ΔC_{RM_T}	rolling moment coefficient due to thrust
ΔC_{YM_T}	yawing moment coefficient due to thrust
ΔC_{M_D}	pitching moment coefficient due to ram drag
C_{D_R}	ram drag coefficient $\sim \frac{M_i\ V}{qS}$

Aerodynamic Coefficients (Direct Thrust Effects Removed)

$C_{L_{Aero}}$	C_{LA}	CLA	lift coefficient
$C_{D_{Aero}}$	C_{DA}	CDA	drag coefficient
$C_{M_{Aero}}$	C_{MA}	CMA	pitching moment coefficient
$C_{R_{Aero}}$	C_{RMA}	CRMA	rolling moment coefficient

Angles

α, Alfa	angle of attack	degrees
ϕ	bank angle	degrees
θ_T	thrust vector angle	degrees
δ_N	nozzle angle - geometric angle	degrees
$\delta_{N_{Fwd}}$	nacelle forward nozzle angle	degrees

$\delta_{N_{Aft}}$	nacelle aft vane angle	degrees
$\delta_{N_{Nose}}$	nose vane angle	degrees
β	sideslip angle	degrees

Dimensions

A	fan exit area - one fan	
S	wing area - 0.7767 m^2	
b	wing span - 2.502 m	
$\bar{c}$	wing mean aerodynamic chord - 0.3231 m	
y	lateral dimension	meters (feet)
x	horizontal dimension	meters (feet)
z	vertical dimension	meters (feet)
H/D, h/D	non-dimensional ground height ; height of fuselage/diameter of one fan	
D	equivalent diameter of one forward fan - 0.1295 m) model used to nondimensionalize height parameter; (1.080 m) full scale airplane	
ℓ_1	horizontal ram drag arm, see Figure 17	meters (feet)
ℓ_2	vertical thrust arm, see Figure 17	meters (feet)
ℓ_3	vertical ram drag arm, see Figure 17	meters (feet)
ℓ_4	horizontal thrust arm, see Figure 17	meters (feet)
ℓ_5	lateral thrust arm, see Figure 17	meters (feet)

Miscellaneous

N	number of fans		
V	wind velocity	meters/sec.	(feet/sec.)
V	nozzle exit velocity	meters/sec.	(feet/sec.)

P_R	pressure ratio, P_T/P_a		
P_T	total pressure behind fan	pascals	(pounds/in^2)
P_a	ambient pressure	pascals	(pounds/in^2)
q	dynamic pressure $\sim 1/2\rho V^2$	newtons/meter^2	(pounds/foot^2)
ρ	air density	kg/meter^3	(slugs/foot^3)
M_i	inlet mass flow	kg/sec.	(pounds/sec.)
FRL	fuselage reference line		

MODEL, APPARATUS AND TEST DESCRIPTION

Model Description

The model represents a multi-mission lift-cruise fan Navy V/STOL aircraft (Figure 2). The model was fabricated to represent either a four fan or a three fan configuration. The approximate model scale is 0.12. For the four fan configuration, the model had two fans located in each of two wing mounted nacelles (Figure 3). One fan in each nacelle was mounted in a standard upright position, and the thrust vectoring was controlled through two swiveling nozzles located on a central plenum (Figure 4a). The second fan was located in the aft portion of the nacelle, and was mounted in a horizontal position exhausting downward (Figure 4b). The thrust vectoring for these fans was controlled by exit louvers and provided flow vectoring from 45° to 105° from the horizontal, although the complete range was not used for this investigation.

The three fan configuration consisted of the two aft fans in the nacelle, as described above, and a similarly mounted fan in the fuselage nose (Figure 5). The vectoring limits of the nose fan are the same as the aft fans. Only 80° was tested.

The propulsion simulators were tip turbine driven fans, Figure 6. The fan face diameter is 13.97 cm (5.5 inches) and the exit diameter including the tip turbine exhaust is 15.25 cm (6 inches). The drive air is delivered internally to the tip turbine ring through separate manual internal control valves. These valves are utilized to distribute the primary mass flow for individual RPM control. The fan exhaust pressure instrumentation is utilized for fan performance determination. The nacelle fan installations are shown in Figure 3. The fuselage nose fan installation is shown in Figure 5. Fan exit total pressure instrumentation can be seen in Figures 3 and 5. The total pressure instrumentation was a rake with five total pressure taps mounted just aft of the fans. These taps were manifolded together and were used to correlate fan thrust

during the testing. The front fan swivel nozzles are shown in Figure 4a and are vectorable from parallel to the FRL (0^{o}) to past the vertical (105^{o}). The louvers utilized to vector the aft fans and the nose fan are also shown in Figure 4b. The vector angles can be varied from 45^{o} to 105^{o}.

The fan thrust vector angles were somewhat different than the nozzle geometric angle. Table 1 presents the thrust vector angle as a function of the nozzle geometric angle. These fan thrust vector angles were determined from the fan calibration tests with the fans shielded. Because of the induced effects on the wing and nacelle, the measured vector angle of the installed fans more nearly equaled the geometric angle. The front fan swivel exhaust nozzle is almost rectangular in shape at the exit. The internal shape of the front nacelle is cylindrical with the nozzles located on either side at a 20^{o} angle cant angle. The duct opening into the nozzles is circular. Figure 3b shows the details of the nozzles. The nozzle area is adjustable by a sliding cover and was adjusted to an area 7.013 m^2 (20.43 in^2) for this test.

The exits of the aft fans and the nose fan are circular and go directly into square sets of deflection louvers. The fan exit cone is truncated at the entrance to the louver system. The base drag of the flat exit cone is accounted for in the thrust calibration.

The model wing is trapezoidal and has an area of 0.7767 M^2 (8.36 ft^2) and a mean aerodynamic chord of 0.323 M (12.72 inches). The wing taper ratio is 0.5, and the sweep of the 0.25c is 3.33 degrees. The basic wing airfoil is a 15% supercritical section. The wing incidence is 5 degrees, and the wing is untwisted. The wing is mounted high on the rectangular fuselage. A 0.25c plain flap is mounted inboard of the nacelle, and a 0.30c single slotted flap extends from the nacelle outer mold line to 0.70 b/2. These flaps were deflected 40^{o} for most of the tests. The wing leading edge was untreated.

The model was tested with the horizontal and vertical tail on at incidence of 0^{o} for all runs.

Figures 7-9 show the complete model mounted in the NASA Langley Research Center V/STOL tunnels.

The ground board fabricated for the wind-on testing was sized to match the airplane model scale, see Figure 2b. The total size was such that the ground board extended beyond the wing tips and fuselage nose and tail for the full ground board. Dimensions of the full ground board were 2.44 by 3.74 meters (8.0 by 9.0 feet). Deck edge locations were required longitudinally at the center of gravity with the board extending forward or aft to represent the landing or takeoff. These positions were achieved during static testing by segmenting the board and removing sections. During forward speed testing, the entire 2.44 meter length was maintained, and the deck edge position was achieved by sliding the

FAN NO.	LOCATION NO.	δ_N	θ	THRUST CONSTANTS i	j	k	l	MASS FLOW CONSTANTS M	N	O	P
364	1	10	7	217.6476	-1290.9127	1637.6488	-564.2361	-226.0997	548.2030	-439.8810	118.6343
		30	25	-883.4905	1790.3770	-1210.5655	303.8194				
		50	45	-2109.8048	2350.8829	-1674.8512	434.0278				
		80	75	-1109.8048	2350.8829	-1674.8512	434.0278				
		90	85	-594.9143	874.0179	-279.0179	0				
		105	102	-1563.2429	3425.0595	-2512.6488	651.0417				
366	2	45	33	-1231.9238	2776.8552	-2152.5298	607.6389	-284.8265	703.4864	-576.8601	159.1435
		60	50	-851.6048	1650.5853	-1102.6786	303.8194	-350.0686	862.5357	-706.9196	195.3125
		70	60	-522.6035	736.9564	-287.0879	72.8438	-288.6063	700.5046	-563.9881	153.3565
		80	70	-2311.8970	5377.4781	-4293.8312	1228.6325				
		90	79	-2311.8970	5377.4781	-4293.8312	1228.6325				
		105	92	-2929.3366	6979.5024	-5662.2128	1612.2766				
365	3	10	7	135.5381	-1029.3849	1371.2798	-477.4306	-242.1297	593.1465	-481.8452	131.6551
		30	25	-76.6095	-417.0734	797.6190	-303.8194				
		50	45	122.4286	-879.8810	1148.0655	-390.6250				
		80	75	45.9286	-745.9226	1090.7738	-390.6250				
		90	85	-420.4762	622.7877	-245.5357	43.4028				
		105	102	313.2429	-1399.5238	1607.1429	-520.8333				
367	4	45	33	-1791.5377	4266.3007	-3475.5491	1000.7482	-304.1959	741.0354	-598.1399	162.0370
		60	50	-1805.2564	4218.0335	-3413.3798	1000.7482	-378.3957	930.5506	-759.5982	208.3333
		70	60	-1213.3765	2564.1402	-1911.8567	561.1672	-416.5671	1030.7768	-847.5446	234.3750
		80	70	-1987.0959	4437.8042	-3404.5214	953.9843				
		90	79	-2290.4622	5211.1552	-4061.6482	1141.0400				
		105	92	-2713.1179	6453.7434	-5255.5315	1515.1515				
421	5	70	69	34.2400	-965.8745	1443.1484	-511.2857	-357.6629	877.1696	-713.8393	195.3125
		80	79	392.1448	-2180.1102	2732.6439	-944.6315	-348.8884	853.8843	-693.3780	189.5255
		90	88	-2221.9070	5196.4727	-4199.8156	1225.2151	-348.8884	853.8843	-693.3780	189.5255

Table 1. Fan Calibration Constants

entire board forward or aft. The lateral deck edge position was achieved by removing sections in both the static and forward speed testing. Lateral deck edge positions in addition to the full board were at the fuselage centerline and at the mid-span point under the right hand wing. Figure 2b shows the dimensions of the ground board relative to the airplane model.

Test Facilities

Several test facilities were utilized in the performance of this study. The fan calibration was done on the balance of the 2.139 x 3.048 meter (7 x 10 foot) contractor's wind tunnel facility. The fan force components were measured on the six component external balance. The individual fans were mounted to the balance with fan drive air supplied by a flexible hose crossing the balance system. Figure 10 shows one fan mounted in the test section. Each fan was tested with a standard bell-mouth inlet and with the normal inlet.

The static tests were done in the contractor's static test stand. Figure 11 shows the model mounted in the test stand. The air is supplied through two pipes above the sting support. A trombone arrangement crosses the balance to reduce the airline tares. The model was mounted to a six-component internal balance located inside the fuselage. The balance was calibrated with the supply pipes pressurized. A segmented ground board was remotely actuated by a three-post screw jack arrangement. The three-post arrangement allowed the adjustment in pitch angle, roll angle and height. The model is not movable. The segmented ground board allowed for the five required deck edge positions, (1) full, (2) aft edge under c.g., (3) forward edge under c.g., (4) 3/4 lateral board, and, (5) 1/2 lateral board. Figure 12 shows the deck edge positions tested during the static and wind-on testing.

The forward speed testing was done in the NASA Langley Research Center (LaRC) 4.42 x 6.36 meter (14.5 x 21.75 foot) V/STOL wind tunnel. The model was mounted on a six-component internal balance with the drive air supplied through an airline inside a hollow sting. Figure 13 shows the model mounted in the LaRC facility with the ground board in place (see also Figures 7-9).

The ground board for the wind-on test was fabricated in segments to allow for the lateral deck edge positions. The longitudinal positioning was accomplished by moving the entire ground board on tracks. Bank angle was achieved by rolling the ground board about a central pivot. Support was provided by telescoping legs. Roll angles of ± 30 are available on the ground board. Figures 14 to 16 show assembly of the ground board.

Data Reduction

The data reduction procedures utilized to reduce the test results are, in general, similar to those discussed in reference (2). The raw data were obtained at specified test conditions. The raw data were corrected for model weight tares, pressure tares, and balance interactions. The model position (height) was corrected for sting and support bending by calibration of the model position as a function of load on the sting. The data were corrected to the stability axis frame of reference (Figure 1) by applying the appropriate transformations. For the static tests the ground board is the frame of reference. The data corrected to stability axis are the total forces on the model which, in coefficient form, are (also see Figure 17):

C_L = total lift coefficient

C_D = total drag coefficient

C_M = total pitching moment coefficient

C_{RM} = total rolling moment coefficient

The model was not yawed in this investigation ($\beta = 0$); therefore, side force and yawing moment coefficients are not listed and are not discussed in this report.

In order to obtain the aerodynamic forces and the forces induced by the thrust, the direct thrust components and the ram drag increments must be subtracted, i.e.,

$$C_{L_A} = C_L - \Delta C_{L_T}$$

$$C_{D_A} = C_D - \Delta C_{D_T} - C_{D_R}$$

$$C_{M_A} = C_M - \Delta C_{M_T} - C_{M_R}$$

$$C_{RM_A} = C_{RM} - \Delta C_{RM_T}$$

These thrust associated increments are fully described in Figure 17. The induced forces can now be obtained by subtracting the power-off forces. The power-off forces utilized are the windmilling case. Variations from the windmilling to the plugged nacelle conditions are small and were neglected. The induced forces are reduced to:

$$\frac{\Delta L}{T} = \frac{C_{L_A} - C_{L_{Power\text{-}off}}}{C_T}$$

$$\frac{\Delta D}{T} = \frac{C_{D_A} - C_{D_{Power\text{-}off}}}{C_T}$$

$$\frac{\Delta PM}{T\bar{c}} = \frac{C_{M_A} - C_{M_{Power\text{-}off}}}{C_T}$$

$$\frac{\Delta RM}{Tb} = \frac{C_{RM_A} - C_{RM_{Power\text{-}off}}}{C_T}$$

This procedure is necessary in the forward speed tests only since all forces are zero for the power-off in the static tests. Therefore, the delta forces divided by thrust shown in all cases represent only the induced forces, and the coefficients terms subscripted "A" represent the aerodynamic forces, including the induced effects.

Figures 18-20 show the breakdown for a typical set of test data for a variation of height with the STOL configuration of 30° deflection of the forward fan nozzles and 60° of the aft fan vanes. The force induced by the thrust is the increment between the power-off curve and the "aerodynamic" curve. The power-off increments due to ground are small and are presented and discussed later in this report. The individual incremental forces are required for analysis of other configurations. Variation in pressure ratio, for example, would result in different velocity ratio V/V_j levels; and, for the same thrust, a change in nozzle equivalent diameter would be experienced. For a fixed height the h/D parameter would vary with pressure ratio. The power-off ground effects are related to the wing geometry as would normally be expected.

In the above discussion, the ram drag contributes to both drag and pitching moment. The ram drag pitching moment arm has been chosen as follows: Front fan ram drag has been assumed to act at the center of the inlet; the aft and nose fan ram drag have been assumed to act 1/4 of an inlet diameter above the inlet. The arm chosen may be slightly low on the aft fan since more pitch-up due to ram drag would reduce the apparent induced pitching moment.

The nondimensional model height used for data correlation in this investigation was defined as follows:

$$\text{Model Nondimensional Height} = \frac{H}{D}$$

where:

H is the model height measured to the bottom of the fuselage at the model moment center (also equal to the forward fan nozzle exit when the nozzles were at 90° vector angle at $\alpha = 0^{\circ}$)

D is the equivalent exit diameter of a single lift/cruise fan and is 0.1295 meters.

The single fan diameter has been used in the above definition for D, rather than the total diameter, to allow for a comparison of three and four fan configurations at comparable real airplane heights. Some previous data have been shown correlated to an equivalent diameter of all fans, and it is felt that this correlation $\left(D_e = \sqrt{\frac{4NA}{\pi}}\right)$ is valid where fan configurations relative to the lifting surface are nearly the same. Large changes in configuration could limit the applicability of the equivalent diameter. The fuselage bottom was chosen for the height measurement since it is at the same height as the forward fan exit for both the nacelle fan and the nose fan. An h/D = 1.0 corresponds to wheel height for this configuration.

Both free stream to fan jet velocity ratio (called velocity ratio for simplicity) and thrust coefficient have been used in the past to correlate V/STOL model data. For this investigation, velocity ratio is used and is defined as:

$$\text{Velocity Ratio} = \frac{V}{V_j}$$

where:

V is the free stream air velocity, and

V_j is the velocity computed assuming an isentropic expansion of the air from average fan exit total pressure to free stream ambient pressure

The ram drag is defined as:

$$D_R = \sum M_i V$$

where:

D_R is the ram drag

M_i is the inlet mass flow rate

V is the free stream velocity

In the above equation, the inlet mass flow rate is determined from a calibration of the inlet flow rate versus fan exit pressure obtained during the fan calibration.

Wind Tunnel Wall Corrections - In the above discussions of data reduction, no mention was made of wind tunnel wall corrections. The theory of wind tunnel wall corrections as applied to models having significant propulsive lift components has been developed by Heyson (reference 5). This theory has been modified and coded for use in the LaRC V/STOL Wind Tunnel data reduction computer programs. In order to assess which data had significant wind tunnel wall effects, wind tunnel wall corrections were applied to representative data points covering the entire test envelope. From this analysis, it was found that the data taken "in ground effect", i.e., over the ground board, had angle of attack corrections less than 0.2° and dynamic pressure corrections less than 1 percent, corrections which are small compared to data scatter due to other reasons. Therefore, all the "in ground effect" (data where $H/D \leq 8$) have not been corrected for wall effects. However, when the model was tested in "free air", wall corrections were found to approach about 3° in angle of attack and 8 percent dynamic pressure under some conditions. Therefore, the "free air" data points of this investigation were all corrected for wall effects

In addition to the corrections of reference 5, all data were corrected for the classical wake and blockage of the model in the LaRC V/STOL tunnel

TEST PROCEDURES

Fan Calibration

The fan calibration was done on each individual fan for each of the configurations shown in Table 2.

Table 2

Configuration	Inlet	Exit	Shields
1. Isolated Fan	Bellmouth	Reference Shroud	On
2. Isolated Fan	Model Inlet	Reference Shroud	On
3. Isolated Fan	Model Inlet	Model Nozzle	On
4. Isolated Fan	Bellmouth	Model Nozzle	On
5. Isolated Fan	Model Inlet	Model Nozzle	Off
6. Ground Board	Model Inlet	Model Nozzle	On

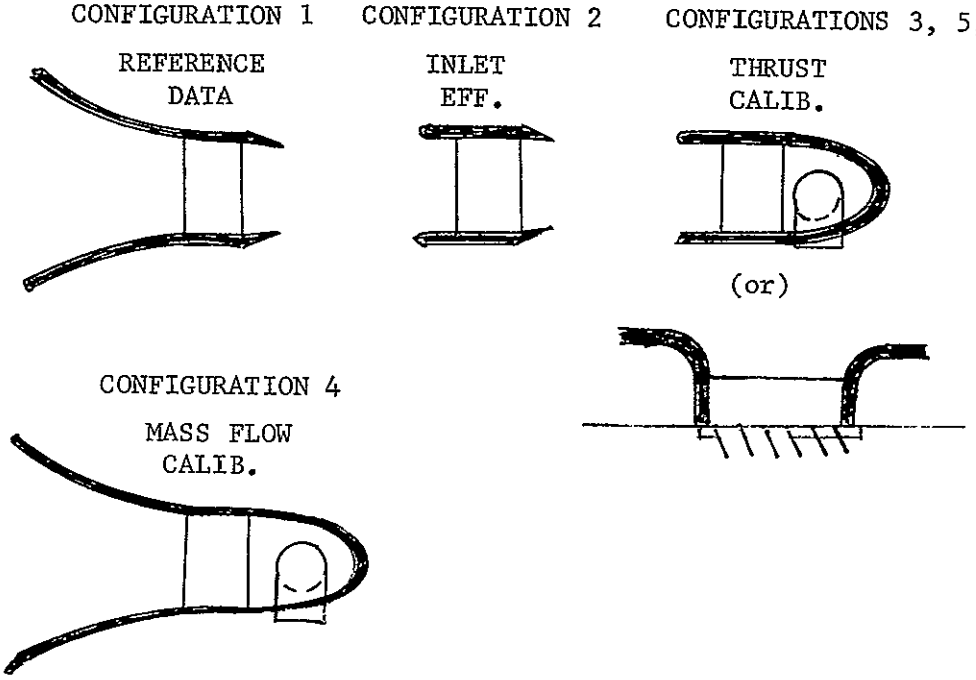

The data gained for each configuration except (5) above consisted of thrust measured from balance, fan RPM, fan exit total pressure and fan exit static pressure at several levels of fan drive pressures and thrust angles. In addition, for configuration (1) and (4) described above, inlet static pressures were obtained for computation of fan secondary mass flow. Configuration (5) data were obtained at normal operating drive pressure only. The above configurations were run in order to obtain the required calibration data for the static and wind-on testing. Considerable extra data were obtained so that if a fan replacement became necessary during later testing the thrust calibration curves could readily be developed. This alternative was never required since all fans performed well during the entire test except for some minor FOD damage on one fan during the LaRC testing.

Figure 21 shows the shields utilized for the fan calibration. The shields were used to protect the fans and fan mounting hardware from any airflows that might be induced by the fan exhaust flows. Thus, losses associated with the installation could be determined. Complete data from the fan calibration are presented in Appendix C.

The calibration data were correlated as a function of the ratio of fan exit total pressure to the ambient static pressure. The correlation on the fan exit pressure ratio was selected for several reasons. The fan pressure ratio will result in a correct measure of thrust under all model speed conditions. Reference 6 demonstrates the effect of forward speed on thrust. The ram effect at forward speed is directly related into a pressure ratio change and any back pressure associated with ground effect is also properly accounted for. Figures 22 and 23 show the installed thrust of the right hand forward and aft fan (#3 and #4). These curves are representative of the calibration data for the remaining fans. The data obtained from the individual fan calibrations were curve fit for thrust and mass flow for each fan and thrust angle by these equations:

Weight Flow (Kg/sec) (From Configuration 4)

$$M_i = 4.536 \left[M + N\left(\frac{P_{T_F}}{P_A}\right) + O\left(\frac{P_{T_F}}{P_A}\right)^2 + P\left(\frac{P_{T_F}}{P_A}\right)^3 \right]$$

Thrust (Newtons) (From Configuration 3 or 6)

$$T = 4.448 \left[i + j\left(\frac{P_{T_F}}{P_A}\right) + K\left(\frac{P_{T_F}}{P_A}\right)^2 + \left(\frac{P_{T_F}}{P_A}\right)^3 \right]$$

The constants for the curve fit are presented in Table 1. Actual thrust angles are also shown in this table. All fans with the exception of the nose fan showed the same thrust calibration in and out of ground effect. The nose fan showed a small loss (approximately 2 pounds) at the h/D = 1.0. Since this occurred at only one height and resulted in about 1% error in total thrust (three engine), it was ignored.

Fan nomenclature is shown in Figure 17.

Static Test

The static tests were conducted on the full span model mounted in the contractor's static test rig. The model was mounted in a fixed position. A movable ground board supported by three screw jack actuators was mounted under the model. The ground board had three degrees of freedom, height, roll and pitch. Angles of $\pm 20^{\circ}$ were possible and heights from zero to approximately 2.438 m (8 feet) were available. The three

screw jacks were driven by three separate drive motors. Calibrated position gages were used on each post to determine ground board position and angle for each data point. Force and moment loads were measured on an internal six-component balance and reduced to airplane stability axes through normal data reduction procedures. Complete static data are presented in Appendix B.

The thrust of the individual fans were balanced in free air at approximately 225 newtons (50 pounds) each for the four fan configuration and 300 newtons (67 pounds) for the three fan configuration. The tests were then made. Small deviations occurred during the runs; however, these are accounted for in the data reduction procedures. In order to account for the different nozzle efficiencies of the forward and aft fans, the aft fans were retarded in RPM. The resultant fan exit pressure ratios were approximately 1.21 for the forward fans and 1.12 for the aft fans for the four fan case.

Forward Speed Test

The forward speed tests were conducted in the Langley Research Center V/STOL wind tunnel. The model was tested in free air and in the presence of the ground board. The thrusts were set as described in the static test discussion at approximately the same magnitudes, 900 newtons (200 pounds). Tunnel dynamic pressure (speed) was varied to obtain the desired ranges in thrust coefficient. The free air data were obtained with the model mounted near the tunnel centerline. Angles of attack of -8 degrees to + 20 degrees were attained. The ground effect data were obtained by setting an angle of attack and varying model height above the ground board. Bank angle was obtained by tilting the ground board. Heights varying from one to eight nozzle diameters were tested. The nozzle diameter of one fan utilized to normalize the height parameter was 12.95 cm (5.1 inches). Data were obtained at angles of attack of 0° and 8° at 0° bank angle, and at an angle of attack of 0° at $\pm 10^{\circ}$ bank angle with the ground board in place.

The ground board was moved forward and aft relative to the model to provide the longitudinal deck edge positions while board segments were removed to provide the lateral deck edge positioning.

The data were obtained for several nozzle angles in both free air and in the presence of the ground. The four fan configuration was tested with nozzle angles of 105° and 90° (VTOL flight condition simulation) and at nozzle angles of 30° forward and 60° aft (STOL flight condition simulation). The three fan configuration was tested with nozzle angle of 80° nose and 90° aft (VTOL flight condition simulation).

All the data obtained during the forward speed testing are presented in Appendix A. The significant findings from these tests are summarized in the following sections of this report.

BASIC DATA

General Discussion - Four Fan Configuration

The free air aerodynamic characteristics of the lift cruise fan configuration are presented in Figure 24 for the STOL configuration with nozzle deflections of 30° forward and 60° aft at various speed conditions. The data show an increase in C_L as the thrust coefficient is increased and a reduction in stability with increasing thrust coefficient. Figure 25 presents the same data with the direct thrust effects removed. The stall angle is increased with increasing thrust coefficient showing the circulation created by the jets. The data presented in Figure 25 have had the thrust increments including ram drag removed as previously discussed.

The effects of ground height on the STOL configuration are shown in Figure 26 for the full deck case. The data show the positive increase in lift to be slightly reduced at an h/D of 2.0 and relatively constant at other conditions. The induced pitch and drag are relatively unaffected by ground height except at the very high C_T value. However, at this high C_T value, the absolute force and moment levels that were induced are small compared to the thrust forces on the model. Similar data for other angles of attack and for the other nozzle angles are presented in Appendix A.

The effect of height on the basic airplane with power off is shown in Figures 27 and 28. The data show an increase in lift as the model approaches the ground for all positions except for #2 position (forward located ground board, see Figure 12) which is essentially unchanged. The most favorable position is the #3 position (aft) which shows a 30% lift increase at an h/D = 1.0 or at the approximate wheel height. Pitching moment and drag show little change due to ground height. A small change in rolling moment is shown with the lateral positioning of the ground board.

The effects of forward speed on the induced effects in free air at 90° and 105° nozzle angles are shown in Figure 29, and in Figure 30 for the 30° forward and 60° aft nozzle angles. The trends are similar for all conditions with a positive lift and pitching moment change as speed is increased. The 90° data indicate a small increase in lift at the low velocity ratios. The 105° nozzle angle data have a greater zero speed lift loss than any of the other nozzle angles, approximately 9% at zero speed, reducing to 5 or 6% at $V/V_j = 0.13$. The 30° forward and 60° aft nozzle angles indicate positive lift and pitching moment increments at all velocities tested.

The propulsion induced interference on the model for static conditions are shown in Figure 31 for free air and in Figure 32 at an h/D of 4 for all ground board configurations. The four fans with the basic nozzles show approximately 5% interference in the presence of the full model. This interference represents an installation loss due to operating the fans on

the model. The thrust used to normalize the data is the summation of the isolated fans with the configuration inlet and nozzle but with the exit shielded from the remainder of the model. The losses shown here are very much affected by the configuration and can be altered by modification to the nozzles. Most of the interference is the result of the forward nozzle configuration. The loss can be readily reduced by variations to the forward nozzle. One modification to the forward nozzles was made to show the effect of minor nozzle changes on the installation losses. A lip extension was added to the inboard lip of the nozzle as shown below:

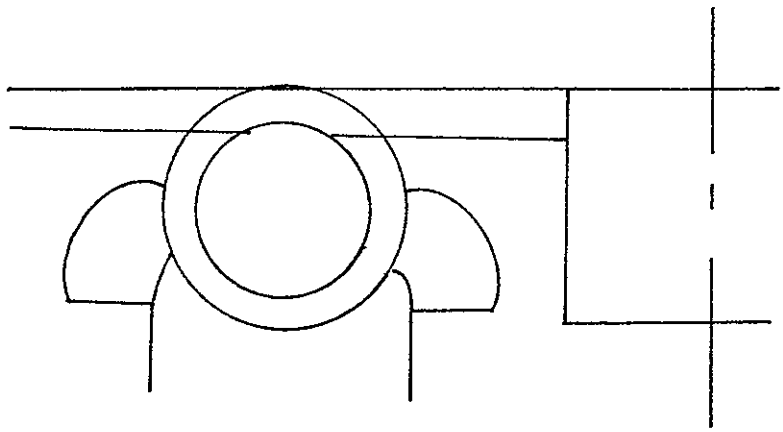

The result of this extension is also shown in Figure 31. The loss was reduced from 5% to 1.5% by the extensions. The three fan version indicates no interference loss at the static condition tested. Since the purpose of this study is to investigate the ground effects, the data in this report were obtained with the basic nozzles.

The effect of the ground board on interference is in general a small additional reduction of lift as can be seen in Figure 32. As much as an additional 5% loss is shown for certain ground board configurations.

Nozzle Angle 105^{o}

The summary of the data with nozzle angle at 105^{o} is presented in Figures 33 to 39 for several conditions tested. The static (V = 0) data show sizable lift losses accompanied by a negative induced pitching moment. A left rolling moment is induced as the ground board is removed from under the right wing.

The lift loss at forward speed is accompanied by an apparent reduction in the aerodynamic drag. These variations would lead one to suspect a reduction in the thrust level as the ground is approached even though no ground effect was indicated during thrust calibrations. One possible

thrust loss explanation is an inlet distortion in the presence of the ground. The total pressure rake used for thrust determination is located on the top quadrant of the fan and might miss an inlet distortion effect. The calibration was done with a fully shielded model so that an inlet distortion would not occur during the fan calibration. One indication of this possible problem was gained during the wind-on test portion of the study. A pitot static tube was mounted on the fuselage nose for comparison with free stream dynamic pressure measurements. During testing at $\delta_N = 105^o$, $\alpha = 8^o$, it was noted that considerable turbulence was present at the probe and that repeatable reading could not be obtained.

The lift loss and drag reduction are affected by the ground board position. At forward speed conditions ground board #3 (aft location) shows an increase in lift and no appreciable effect on drag. The data show that where the front fan exhaust does not strike the ground, the characteristics are entirely different. This condition tends to strengthen the possibility of an inlet distortion.

The 105^o nozzle angle condition would not be used near proximity of a deck and is utilized primarily as a descent and deceleration device such that a lift loss will not materially limit the performance. In the descent an additional lift loss will only require a slightly higher thrust level without approaching the maximum thrust level of the propulsion system. The use of the full forward thrust angle in maneuvering around the deck is also rather unlikely.

Increasing the angle of attack to 8^o also is undesirable in that the lift losses are increased (Figure 39).

Nozzle Angle 90^o

The 90^o nozzle angle condition is of the greatest interest for VTOL operation around the ship. Figures 40 to 50 present the summary of the 90^o nozzle condition. The data show the aerodynamic characteristics due to ground to be a generally small lift loss in ground effect and a pitch down at intermediate heights for the static or zero speed case (Figure 40).

The rolling moments induced by the removal of the ground board from under the right hand wing are as expected for the zero bank case. Removal of the ground board from under the right hand wing induces a left or negative roll, see Figure 41. During banked conditions the effect of removing the ground board from under the right wing is affected by the direction of bank. Positive bank $+10^o$ (right wing down) results in a positive moment for the full deck. As portions of the deck are removed, the positive moment decreases; and, with the deck edge at the centerline, the induced moment is negative. Negative bank -10^o induces a negative moment for full deck. These negative moments are relatively unchanged due to the removal of the deck from under the right hand wing. This variation in rolling

moment can be explained by an analysis of the primary contributors to the moments. The primary contributor to the moment is the change in fountain position with a secondary contribution due to the negative pressure on the bottom surfaces of the wing.

Unbanked — Symmetrical Fountain, Symmetrical pressures

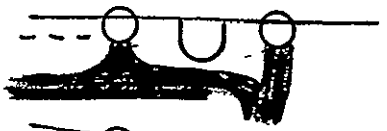

Negative roll from pressures

Right Bank (Positive) $\phi = +$ — Positive roll from fountain, Small positive roll from pressures

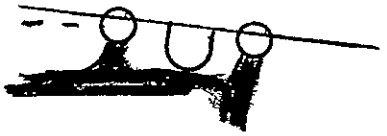

Negative roll from pressures

Left Roll (Negative) $\phi = -$ — Negative roll from fountain, Small negative roll from pressures

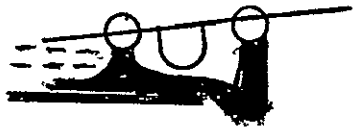

Negative roll from pressures

The removal of the ground board alters the position of the fountain since there is no counteracting jet reflecting from the side with the board removed. The data presented in Figure 41 are the summation of the pressure changes due to the nearness to the ground of the downgoing wing, the fountain shifts occurring due to bank angle, and the elimination of the fountain due to removal of the ground board.

The induced forces at forward speed are similar to those at the static condition with some exceptions. The lift loss in ground effect is somewhat higher and with deck #2 is much higher (Figure 42). Again, as discussed in the 105° nozzle angle case, this condition may be due to some external effect. The pitching moments and rolling moment excursion are somewhat reduced with the maximum rolling moment occurring at $h/D = 4$ rather than at zero for the $V/V_j = 0$ condition (Figure 43). Increasing the angle of attack to 8°, shows an increase in lift loss as was experienced at 105°.

Figures 47 and 48 present the $\delta_N = 90^{\circ}$, $\alpha = 0$, longitudinal data as a function of velocity ratio at constant h/D. With the exception of

ground board #2, the lift increases as speed increases. The pitch down is reduced and the drag is relatively constant.

The effects of the #2 ground board configuration have been shown to be a loss in lift and a reduction in drag. There are several possible explanations for this characteristic. The data assume this lift loss to be a true deck edge characteristic. Other possible explanations which may be present are: The full ground board is located ahead of the model center of gravity and, therefore, extends some distance ahead of the model. There could exist a flow ahead of the model which because of the length of the board would cause the flow to be deflected off the deck and into the fans creating an inlet distortion not picked up by the instrumentation, as discussed previously.

The second possibility also lies in the ground board configuration. The ground board as can be seen in Figure 13 covers only part of the tunnel width. The quality of the flow off the front corners of the ground board is not known. The flow may be creating a turbulence field which is affecting the model characteristics. If the board created a turbulence, it would be different from a ship turbulence and, therefore, these results would not be relatable to an airplane operating near the ship. The reason for this apparent lift loss can not be determined from the available data. Additional studies and instrumentation would be required to define the reason for this lift loss at the #2 deck position.

The effect of the ground board configuration on longitudinal control is shown in Figure 49. A thrust unbalance of approximately 10% nose up was investigated. The greatest effect occurs at $V/V_j = 0$ where considerable effect of the deck edge as well as a basic ground effect is shown. The data show a ratio of pitching moment obtained to pitching moment input. In free air a ratio 1.5 was obtained and at an h/D of 4 the ratio was less than 0.10 for the full deck and for deck #3. Investigation of surface pressures (wing, nacelle, and fuselage) show a trend to reduce the moment but do not indicate the magnitude necessary to reduce the moments to zero. At forward speed some reduction of control input is experienced in ground effect with the greatest occurring with the full deck.

Rolling moment control effectiveness is shown in Figure 50. A 10% thrust unbalance to produce a positive rolling moment was input. Again a reduction is indicated with the full deck showing the largest loss, 50% in a left roll. It should be recognized no attempt was made to affect the rolling or pitching moment control effectiveness by configuration changes since the objective of the study was to investigate the effect of the deck edge location. The addition of strakes and strake boxes have been shown to materially affect these induced effects. Other items available are realignment of the nozzles and height changes to the nozzle exits.

Nozzle Angle 80°

The induced effects of the ground at a nozzle angle of 80° for the $V/V_j = 0$ condition are shown in Figures 51 and 52. The results are similar to the 90° condition.

Nozzle Angle 30°/60°

The deck effects of the four fan configuration in a STOL condition are shown in Figures 53 to 56 for a nozzle angle of 30° forward and 60° aft. The longitudinal data are presented for decks 1, 2, 3 and 4 which represent conditions which might be experienced during takeoff and landings. The data show positive induced lift and moments for all conditions tested. The deck effects are slightly greater than the free air case with the single exception of the lift with deck #2 at an h/D of 1.0. This is not a realistic flight condition since it would entail a landing with the wheels at deck level as the airplane crosses the deck edge.

The induced rolling moments due to thrust are generally small and are greatest with full decks.

Three Fan Nozzle Angle 80°/90°

The three fan configuration, nose plus the two aft fans, was investigated in a VTOL operation mode. The summary data are presented in Figures 57 to 61. The static results show moderate lift changes and a rather large pitch change as the model approaches the full deck. Wind-on conditions indicate small longitudinal induced effects and moderate rolling moments. Higher angle of attack data show again a sizable lift loss with ground board #2. As discussed previously for the four fan configuration, the reason for the lift loss with the #2 board again can not be determined.

EXTRAPOLATION TO FULL SCALE

In order to gain an insight into the possible penalties of operating a full scale aircraft over a partial deck, the model was scaled up to full scale utilizing a 0.12 scale factor. A weight representative of a V/STOL configuration and typical inertias were assigned based on previous in-house studies. While none of these parameters are exact, they are certainly representative of the configuration tested and approximate a full scale airplane of the type discussed. A wing loading of 2876 N/M^2 (60 lbs/ft^2) for vertical operation and 4074 N/M^2 (85 lbs/ft^2) for STOL

operation have been picked for the analysis of data. This results in the following airplane.

Wing Area	53.88 M^2	(580 ft^2)
Aspect Ratio	8.06	
Span	20.85 M	(68.4 ft)
Root Chord	3.46 M	(11.36 ft)
Tip Chord	1.73 M	(5.68 ft)
MAC	2.69 M	(8.83 ft)
W/S Vertical	2876 N/M^2	(60 lbs/ft^2)
STOL	4074 N/M^2	(85 lbs/ft^2)
Weight Vertical	154,945 N	(34,833 lbs)
STOL	219,506 N	(49,347 lbs)
Lateral Arm	5.88 M	(19.3 ft)
Longitudinal Arm	3.73 M	(12.25 ft)
Pitch Inertia	14.9×10^6 Kg/M^2	(95,000 $slugs/ft^2$)
Roll Inertia	15.7×10^6 Kg/M^2	(100,000 $slugs/ft^2$)

Thrust variations required to perform the required 0.5 radians per second pitch acceleration accounts for a thrust differential of 34,496 N (7755 pounds) of thrust front and rear, or 8620 N (1938 pounds) of thrust per engine for the four engine configuration. The roll requirement for the .9 radian/sec acceleration amounts to 10,373 N (2332 pounds) of thrust per engine. Using the higher number as a limit (2132 pounds) for the thrust variation shows that a pitch control of $PM/T\bar{c} = \pm 0.185$ is available for pitch control from the trim condition. This thrust unbalance would allow an increase in pitch acceleration from 0.5 rad/sec to 0.6 rad/sec. This would occur at a thrust of 154,798 N (34,800 pounds) or equal to the vertical operating weight. No moments of this magnitude are indicated in the data for the four fan configuration.

The lateral coefficient of RM/Tb reduces to ± 0.038, far greater than any induced moments encountered.

Much of the data is correlated on the velocity ratio (V/V_j). Conversion of the V/V_j to velocity for an airplane engine operating at a fan pressure ratio of 1.25 is presented in Figure 62 (sea level, standard day).

The vertical flight condition (90^o nozzle) has been analyzed to show the effects on a full scale airplane. The airplane was discussed previously. Considering the selected airplane pressure ratio, the data can now be converted to a speed. $V/V_j = 0$ is, of course, zero velocity. A $V/V_j = 0.09$ corresponds to approximately 35 knots which is the upper speed region for wind over the deck. These speeds were chosen to show the effect of deck and deck edge on the control requirements. A basic set of control requirements have been chosen to correlate with the deck edge inputs. These control requirements (from reference 1) are as follows:

Lift	+ 10% of weight
Pitch	0.5 radians per $(\text{second})^2$
Roll	0.9 radians per $(\text{second})^2$

The airplane damping was not considered in the analysis. A positive damping can be expected on a real configuration which would increase the basic control requirements to obtain the angular accelerations. Therefore, the ratios shown in this analysis may be slightly large. Figures 63 to 66 present the control required in ground effect on the airplane from a trimmed in free air condition as a percent of control available. The most significant deck edge input occurs in the lift requirement with deck #2 at a velocity of 35 knots ($V/V_j = 0.09$). In this condition slightly more than the full control allowance is required.

A similar presentation for the three fan is presented in Figures 67 and 68 for the largest excursions shown. The weights, inertias, etc., of the three fan are the same as used for the four fan configuration. Approximately 90% of the lift control is required with either the deck #2 or #3 at a h/D of 1.0. The most significant three fan variation is shown in the full deck pitching moment at $V/V_j = 0$. Although the data show pitching moment required to trim the airplane in ground effect would exceed the single axis pitch control by approximately 50%, data from other three fan configurations (e.g., reference 4) do not show this trend. This phenomenon is probably very configuration dependent and will require testing during configuration development of any new configuration.

The effects of the forces induced by the deck and deck edge depend to a great extent on the approach pattern used by the V/STOL airplane. One study, reference 7, used an approach as shown in Figure 69. In this study the deceleration was done in free air with initial hover at 50 feet above the deck. The airplane was then translated laterally at 50 feet and the landing made vertically. This type of approach would then eliminate most deck edge effects. Deck edge would only be of interest if the airplane wandered off the deck in the final landing maneuver or if the deck was of such a size that partial overhang was a requirement. In order to investigate the deck edge effect, a four fan airplane configuration was assumed to approach a ship straight in from the rear at 6.1 M (20 feet) (h/D = 4.0). This approach (Figure 70) was made at 10 knots carrier speed and 10 knots closing speed. This condition encompasses the worst deck edge effects found in the study. The approach was made with no control and repeated with pitch control only. The airplane required 1.75 seconds to cross from deck position #2 to the full deck. The deck edge effects were assumed to act as a step input. The forces and moments were input as the airplane center of gravity crossed the deck edge and removed as the tail crossed the deck. In reality the forces will come in and reduce over a finite time period. For purposes of this study the total time the forces are felt is most likely longer than actual so that the study should be applicable. During this time the airplane lost five feet altitude with no control and three

feet with pitch control only. Little, if any, altitude would be lost if height control were also used. The dynamic effects of the force and moment changes at the deck edge will need to be investigated on a simulator.

Utilizing the approach of reference 7, this condition would not be experienced, because the deck is crossed at 15.2 M (50 feet); however, investigating the data presented shows that if the airplane inadvertently got into this position (#2) and remained there for one second with no corrective action taken, only 1.5 feet of altitude would be lost.

The STOL configuration does not encounter significant inputs due to deck edge proximity. The airplane, of course, must cross both deck #2 and #3 on each takeoff or landing; but, as seen previously, at the airplane heights expected during operation, no significant inputs are seen. The other deck edge location of interest for STOL is with partial wing overhang (#4). This could occur during operation from a narrow deck. Deck #4 has essentially the same longitudinal induced effects as the full deck.

CONCLUSIONS

The operation of a V/STOL multi-mission low pressure ratio fan powered airplane configuration in the proximity of a small ship will induce some forces and moments on the aircraft. In most cases these forces are relatively small and manageable. The more significant variations which occur at static or wind over the deck speeds in the vertical mode of operation are:

(1) A lift loss is experienced at wind over the deck speeds for the ground board under the forward part of the model (deck position #2).

(2) A change in trim is experienced in ground effect (all deck positions).

(3) The three fan configuration shows a sizable pitching moment (150% of single axis control) with full deck and zero wind over the deck. This is apparently very configuration dependent and is not generic to three fan configurations.

(4) The four fan configuration shows a 5% loss in lift in free air. This loss can materially be reduced by modifications to the front fan nozzles.

Operation of the four fan configuration in a STOL mode from a small deck appears to present no operational problems.

RECOMMENDATIONS

The results of the deck edge test and analysis have shown several areas where additional studies would be beneficial. It is recommended that these areas be investigated further.

A simulation study is recommended to investigate if the forces and moments due to deck and deck edge proximity would materially increase the pilot's work load.

Because it has been shown that the deck edge effects are configuration oriented, a study on both the three and four fan is recommended to determine the type of configuration modifications which would minimize the deck edge effects.

The fans used for this study had a low exit pressure ratio (approximately 1.2). Because several current configuration analyses have indicated that higher pressure ratio fans are desirable, a study of the effect of fan pressure ratio on deck and deck edge effects is recommended.

The operation around small ships also involves an additional force on the airplane, one of turbulence. It is recommended that the model used in this study be utilized for a study of ship turbulence on the steady state and dynamic characteristics of the configuration.

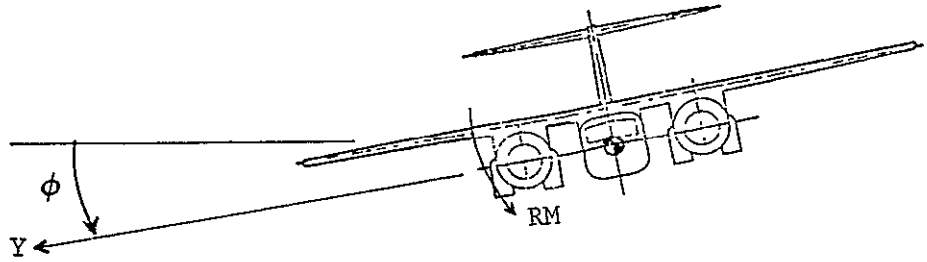

FRONT VIEW

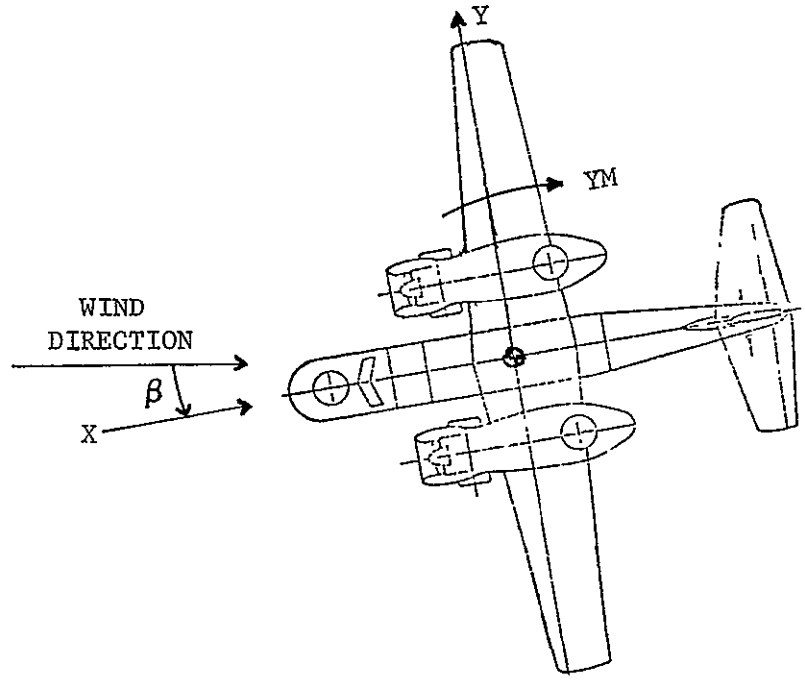

TOP VIEW

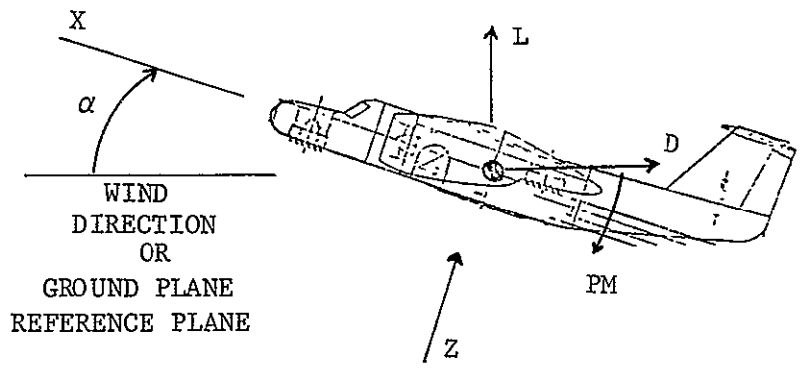

SIDE VIEW

Figure 1. Model Axes System

WING:		
AREA	0.7767 m^2	(8.36 Ft^2)
SPAN	2.5002 m	(8.209 Ft.)
CHORD		
ROOT	0.4154 m	(16.355 in.)
TIP	0.2077 m	(8.178 in.)
MAC	0.3231 m	(12.721 in.)
ASPECT RATIO	8.06	
TAPER RATIO	0.50	
F.S. 25 $\bar{c}$ (C.G.)	0.8610 m	(33.9 in.)
INCIDENCE	5.0°	
WRP AT L.E.	0.1516 m	(5.97 in.)
SWEEP		
L.E.	5.717°	
1/4 CHORD	3.334°	
T.E.	-3.817°	
AIRFOIL SECTION - 15% SUPERCRITICAL		

HORIZONTAL TAIL:		
AREA	0.1956 m	(2.106 Ft^2)
SPAN	0.8661 m	(34.1 in.)
$\bar{c}H$	0.2281 m	(8.98 in.)
ASPECT RATIO	3.83	
TAPER RATIO	0.509	
W.P.	0.3762 m	(14.81 in.)
F.S. 0.25 $\bar{c}$	1.7886 m	(70.417 in.)

VERTICAL TAIL:		
AREA	0.1076 m^2	(1.158 Ft^2)
SPAN	0.3283 m	(12.925 in.)
$\bar{c}V$	0.2337 m	(9.2 in.)

BODY:		
DEPTH	0.2565 m	(10.1 in.)
WIDTH	0.2540 m	(10.0 in.)
LENGTH	1.9986 m	(78.685 in.)

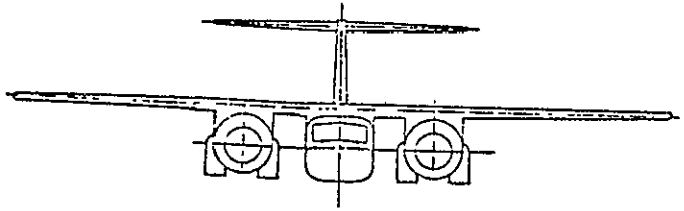

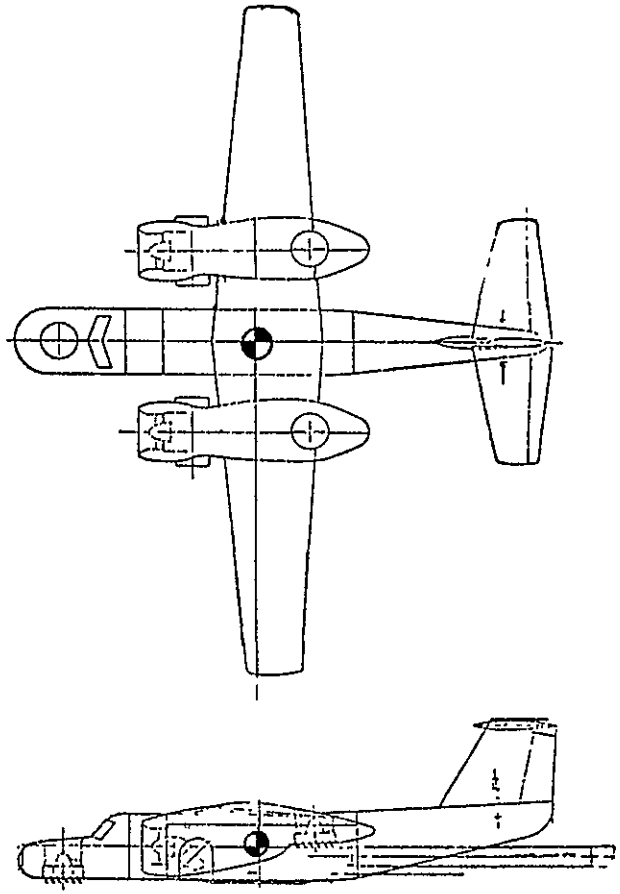

a. 0.12 Scale Model

Figure 2. Model Dimensions

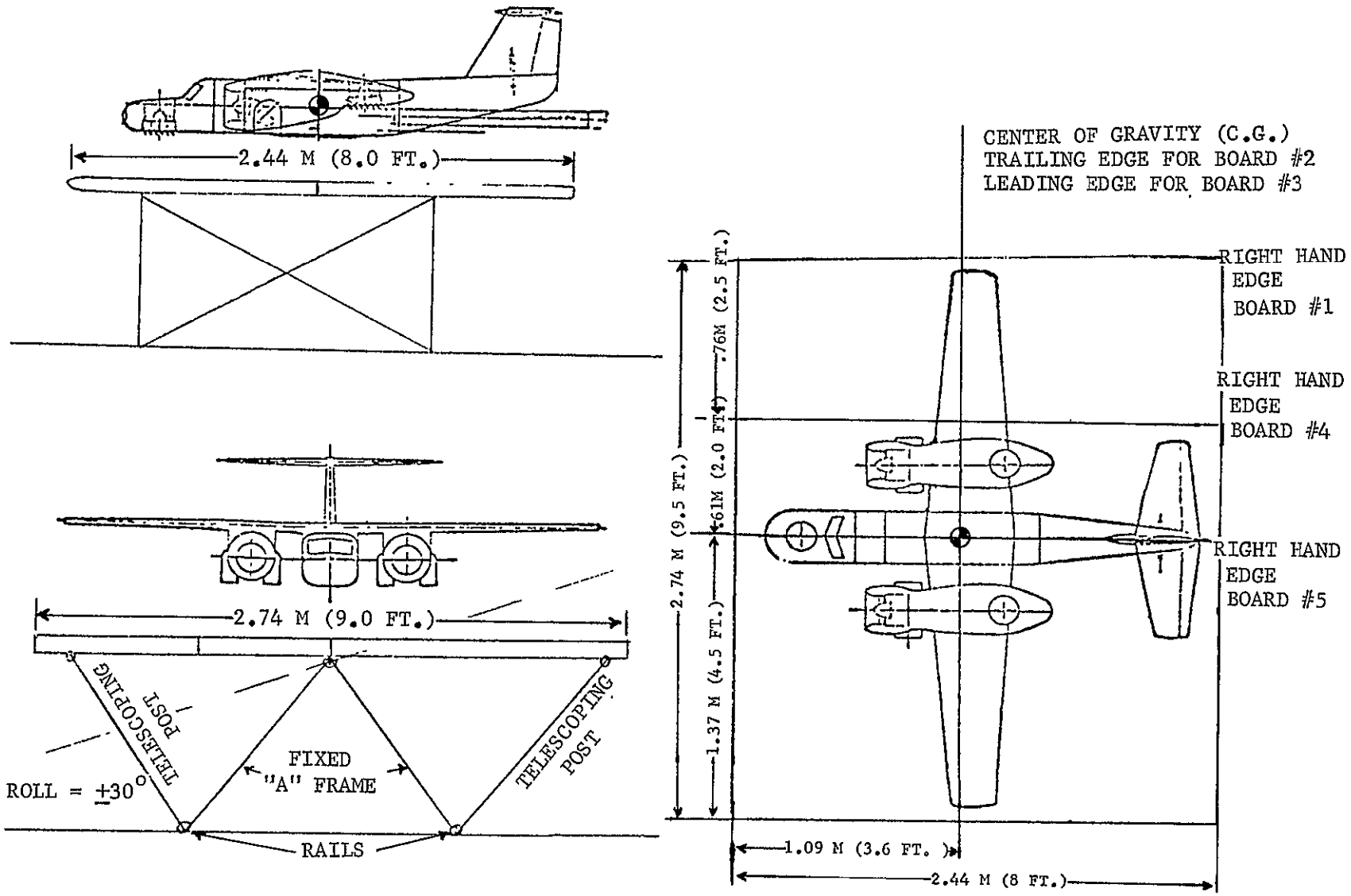

b. Ground Board

Figure 2. Model Dimensions (Concluded)

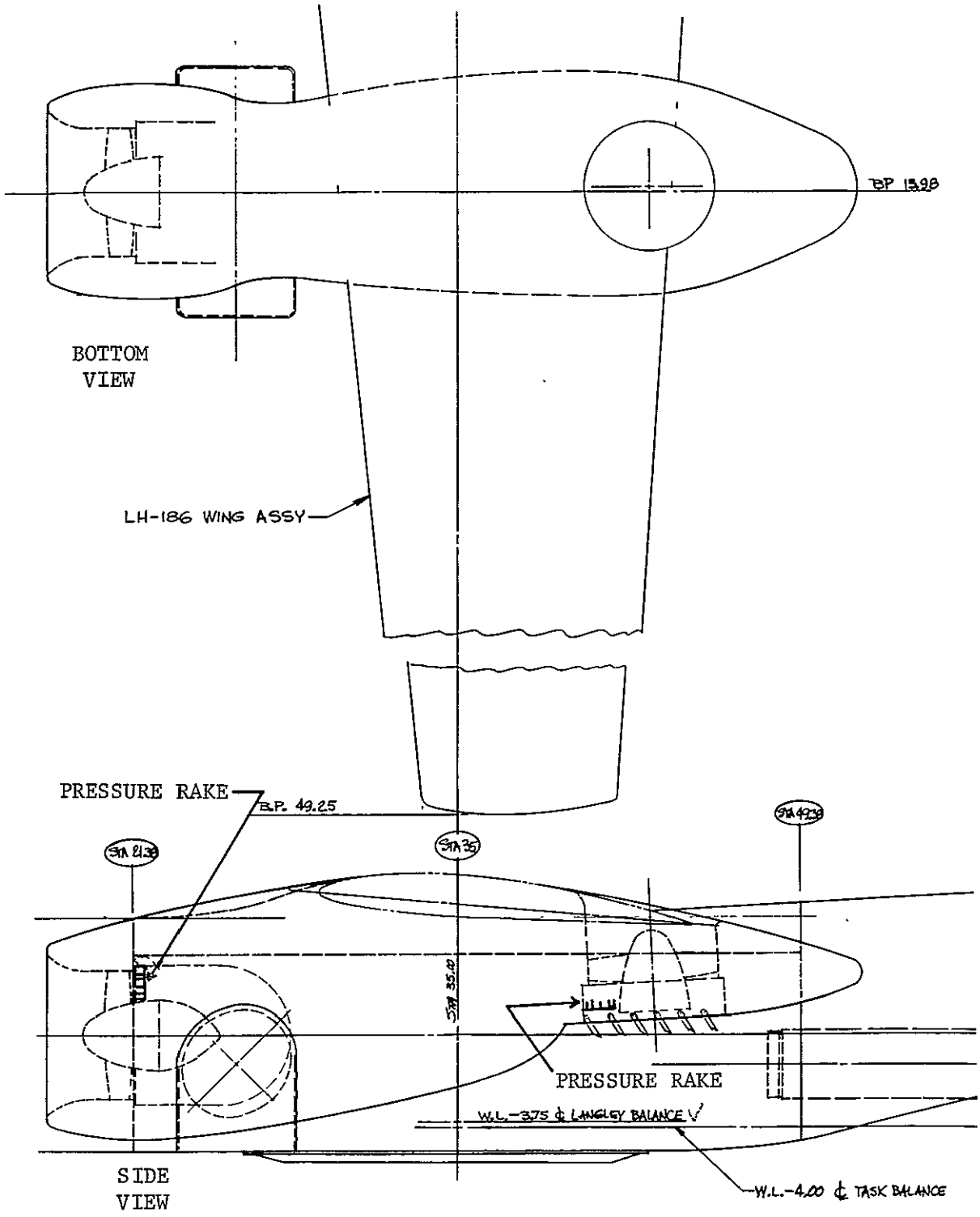

a. Nacelle Details

Figure 3. Nacelle Fan Installation

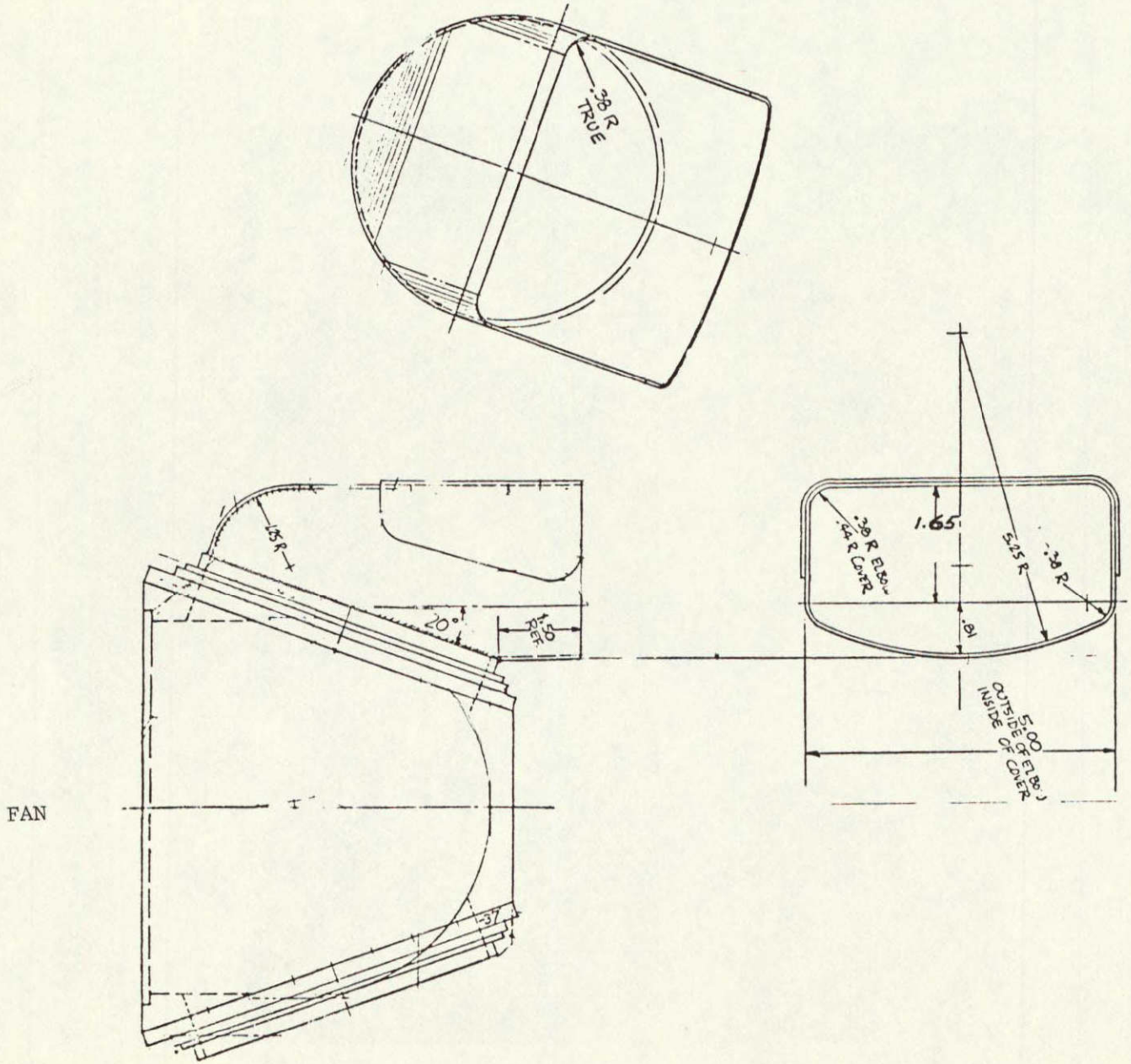

b. Forward Nozzle Detail

Figure 3. Nacelle Fan Installation (Concluded)

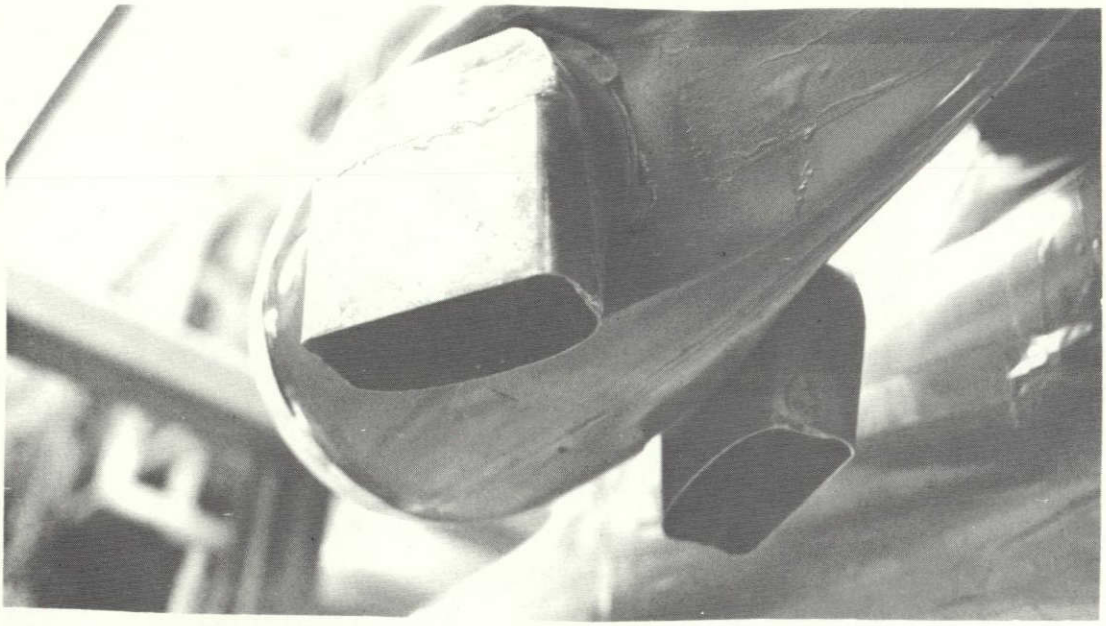

a. (Front Fan)

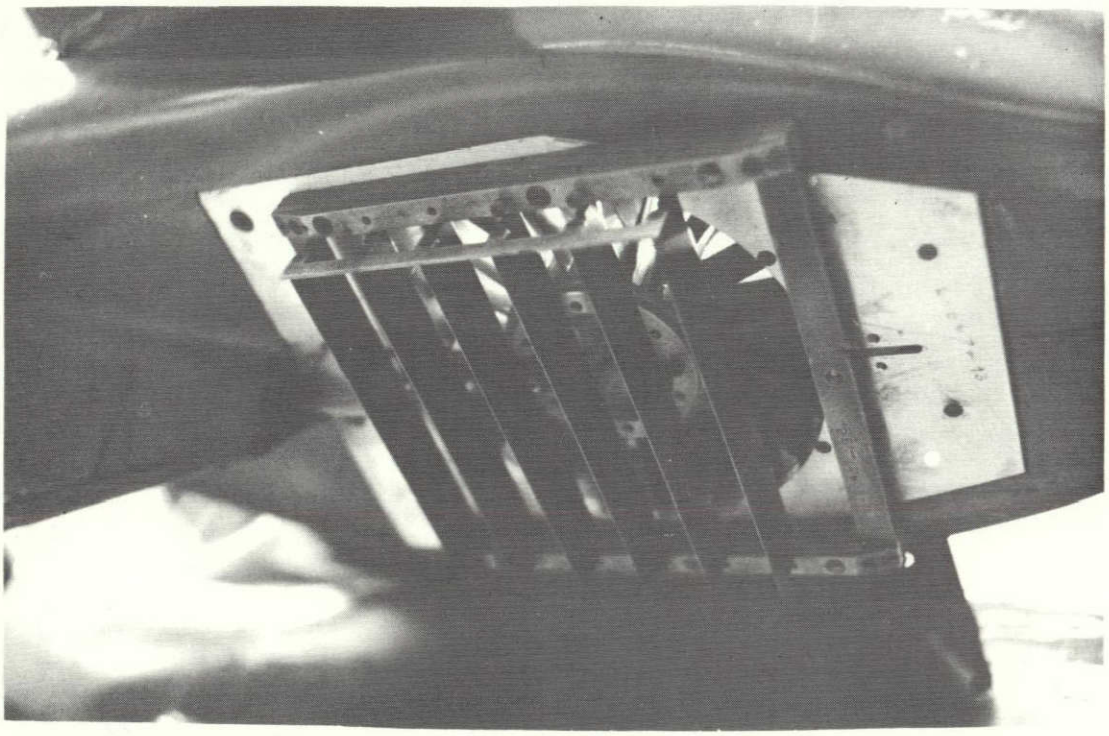

b. (Aft or Nose Fan)

Figure 4. Model Fan Exit

REPRODUCIBILITY OF THE
ORIGINAL PAGE IS POOR

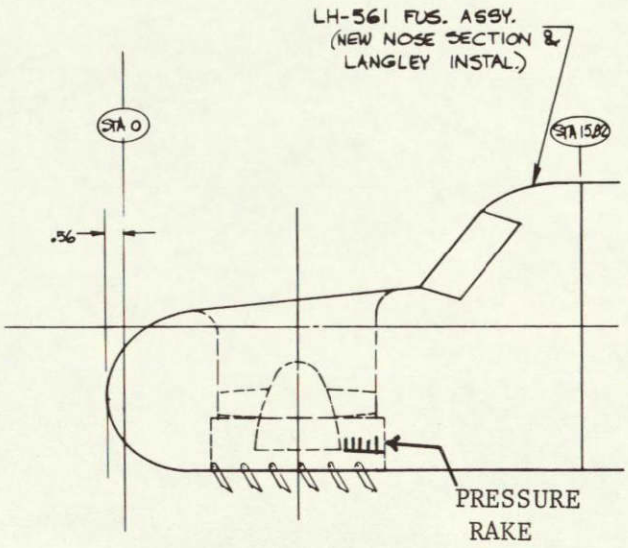

Figure 5. Nose Fan Installation

ITEM NO.	PART NAME
	5.5 IN. CRUISE FAN
1	SPINNER
2	WASHER
	PIN 1/32 DIA. X .125 LG
3	LOCKNUT 1/4-28 #LH6521-048 (ESNA)
4	SPINDLE
	PIN 1/16 DIA. X .125 LG
	T/C WIRE NN-30-J X 12" FREE LENGTH
5	SCREW #2-56 X 1/4 LG NYLOK SOC HD CAP
6	ROTOR ASSY
	HUB
	RETAINER BLADE
	ROTOR BLADE
	TURBINE
	SCREW #4-40 X 1/4 LG NYLOK FL HD CAP
	SHIM
7	STATOR ASSY
	HUB
	RING
	STATOR BLADE
8	SCREW #6-32 X 3/4 LG NYLOK SOC HD CAP
9	SPEED PICKUP (ELECTRO-PRODUCTS #3080)
10	SPACING WASHER
11	SHIM - WASHER
12	WASHER - PRELOAD
13	WAVY SPRING WASHER (ASSOCIATED SPRING #W925-010)
14	SCREW #4-40 X 5/8 NYLOK SOC HD CAP
15	DOWEL PIN
16	O-RING (PRECISION RUBBER #010-8307)
17	HOUSING - STRAIGHT
18	OIL FITTING
	NUT
	TUBE
19	BEARING (BARDEN 101SSTX1K5) (MOD)
20	SPACER, BEARING
21	SET SCREW #8-32 X 15/64 LG NYLON TIP

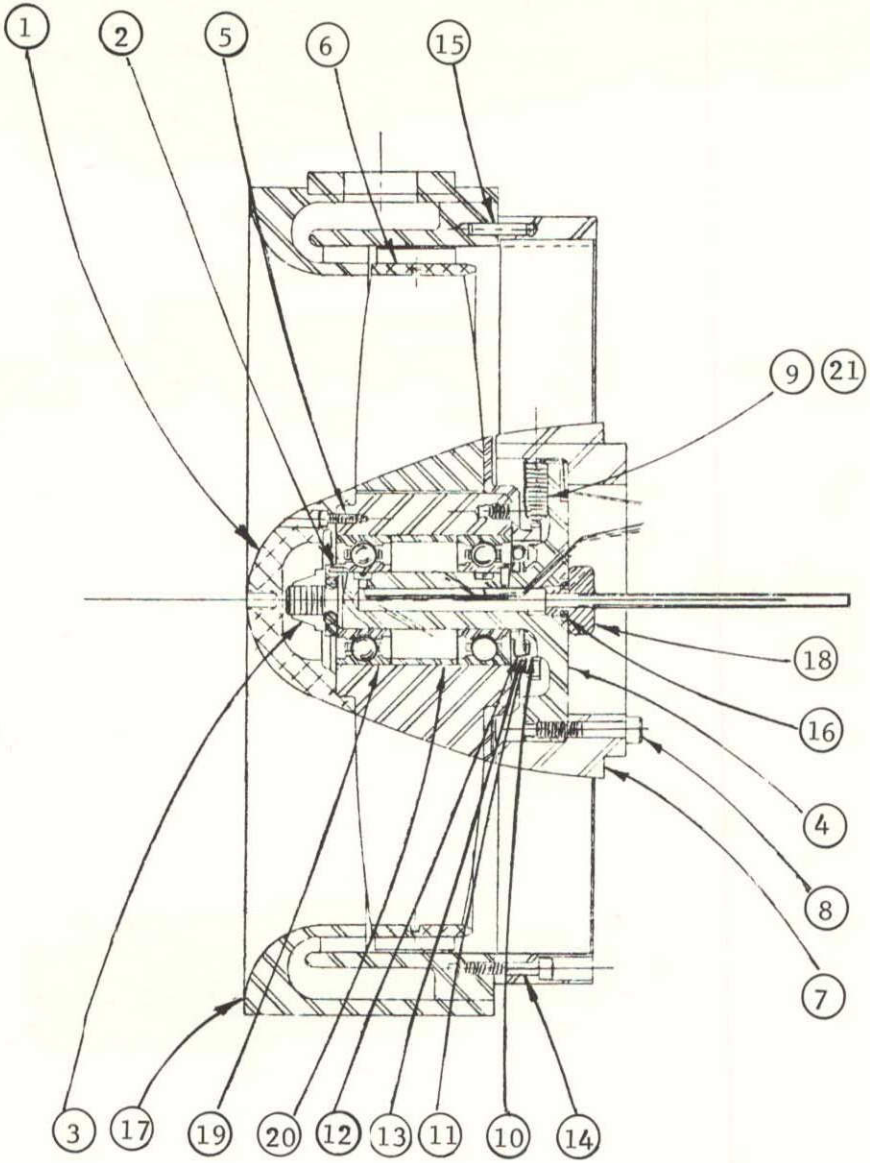

Figure 6. Fan Details

Figure 7. Model Front View

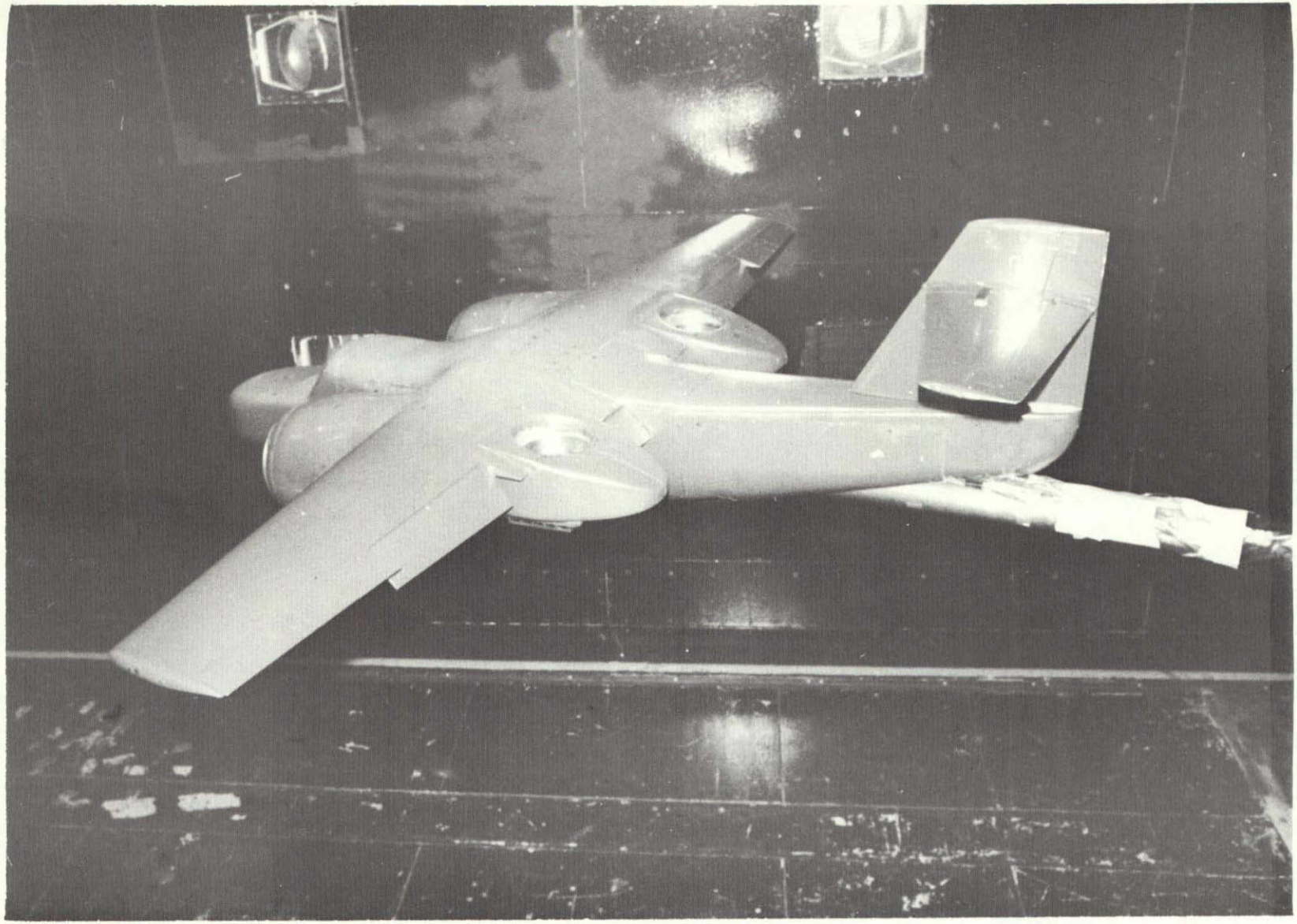

Figure 8. Model 1/2 Top View

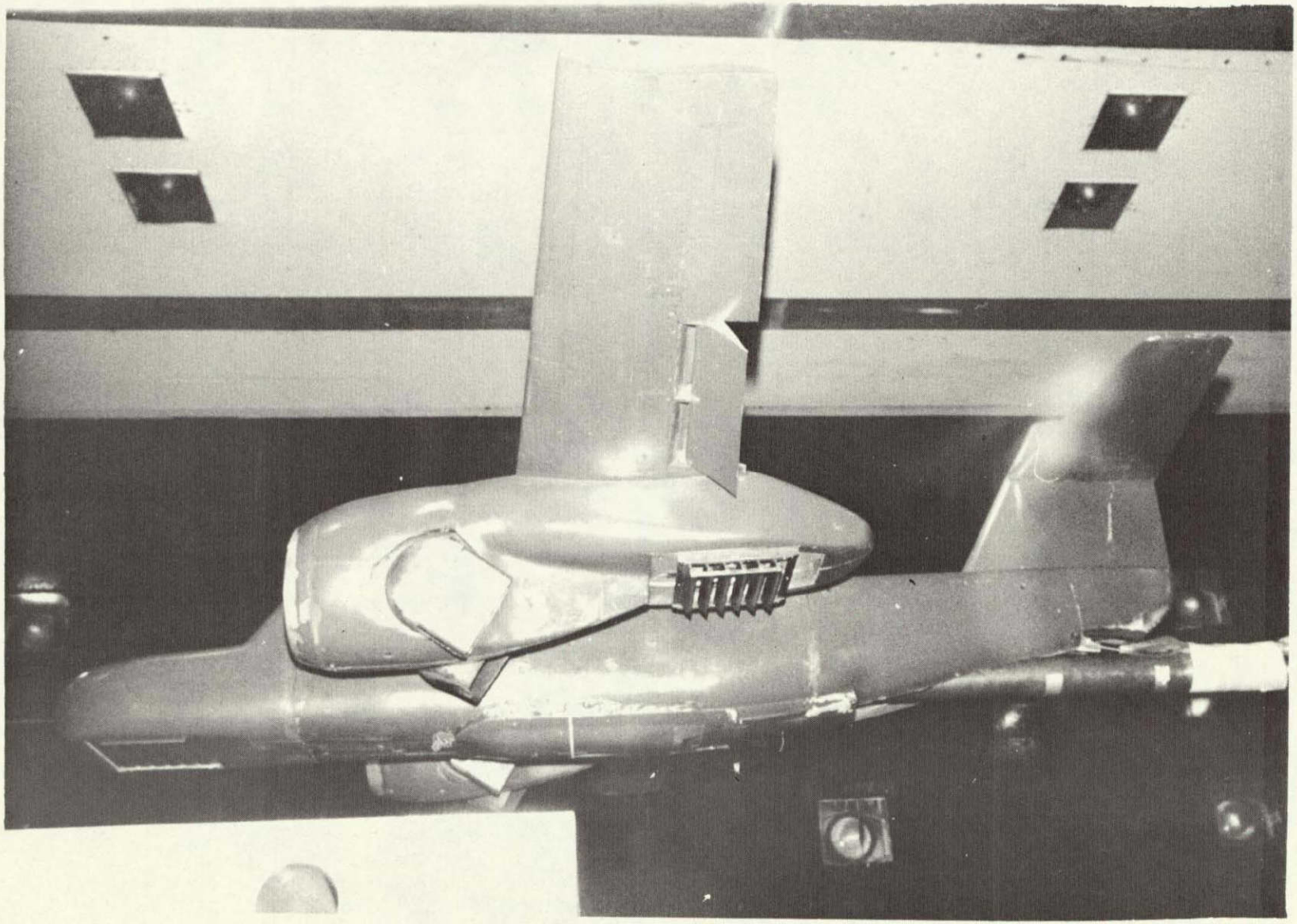

Figure 9. Model 1/2 Bottom View

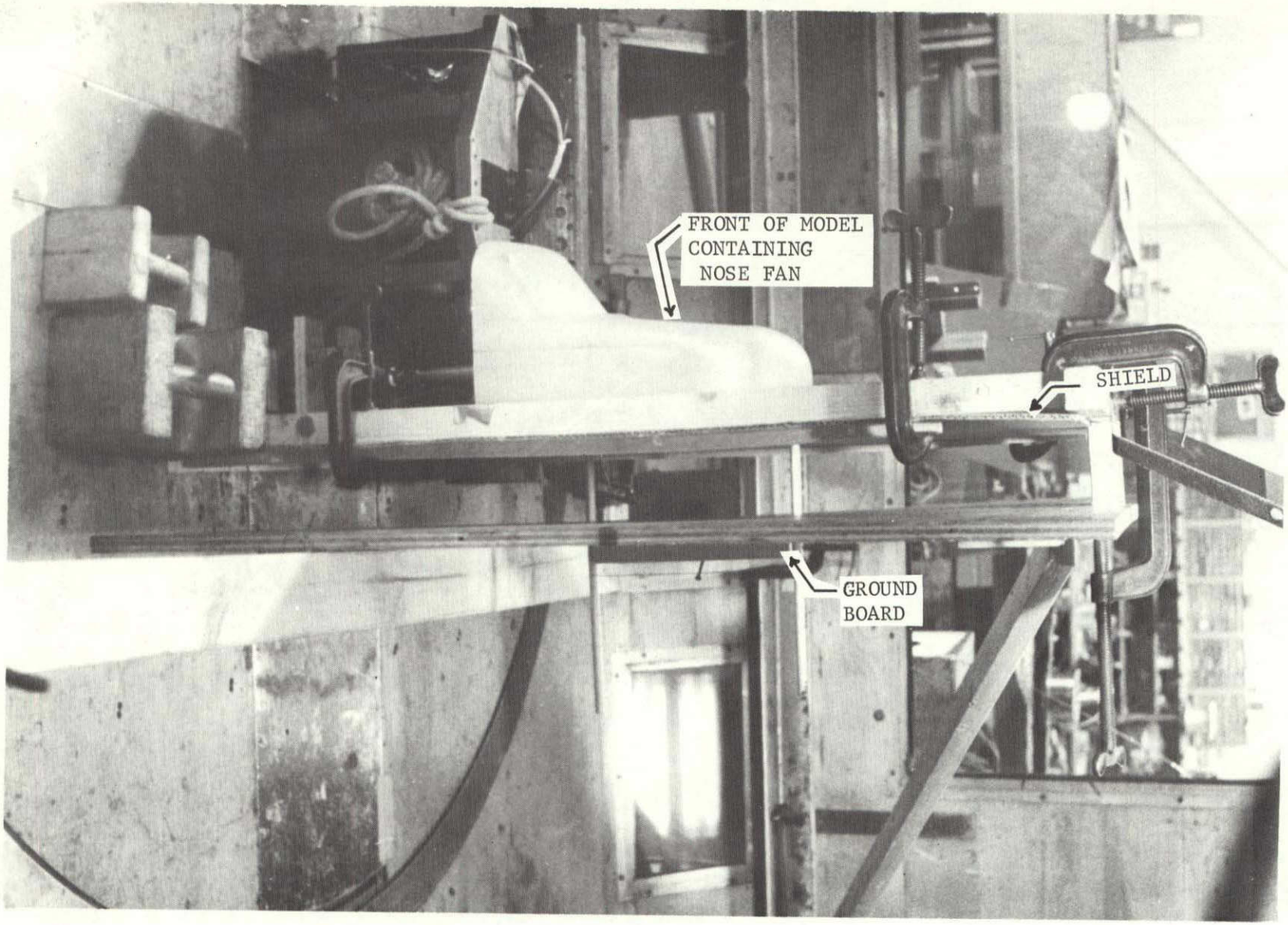

Figure 10. Fan Calibration Setup - Nose Fan

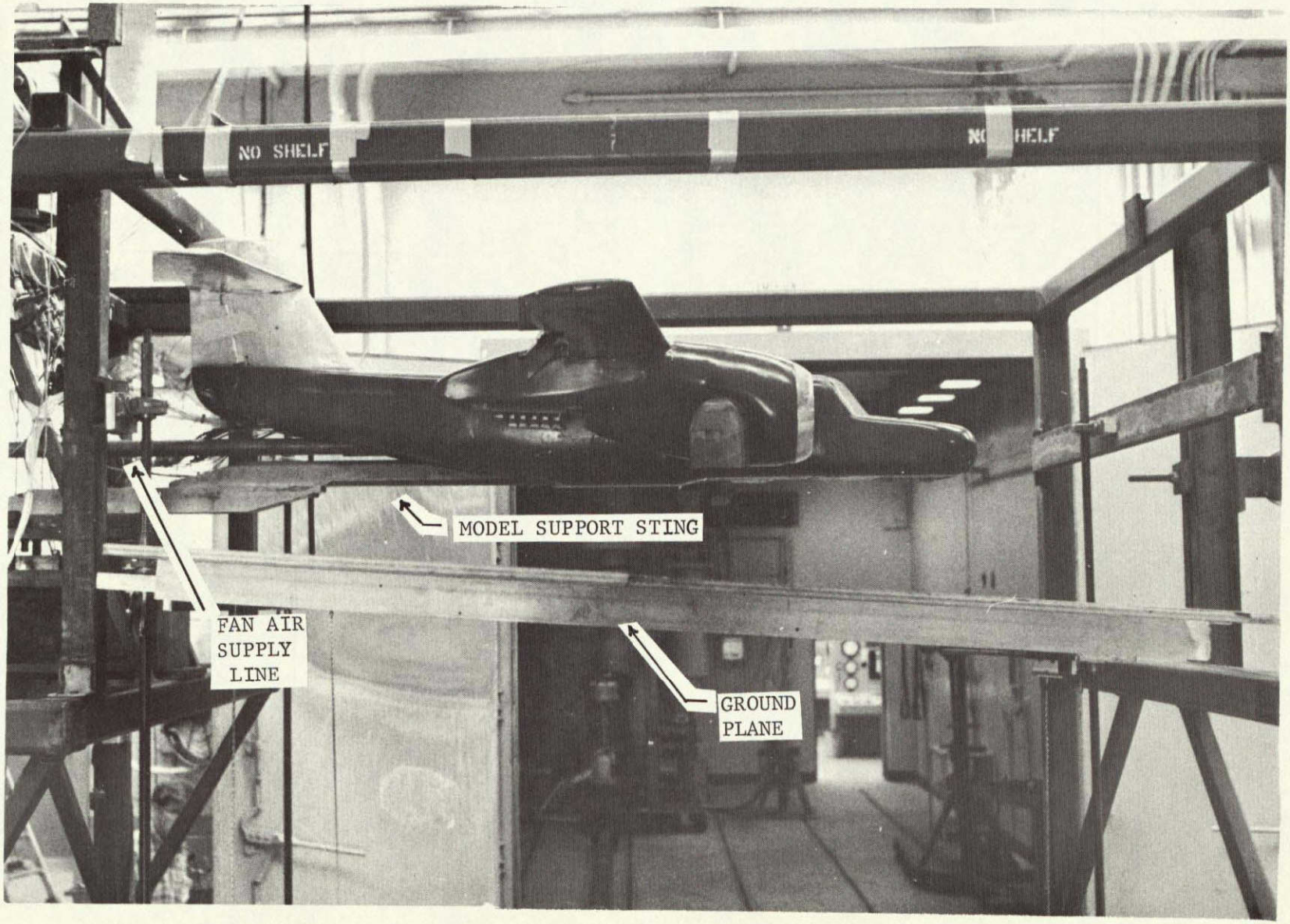

Figure 11. Model in Static Thrust Stand

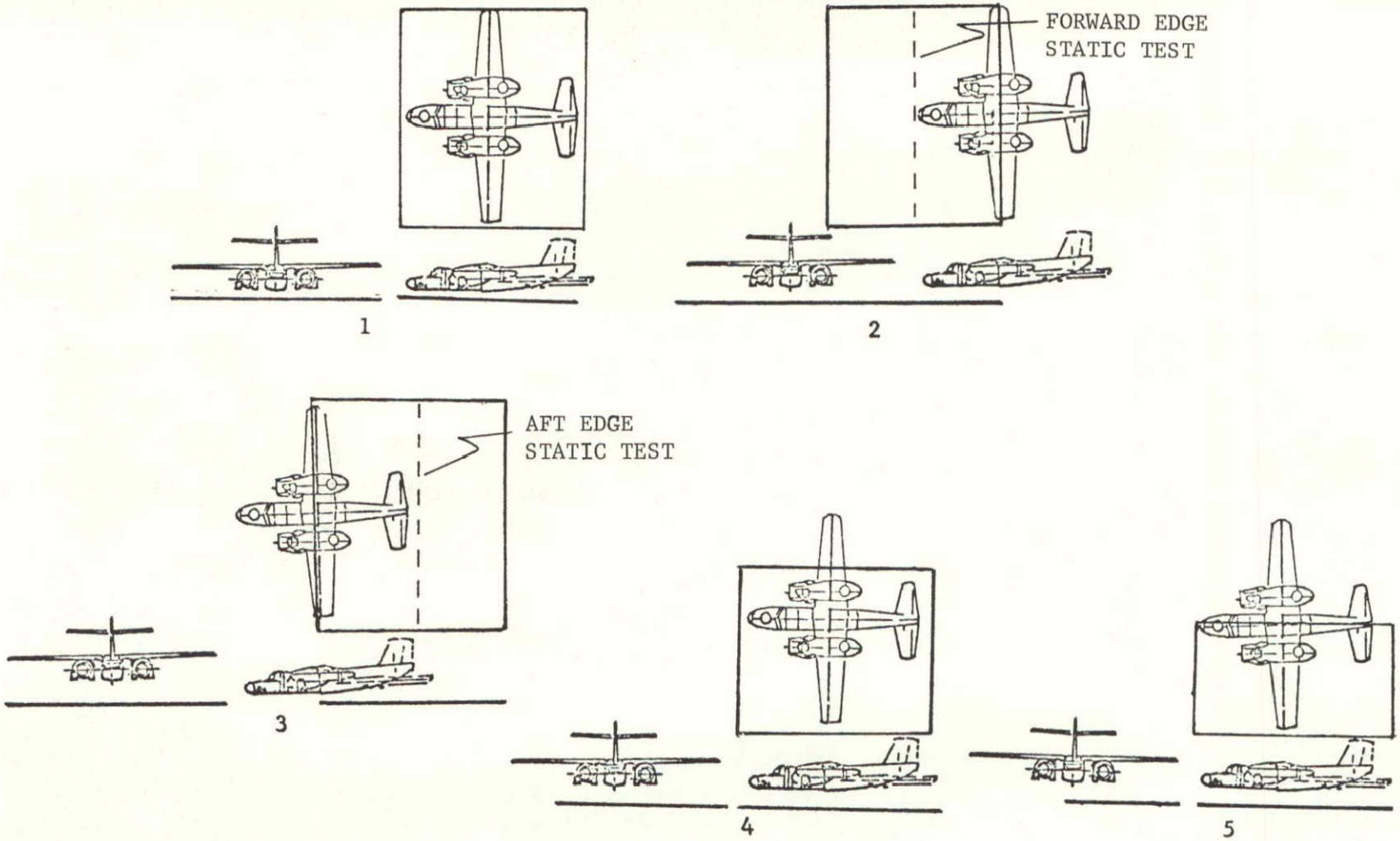

Figure 12. Ground Board Configurations

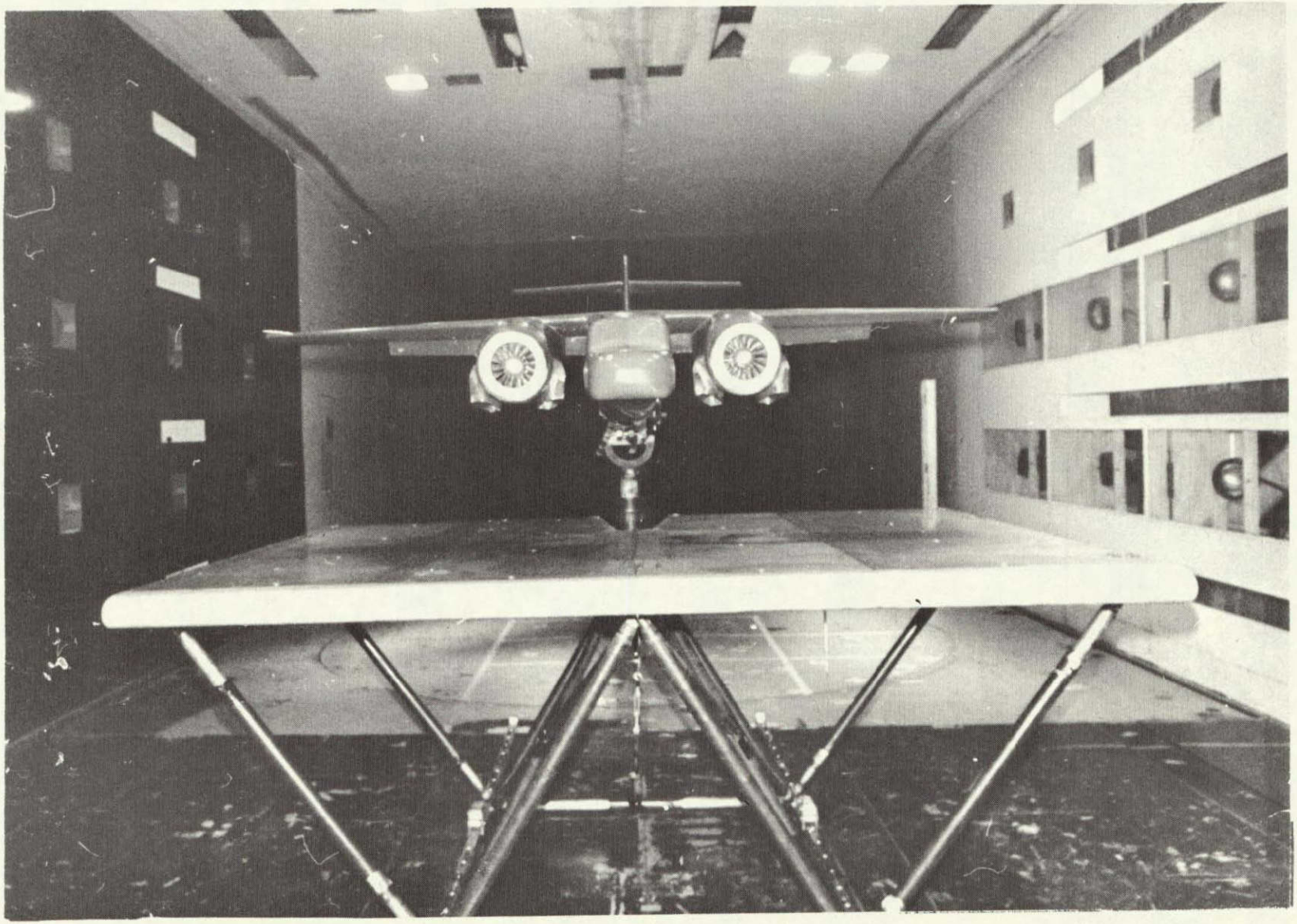

Figure 13. Model in LaRC V/STOL Tunnel with Ground Board

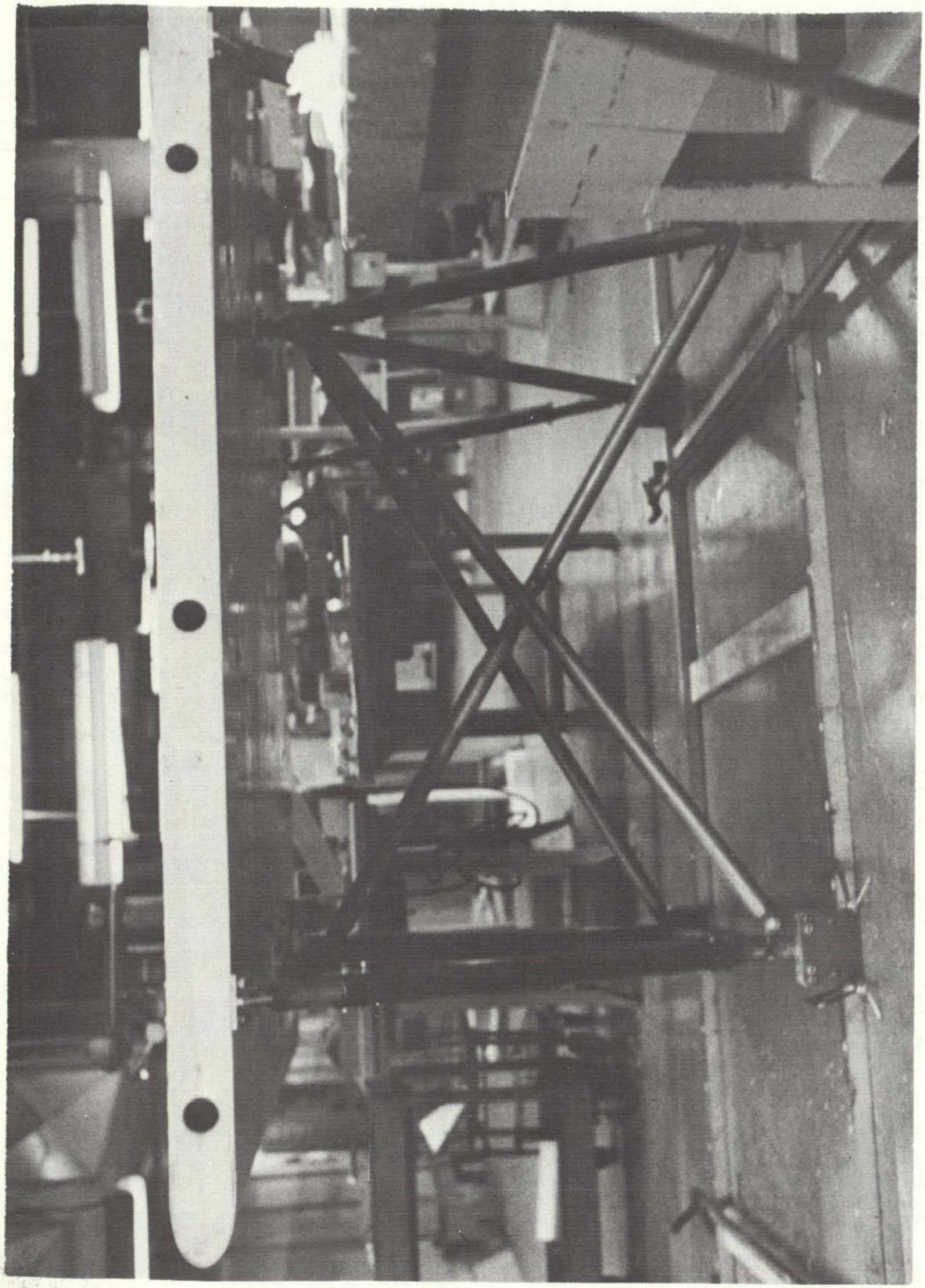

Figure 14. Ground Board Side View

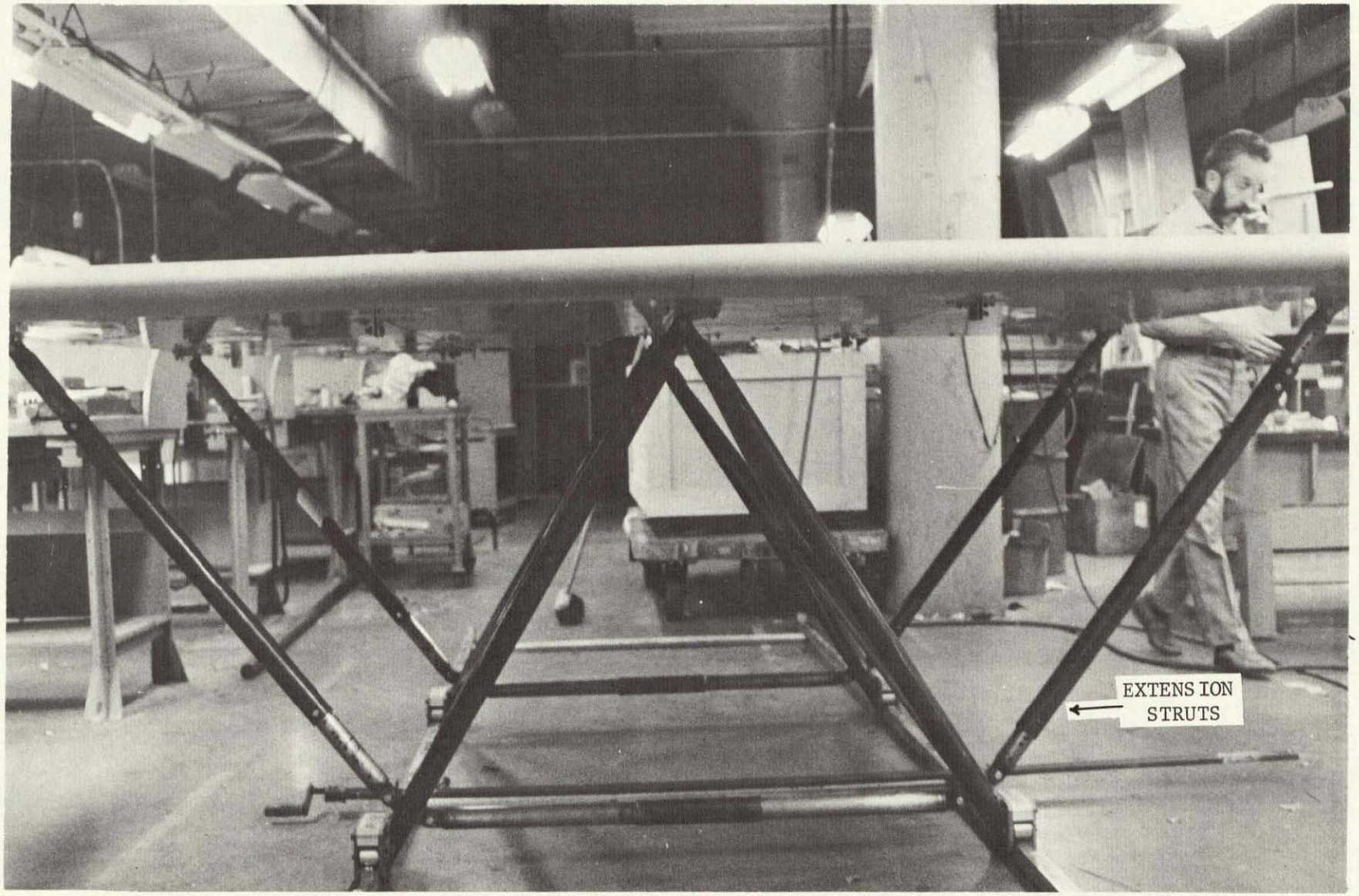

Figure 15. Ground Board Front View

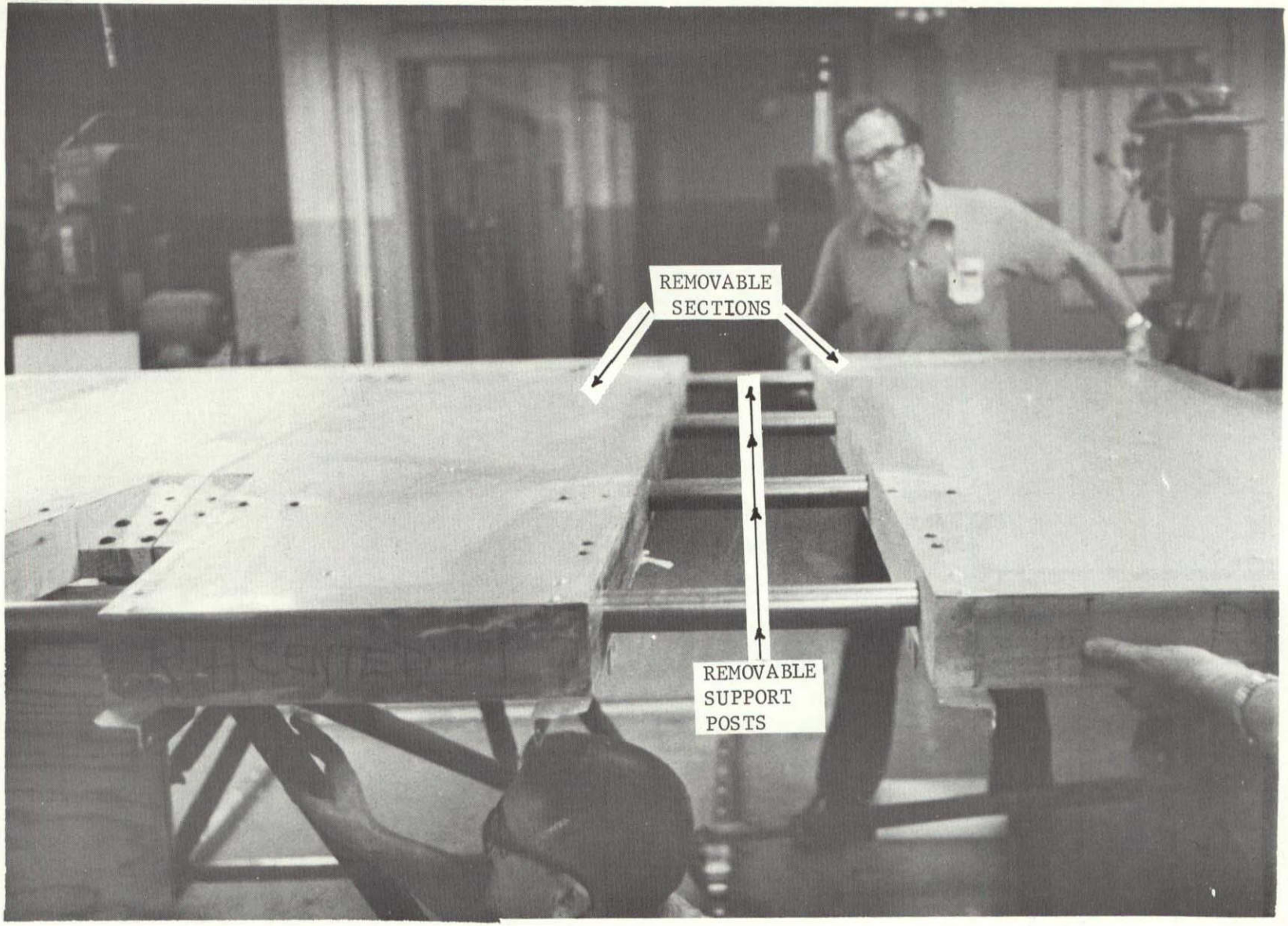

Figure 16. Ground Board Assembly

Thrust Coefficients Nomenclature

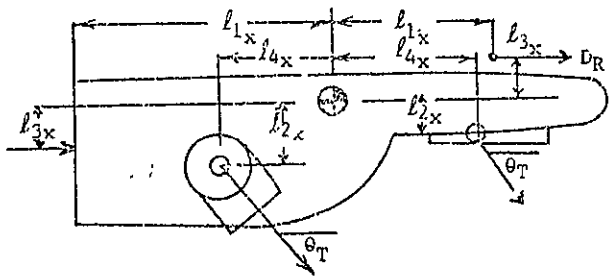

ℓ_{1_x} Horizontal Ram Drag Arm - meters (feet)

ℓ_{4_x} Horizontal Thrust Arm - meters (feet)

ℓ_{3_x} Vertical Ram Drag Arm - meters (feet)

ℓ_{2_x} Vertical Thrust Arm - meters (feet)

ℓ_{5_x} Lateral Thrust Arm - meters (feet)

θ_{T_x} Thrust Angle

ΔC_{L_T} Lift Coefficient due to Thrust

ΔC_{D_T} Drag Coefficient due to Thrust

ΔC_{RM_T} Rolling Moment Coefficient due to Thrust

ΔC_{M_T} Pitching Moment Coefficient due to Thrust

ΔC_{YM_T} Yawing Moment Coefficient due to Thrust

$C_{L_{Aero}}$ Aerodynamic Lift Power On

$C_{D_{Aero}}$ Aerodynamic Drag Power On

$C_{M_{Aero}}$ Aerodynamic Pitching Moment Power On

$C_{RM_{Aero}}$ Aerodynamic Rolling Moment Power On

$C_{YM_{T_{Aero}}}$ Aerodynamic Yawing Moment Power On

x = fan number (1⟶5)

Fan Nomenclature

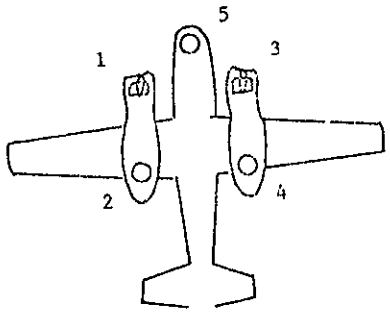

MOMENT ARMS

Fan	ℓ_1	ℓ_2	ℓ_3	ℓ_4	ℓ_5
1	.413 (1.354)	.061 (.20)	.031 (.103)	.210 (.688)	.355 (1.165)
2	-.234 (-.771)	.013 (.041)	.130 (.425)	-.239 (-.783)	.350 (1.150)
3	.413 (1.354)	.061 (.20)	.031 (.103)	.210 (.688)	.355 (1.165)
4	-.234 (.771)	.013 (.041)	.130 (.425)	-.239 (-.783)	.350 (1.150)
5	.711 (2.333)	.160 (.525)	.025 (.083)	.711 (2.333)	0

Figure 17. Data Reduction Equations

Compute Aerodynamic Coefficients (Power On)

$$\theta_T = \sin^{-1} \Sigma T_x \sin \theta_x \Big/ \left[\left(\Sigma T_x \cos \theta_x \right)^2 + \left(\Sigma T_x \sin \theta_x \right)^2 \right]^{1/2}$$

$$\Delta C_{L_T} = C_T \sin(\theta_T + \alpha)$$

$$\Delta C_{D_T} = -C_T \cos(\theta_T + \alpha)$$

$$\Delta C_{M_{T_x}} = T_x (\ell_{4_x} \sin \theta_{T_x} + \ell_{2_x} \cos \theta_{T_y}) / qS\bar{c}$$

$$\Delta C_{M_T} = \Sigma \Delta C_{M_{T_x}} \quad \text{Fan 1, 2, 3, 4, 5}$$

$$\Delta C_{M_{D_x}} = D_R (\ell_{3_x} \cos \alpha + \ell_{1_x} \sin \alpha) / qS\bar{c}$$

$$\Delta C_{M_D} = \Sigma \Delta C_{M_{D_x}} \quad \text{Fan 1, 2, 3, 4, 5}$$

$$\Delta C_{R\ell_x} = T_x \ell_{5_x} \left[\sin \theta_x \cos \alpha + \cos \theta_x \sin \alpha \right] / qSb$$

$$\Delta C_{YM_x} = T_x \ell_{5_x} \left[\cos \theta_x \cos \alpha - \sin \theta_x \sin \alpha \right] / qSb$$

$$C_{L_{Aero}} = C_L - \Delta C_{L_T}$$

$$C_{D_{Aero}} = C_D + \Delta C_{D_T} - C_{D_R}$$

$$C_{M_{Aero}} = C_M - \Delta C_{M_T} - \Delta C_{M_D}$$

$$C_{R\ell_{Aero}} = C_{R\ell} - \Sigma \Delta C_{R\ell_x}$$

$$C_{YM_A} = C_{YM} - \Sigma \Delta C_{YM_x}$$

$$D_R = M_1 V$$

$$C_{D_R} = \frac{D_R}{qS}$$

$$\frac{\Delta L}{T} = \frac{C_{L_{A_{Power\ On}}} - C_{L_{Power\ Off}}}{C_T}$$

$$\frac{\Delta D}{T} = \frac{C_{D_{A_{Power\ On}}} - C_{D_{Power\ Off}}}{C_T}$$

$$\frac{\Delta M}{T\bar{c}} = \frac{C_{D_{A_{Power\ On}}} - C_{D_{Power\ Off}}}{C_T}$$

$$\frac{\Delta RM}{Tb} = \frac{C_{RM_{A_{Power\ On}}} - C_{RM_{A_{Power\ Off}}}}{C_T}$$

Figure 17. Data Reduction Equations (Concluded)

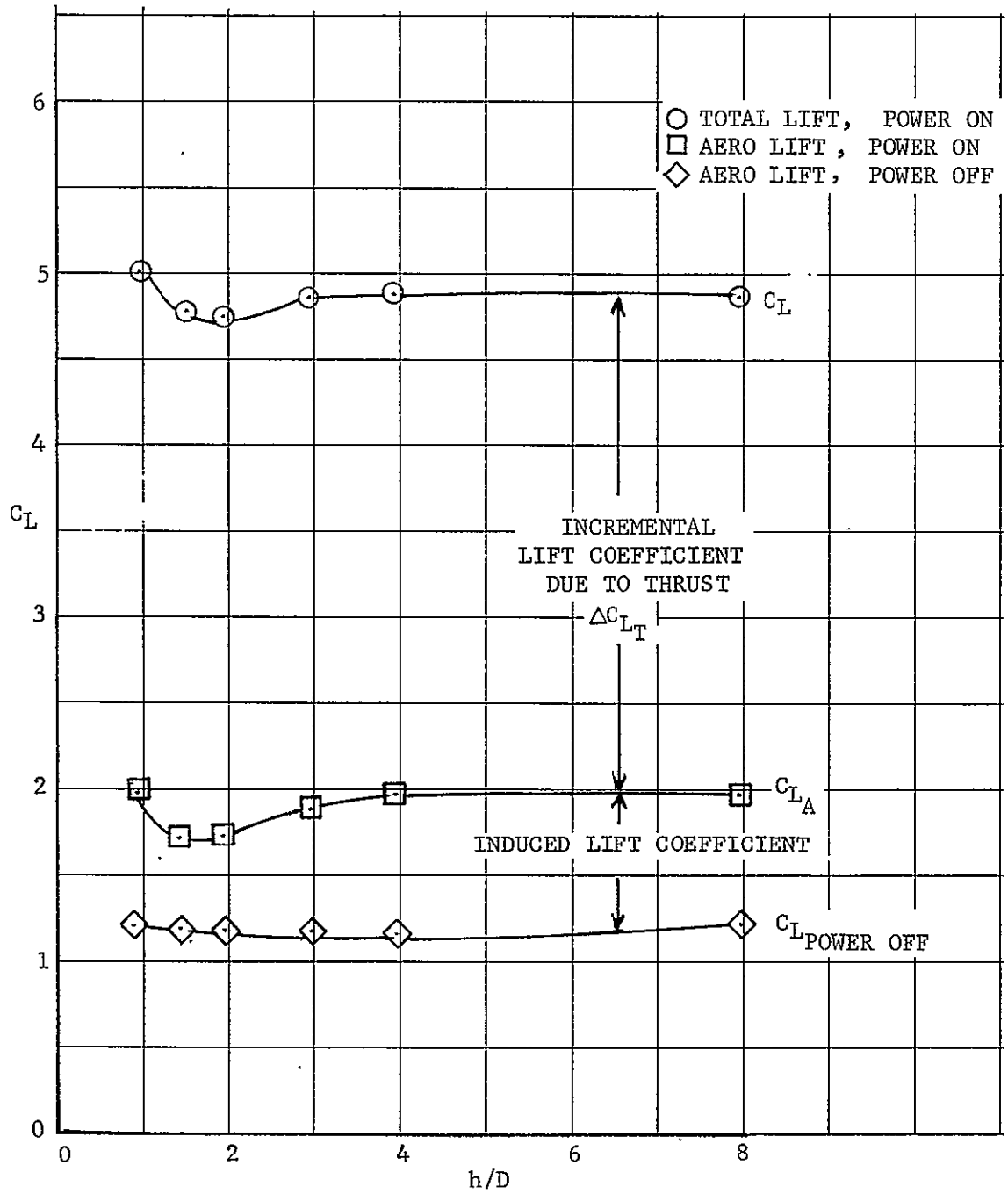

Figure 18. Lift Coefficient Incremental Buildup Due to Power; $\delta_{N_{Fwd}} = 30^\circ$, $\delta_{N_{Aft}} = 60^\circ$ $C_T = 5.1$, $\alpha = 0^\circ$, $\emptyset = 0^\circ$, $V/V_j = .12$

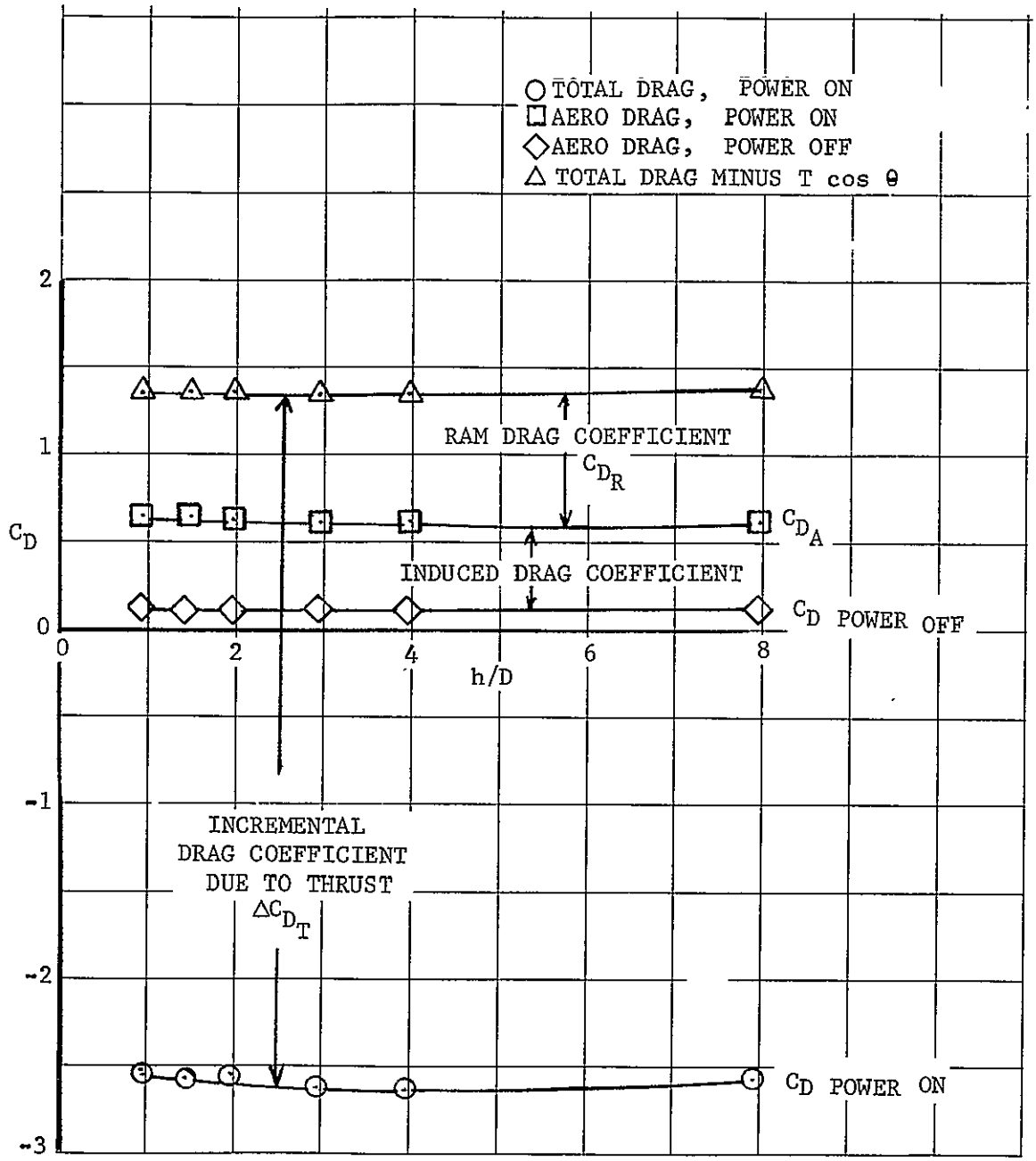

Figure 19. Drag Coefficient Incremental Buildup Due to Power; $\delta_{N_{Fwd}} = 30$, $\delta_{N_{Aft}} = 60^o$, $C_T = 5.1$, $\alpha = 0^o$, $\emptyset = 0^o$, $V/V_j = .12$

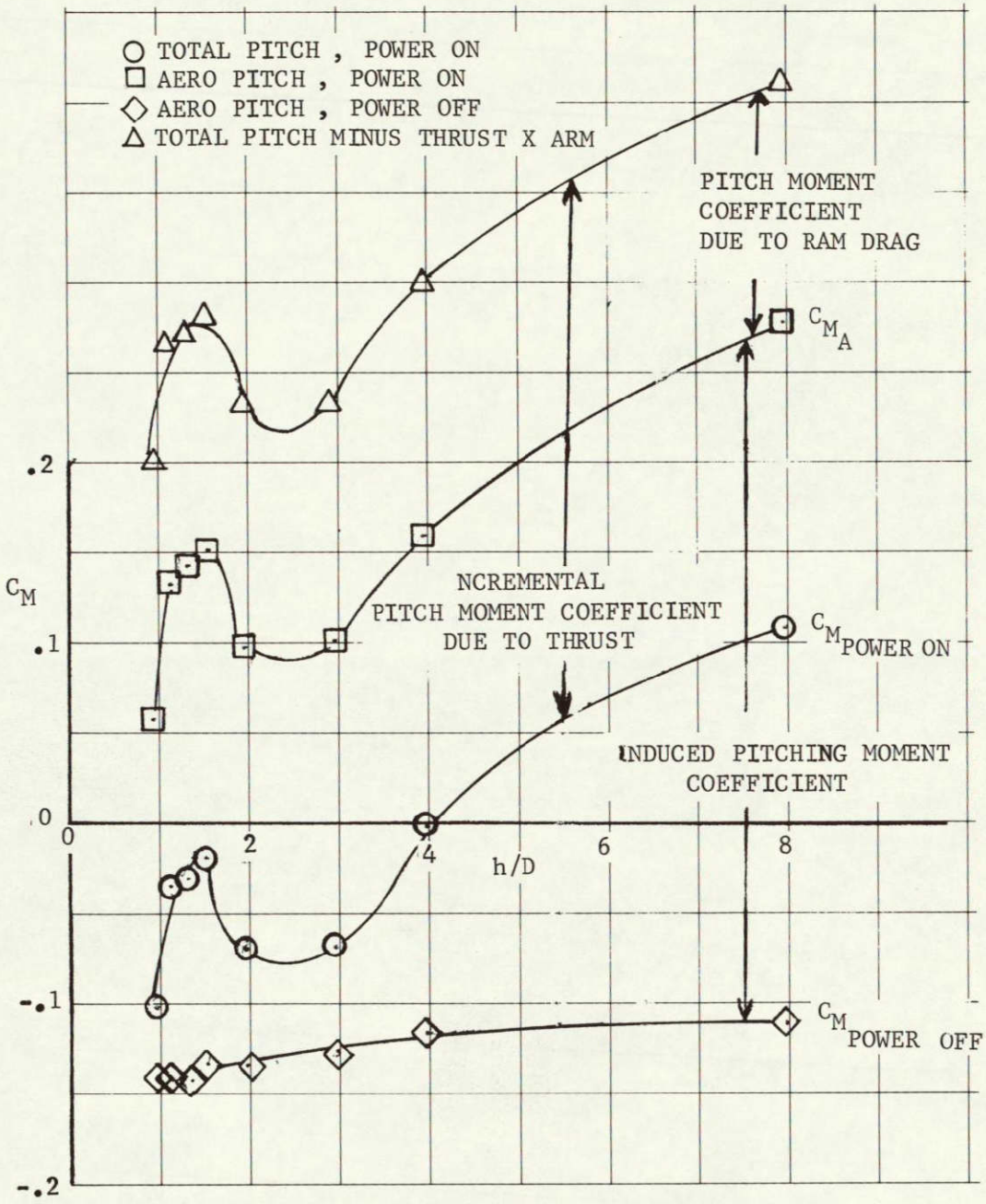

Figure 20. Pitching Moment Coefficient Incremental Buildup Due to Power, $\delta_{N_{Fwd}} = 30^o$, $\delta_{N_{Aft}} = 60^o$, $C_T = 5.1$, $\alpha = 0^o$, $\emptyset = 0^o$, $V/V_j = .12$

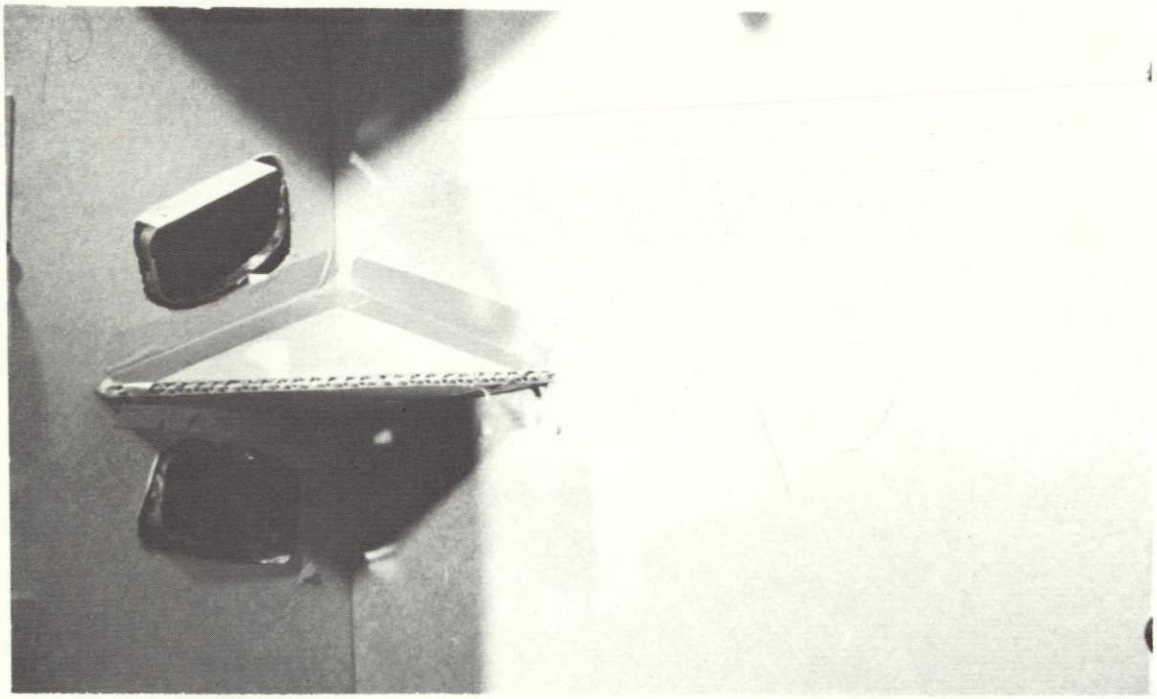

a. Forward Fan in Nacelle

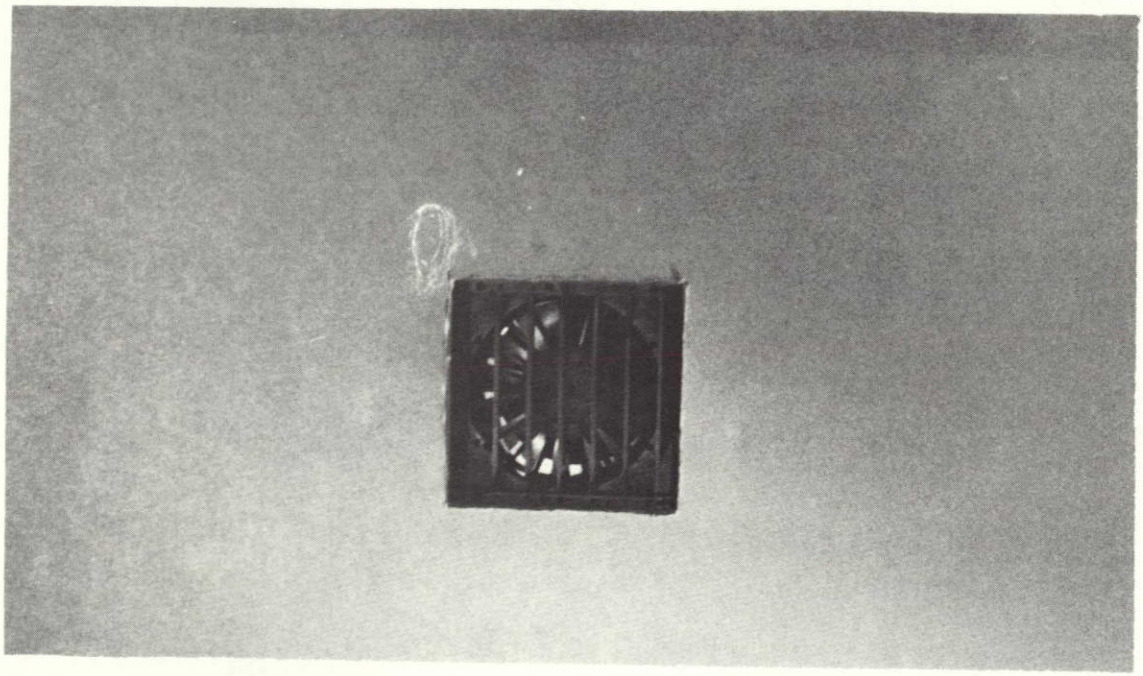

b. Aft Fan in Nacelle or Nose Fan

Figure 21. Fan Exits with Shields

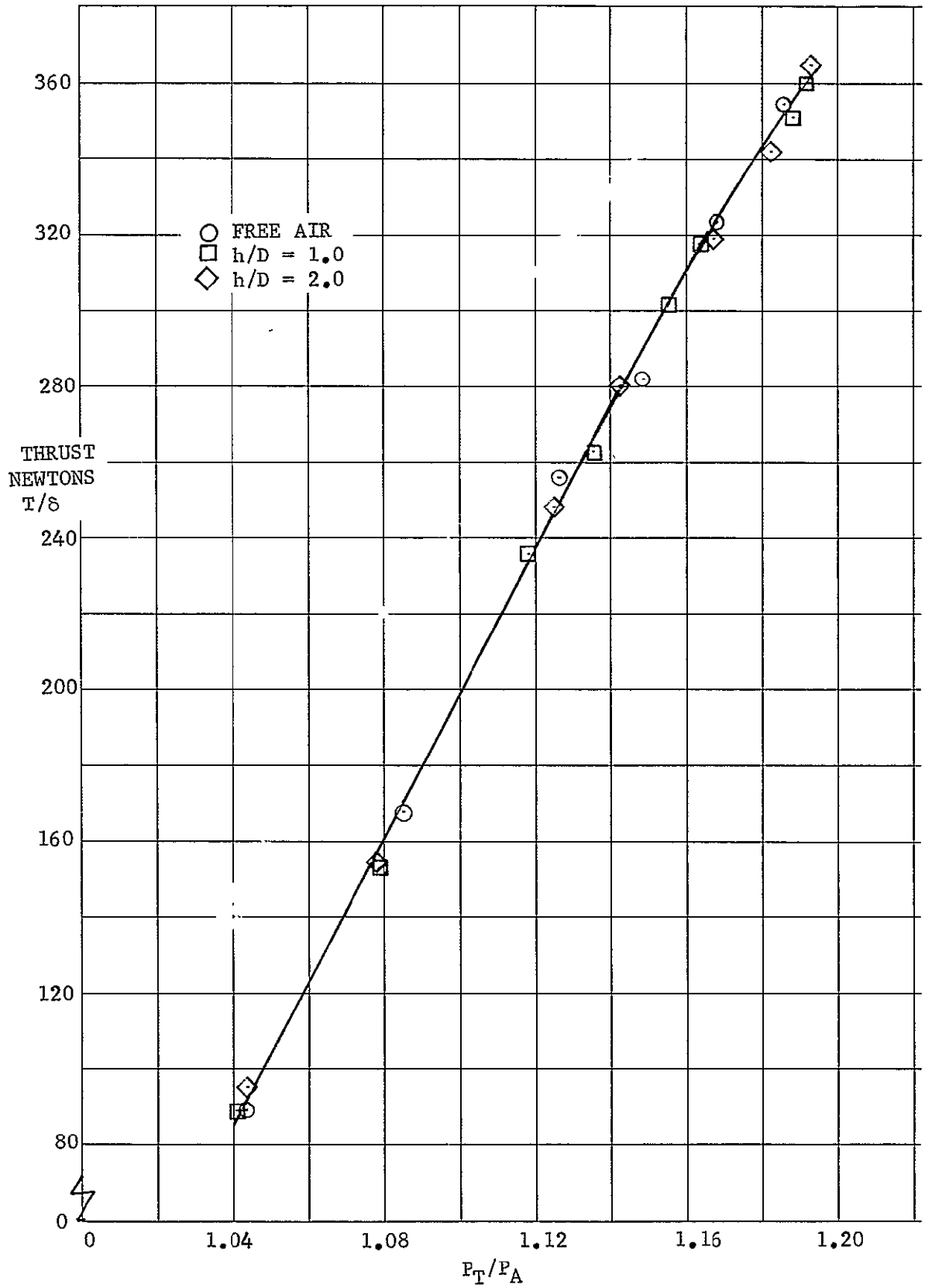

Figure 22. Variation of Thrust with Pressure Ratio at Various Heights, Right Hand Aft Fan #4, $\delta_N = 90^o$

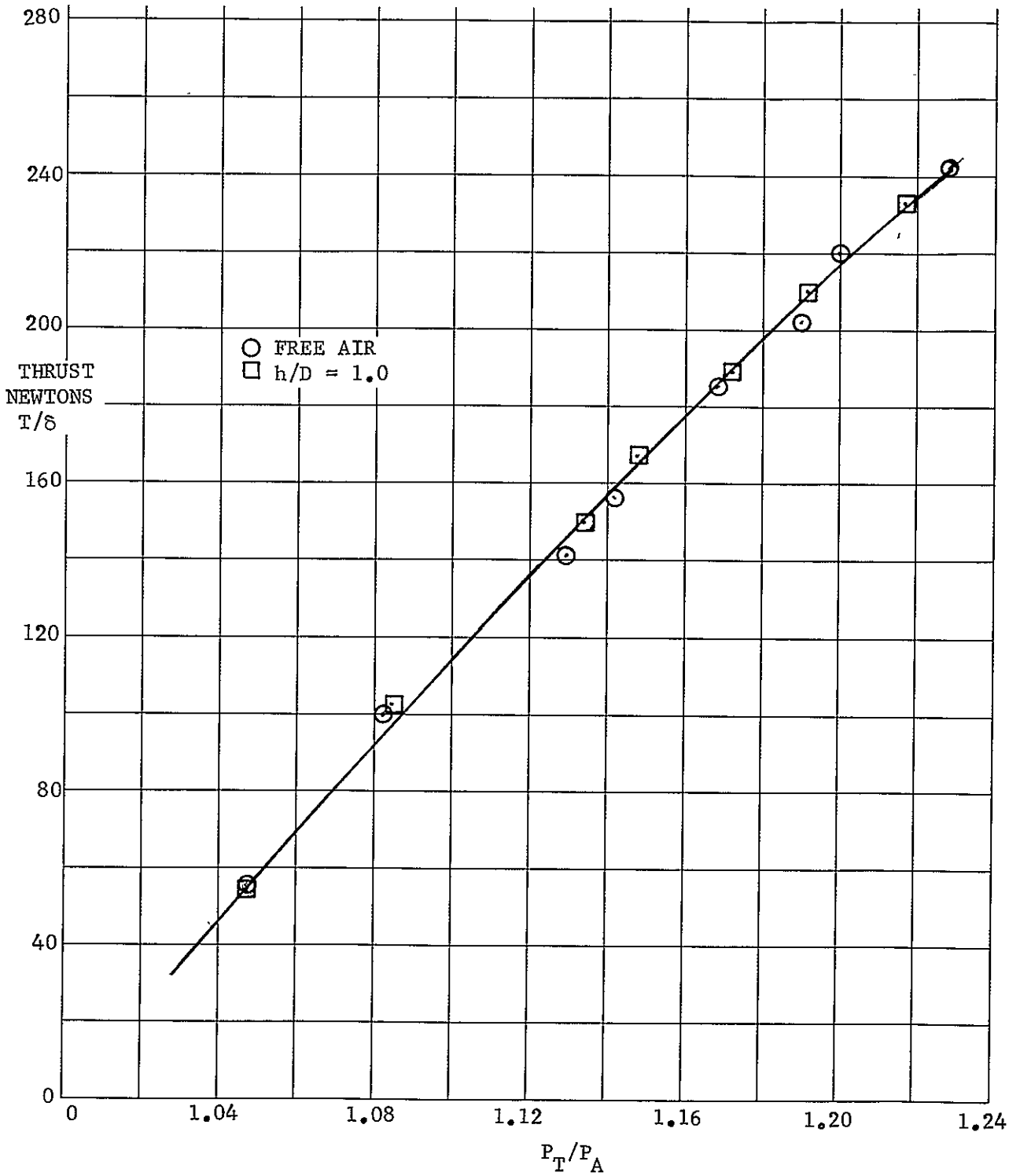

Figure 23. Variation of Thrust with Pressure Ratio at Various Heights, Right Hand Forward Fan #3, $\delta_N = 90^o$

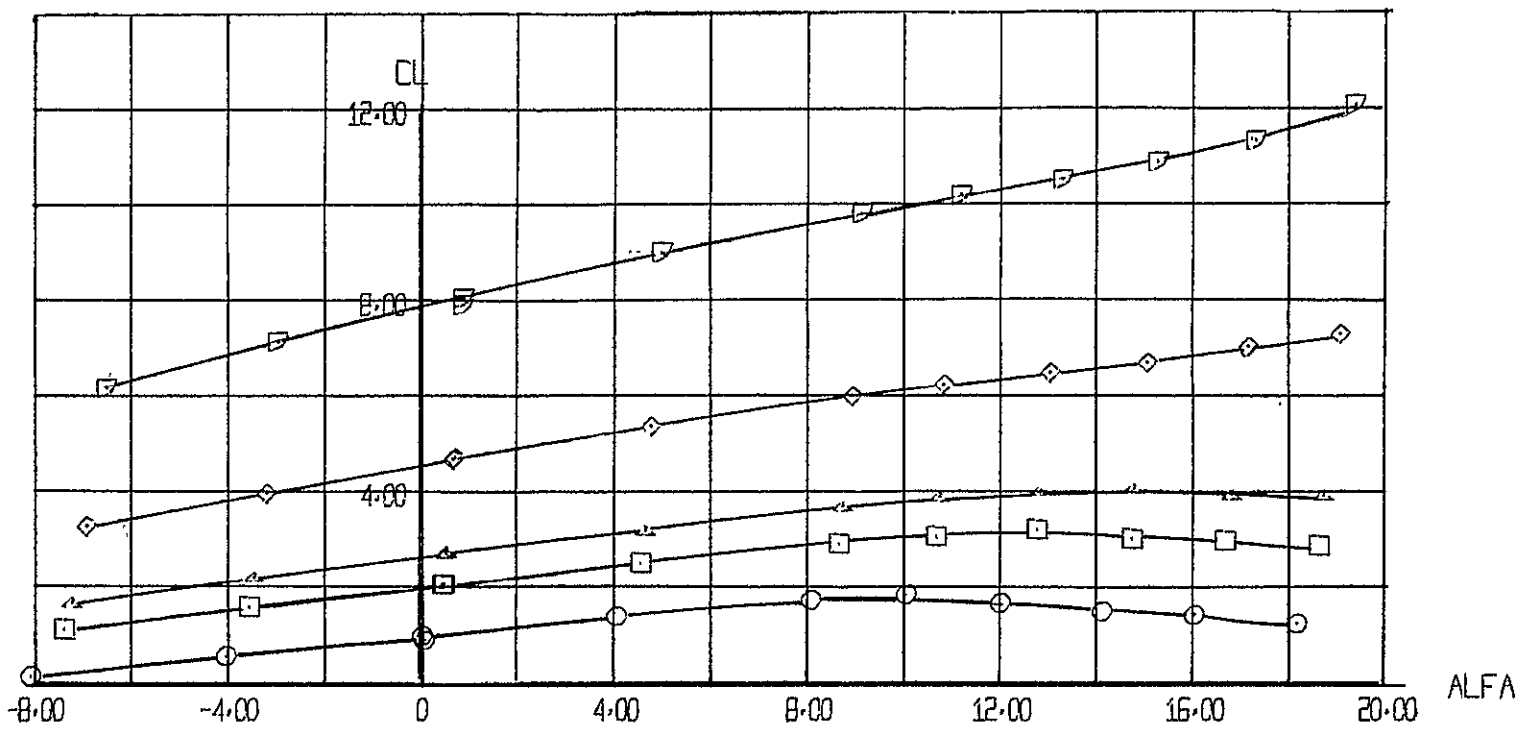

RUN		C_T	V/V_j
24	⊙	0	-
26	□	1.0	.26
22	△	2.0	.19
28	◇	5.0	.12
30	▷	10.1	.08

Figure 24. Effect of Thrust on the Basic Aerodynamic Characteristics, Free Air - $\delta_{N_{Fwd}} = 30^{\circ}$, $\delta_{N_{Aft}} = 60^{\circ}$

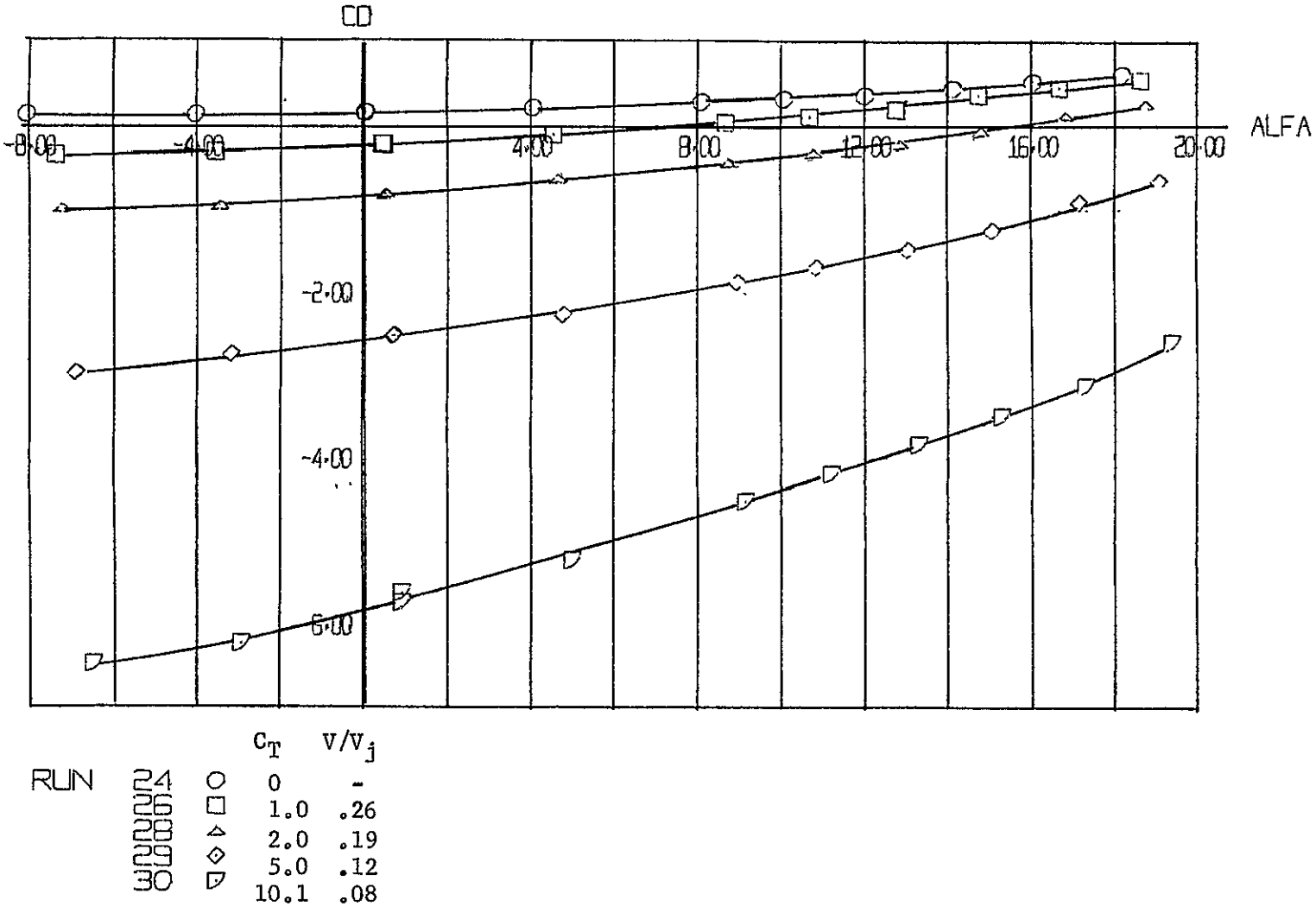

Figure 24. Effect of Thrust on the Basic Aerodynamic Characteristics, Free Air - $\delta_{N_{Fwd}} = 30^{\circ}$, $\delta_{N_{Aft}} = 60^{\circ}$ (Continued)

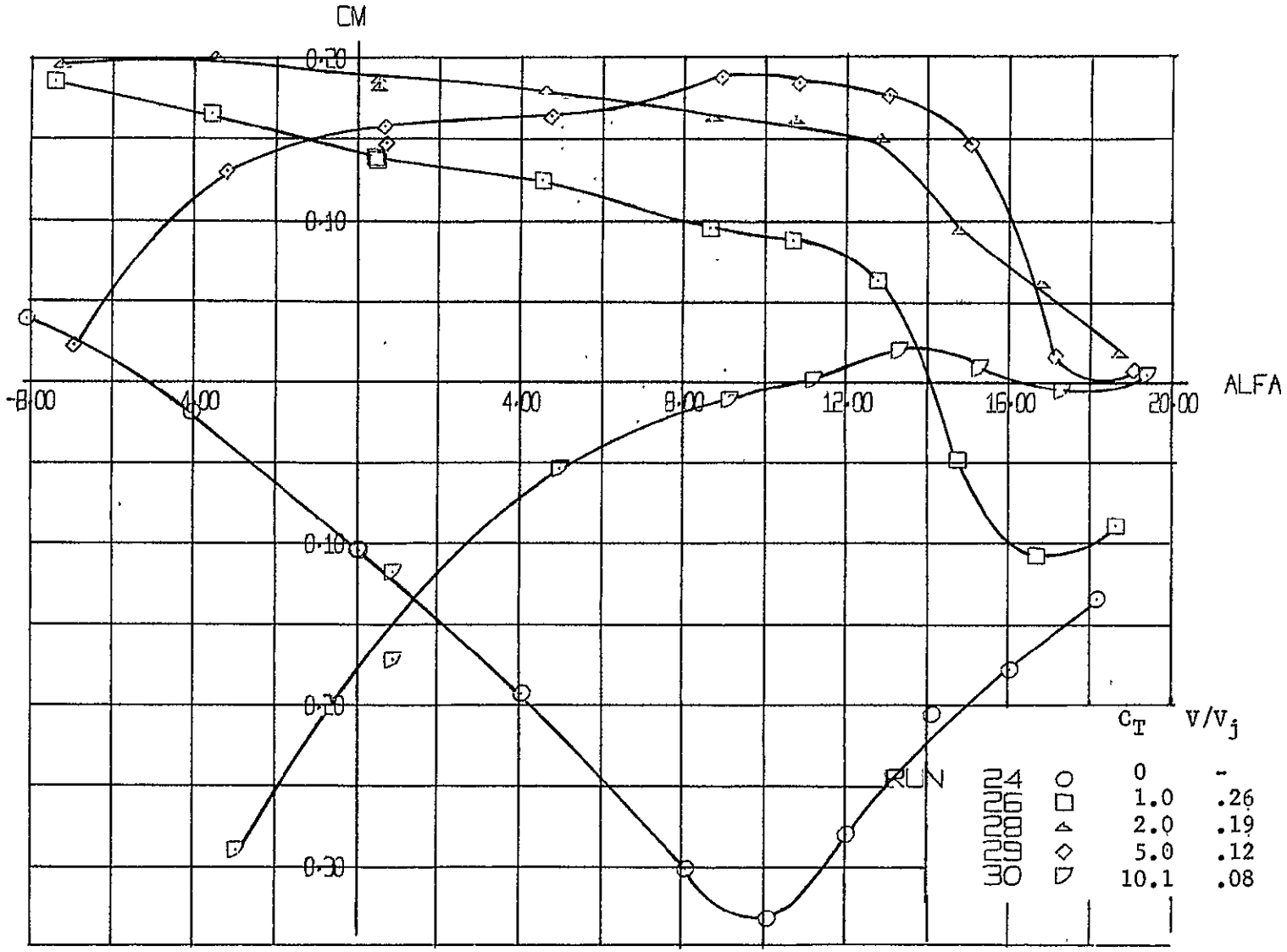

Figure 24. Effect of Thrust on the Basic Aerodynamic Characteristics, Free Air - $\delta_{N_{Fwd}} = 30^{\circ}$, $\delta_{N_{Aft}} = 60^{\circ}$ (Continued)

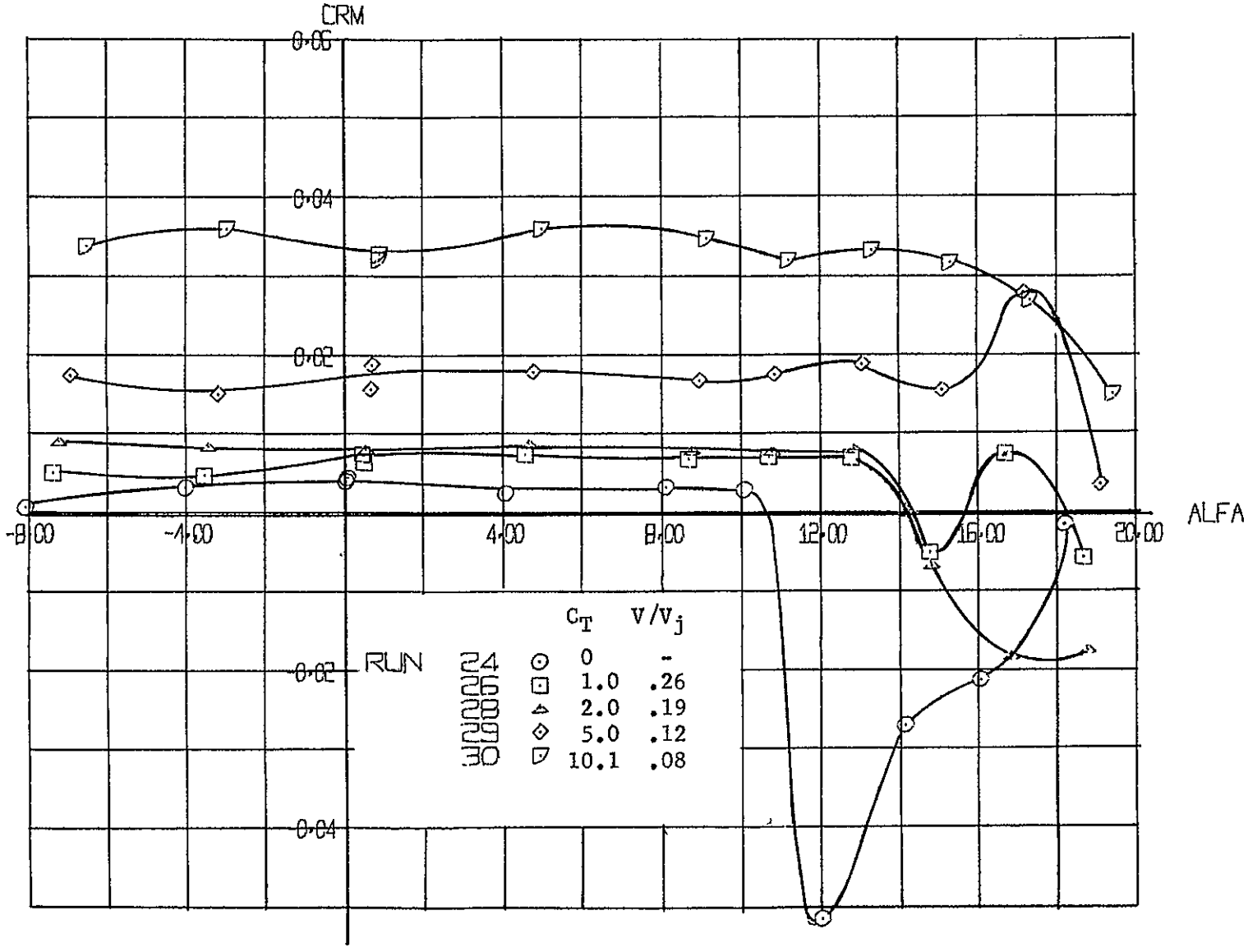

Figure 24. Effect of Thrust on the Basic Aerodynamic Characteristics, Free Air - $\delta_{N_{Fwd}} = 30^\circ$, $\delta_{N_{Aft}} = 60^\circ$ (Concluded)

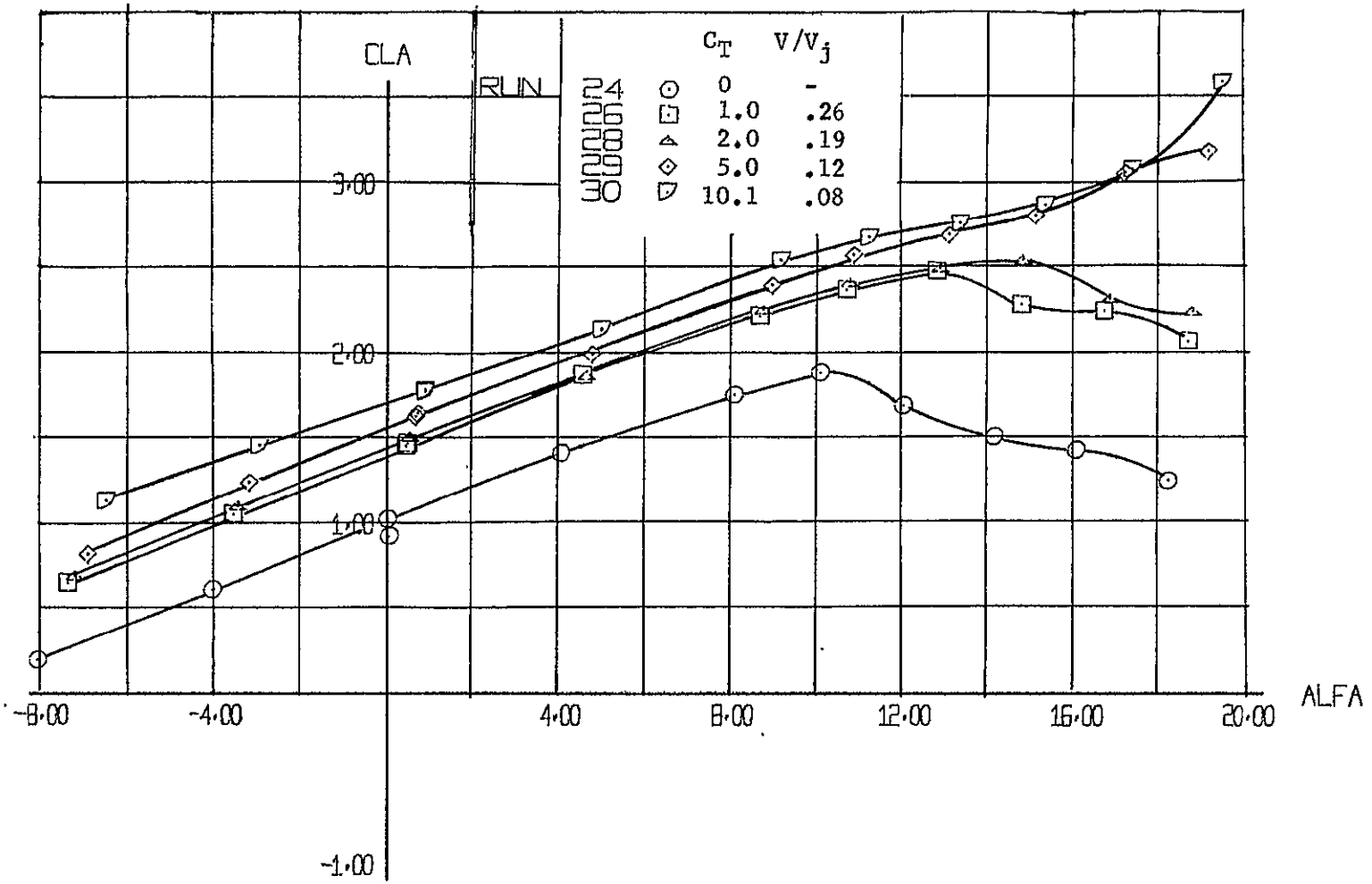

Figure 25. Effect of Thrust on the Aerodynamic Coefficients, Free Air - $\delta_{N_{Fwd}} = 30^{o}$, $\delta_{N_{Aft}} = 60^{o}$

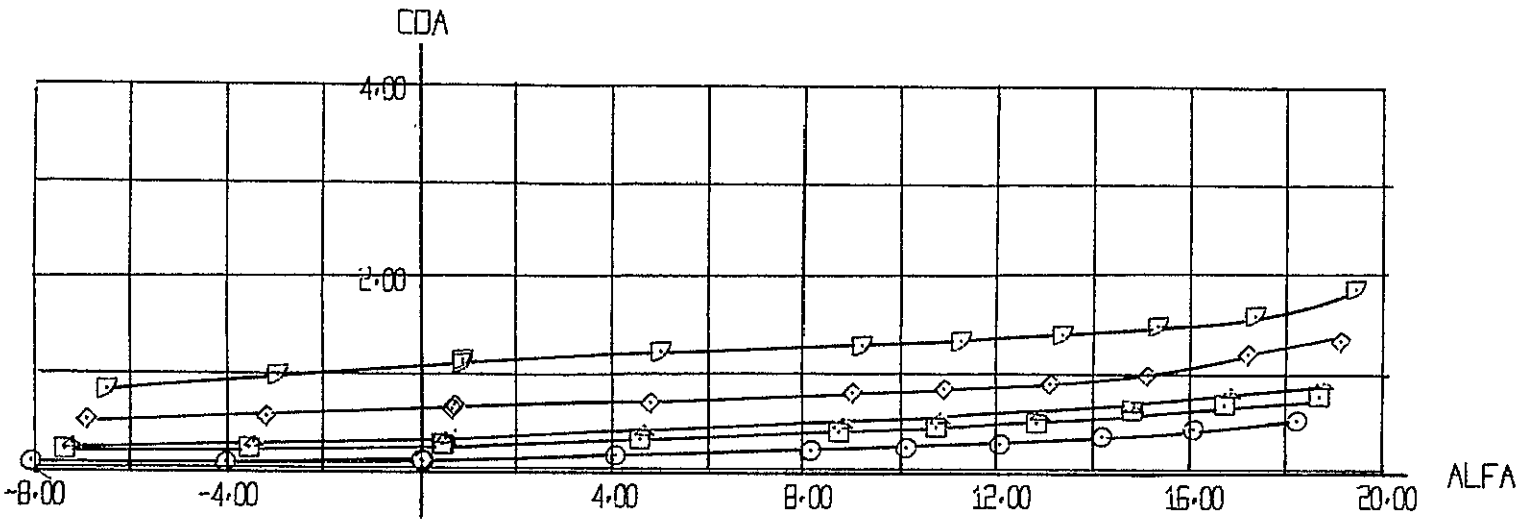

Figure 25. Effect of Thrust on the Aerodynamic Coefficients, Free Air - $\delta_{N_{Fwd}} = 30^{\circ}$, $\delta_{N_{Aft}} = 60^{\circ}$ (Continued)

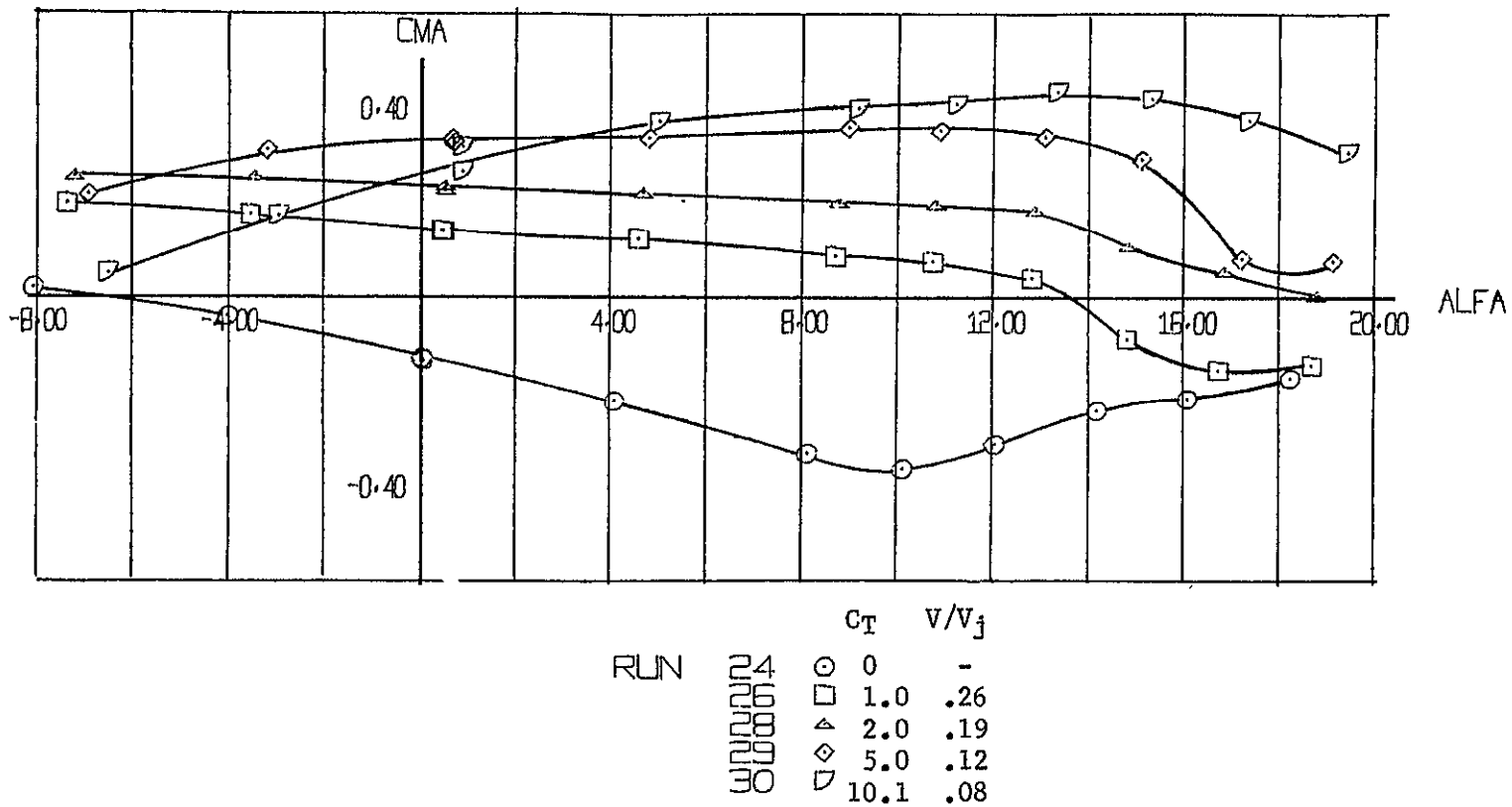

Figure 25. Effect of Thrust on the Aerodynamic Coefficients, Free Air - $\delta_{N_{Fwd}} = 30^{\circ}$, $\delta_{N_{Aft}} = 60^{\circ}$ (Continued)

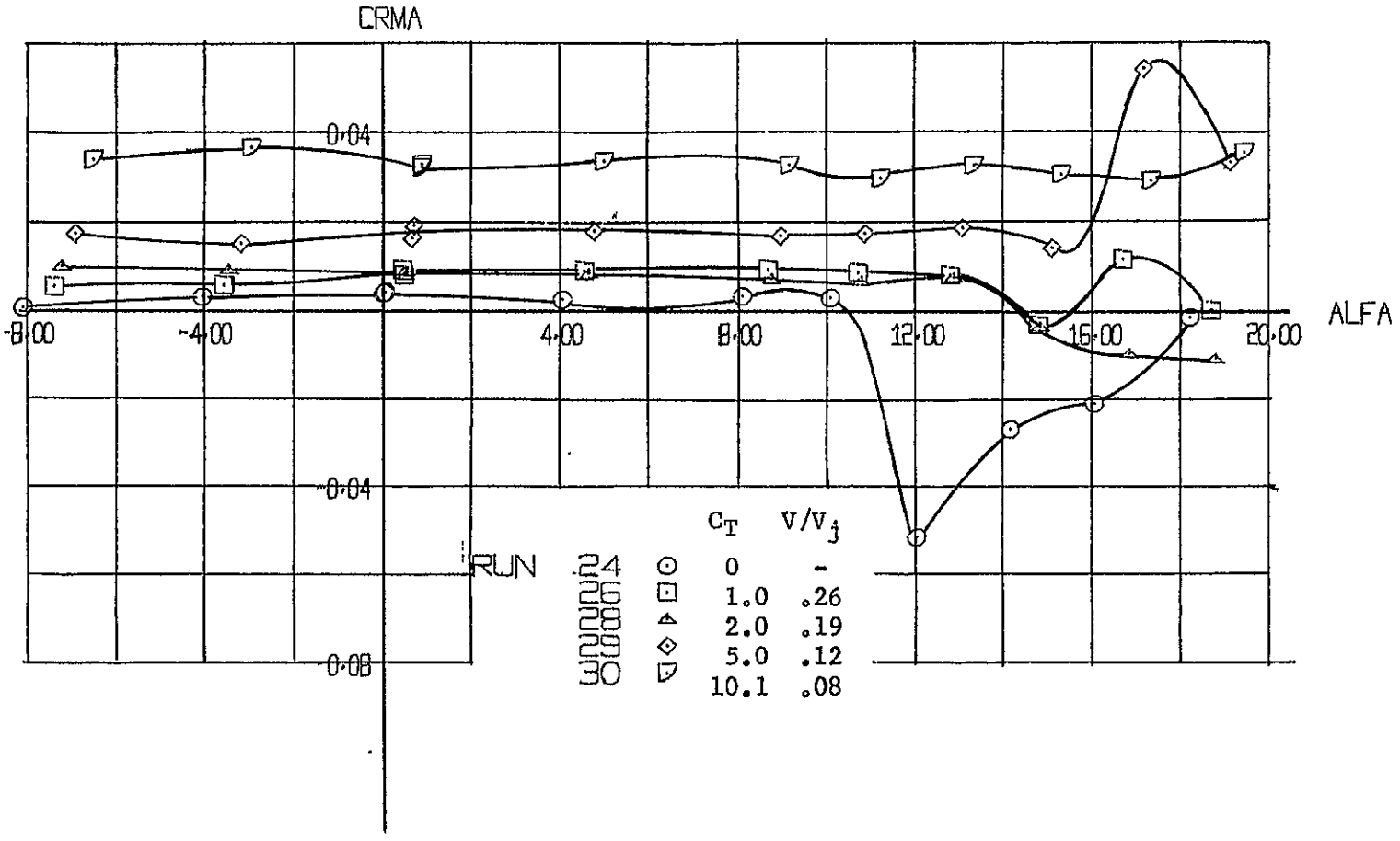

Figure 25. Effect of Thrust on the Aerodynamic Coefficients, Free Air - $\delta_{N_{Fwd}} = 30^{\circ}$, $\delta_{N_{Aft}} = 60^{\circ}$ (Concluded)

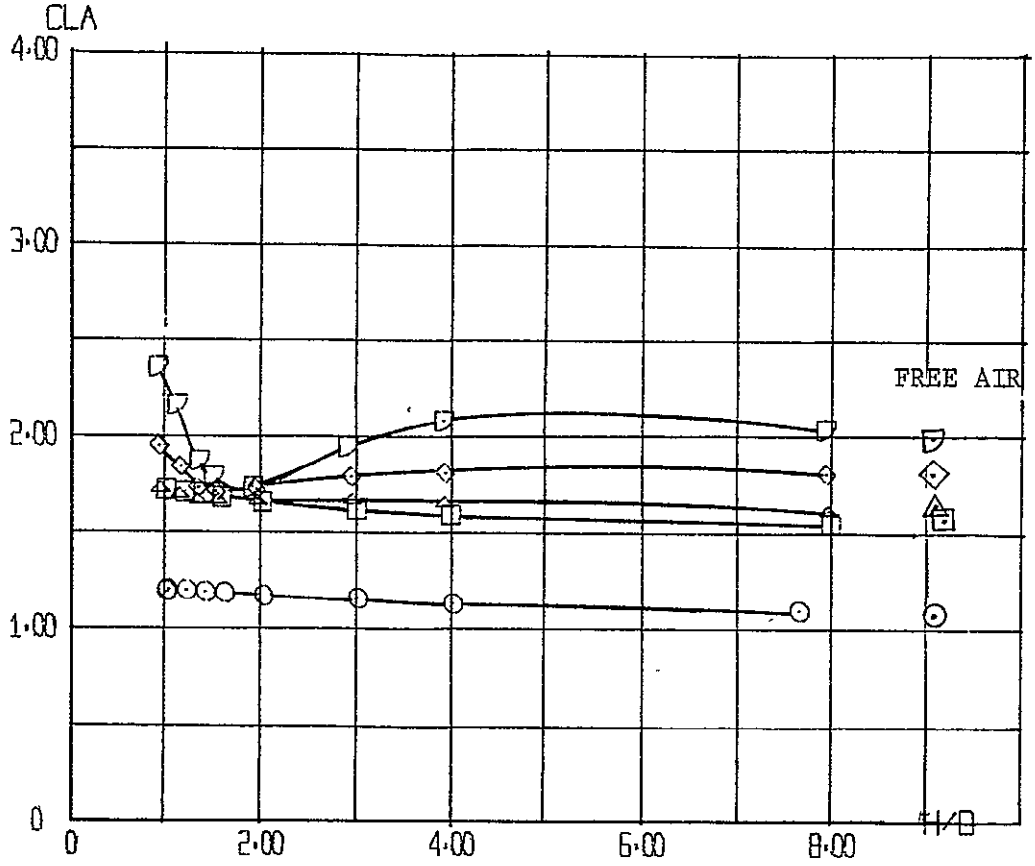

RUN			C_T	V/V_j
	31	○	0	-
	33	⊡	1.1	.26
	36	△	2.1	.19
	37	◇	5.1	.12
	40	▽	10.1	.08

Figure 26. Effect of Height and Velocity Ratio on the Aerodynamic Coefficients, Ground Board Configuration 1, $\delta_{N_{Fwd}} = 30^{\circ}$, $\delta_{N_{Aft}} = 60^{\circ}$, $\alpha = 0$, $\emptyset = 0$

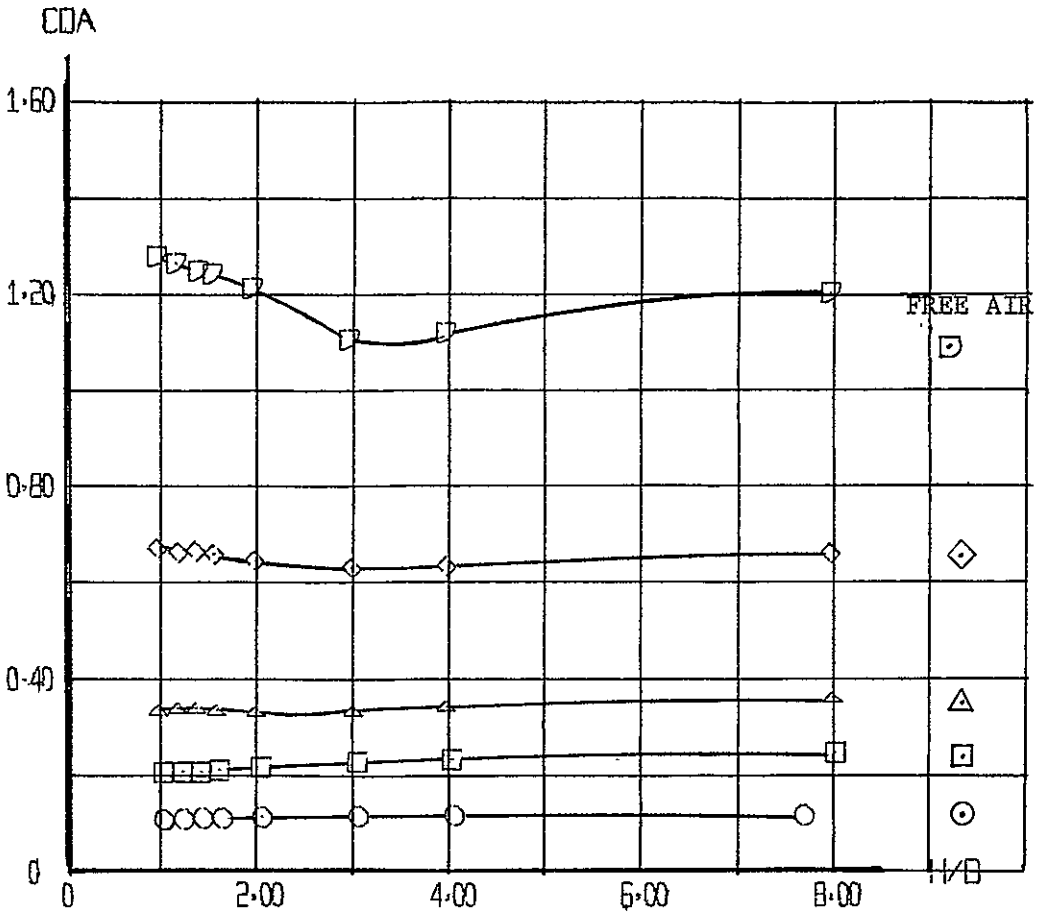

RUN		C_T	V/V_j
33	○	0	-
34	□	1.1	.26
36	△	2.1	.19
37	◇	5.1	.12
40	▽	10.1	.08

Figure 26. Effect of Height and Velocity Ratio on the Aerodynamic Coefficients, Ground Board Configuration 1, $\delta_{N_{Fwd}} = 30^{o}$, $\delta_{N_{Aft}} = 60^{o}$, $\alpha = 0$, $\emptyset = 0$ (Continued)

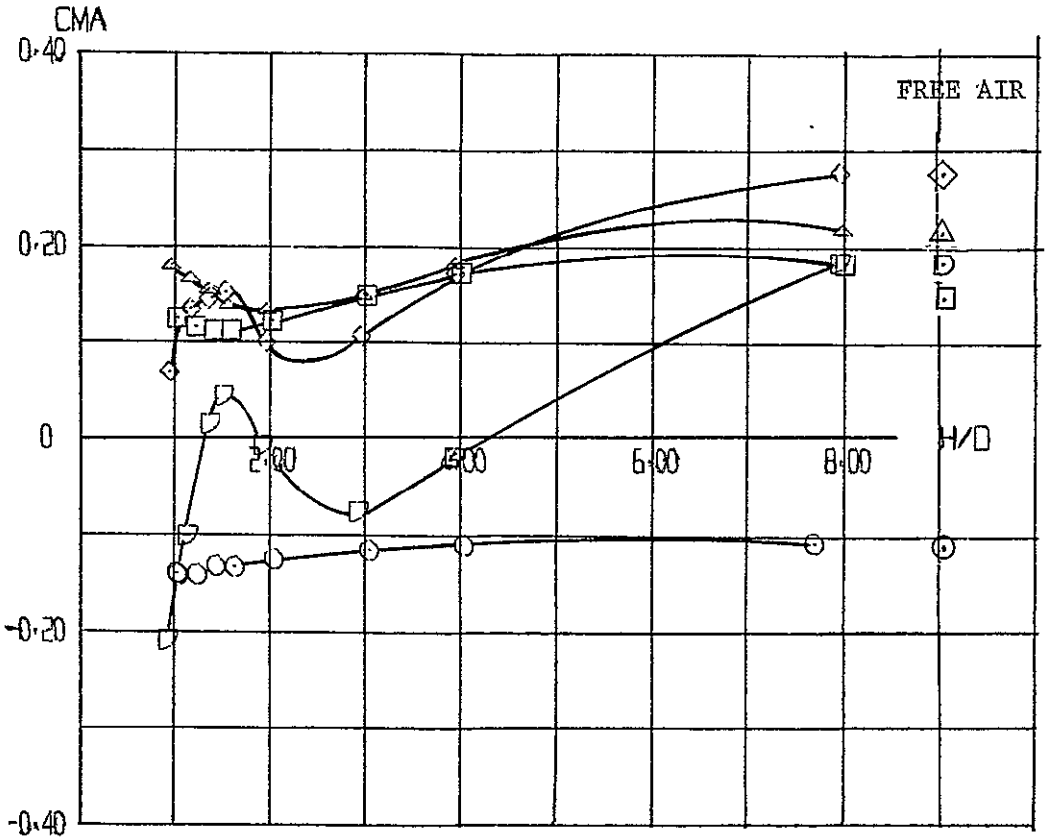

RUN			C_T	V/V_j
	31	○	0	-
	33	□	1.1	.26
	36	△	2.1	.19
	37	◇	5.1	.12
	40	▽	10.1	.08

Figure 26. Effect of Height and Velocity Ratio on the Aerodynamic Coefficients, Ground Board Configuration 1, $\delta_{N_{Fwd}} = 30^{o}$, $\delta_{N_{Aft}} = 60^{o}$, $\alpha = 0$, $\emptyset = 0$ (Continued)

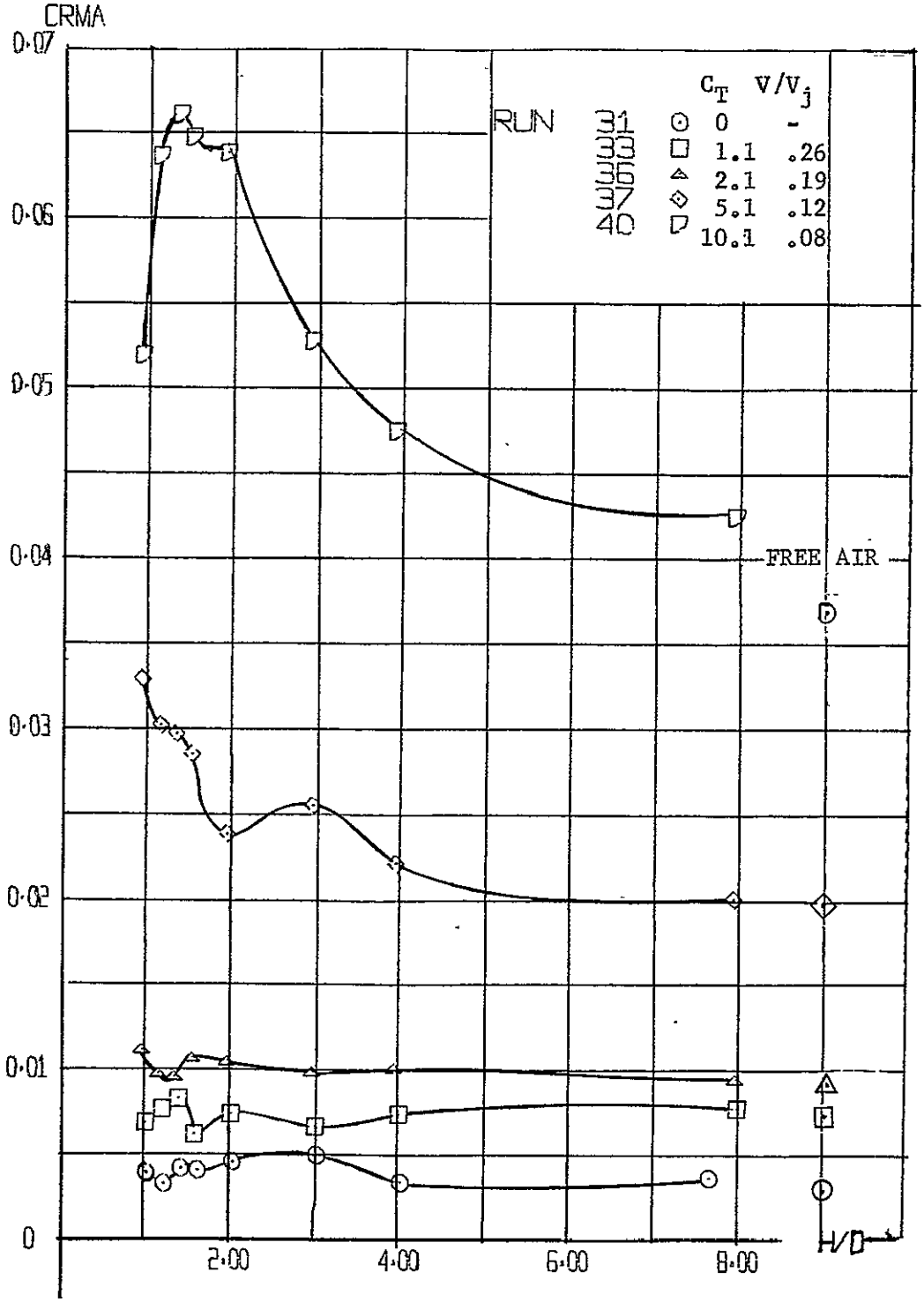

Figure 26. Effect of Height and Velocity Ratio on the Aerodynamic Coefficients, Ground Board Configuration 1, $\delta_{N_{Fwd}} = 30^{o}$, $\delta_{N_{Aft}} = 60^{o}$, $\alpha = 0$, $\emptyset = 0$ (Concluded)

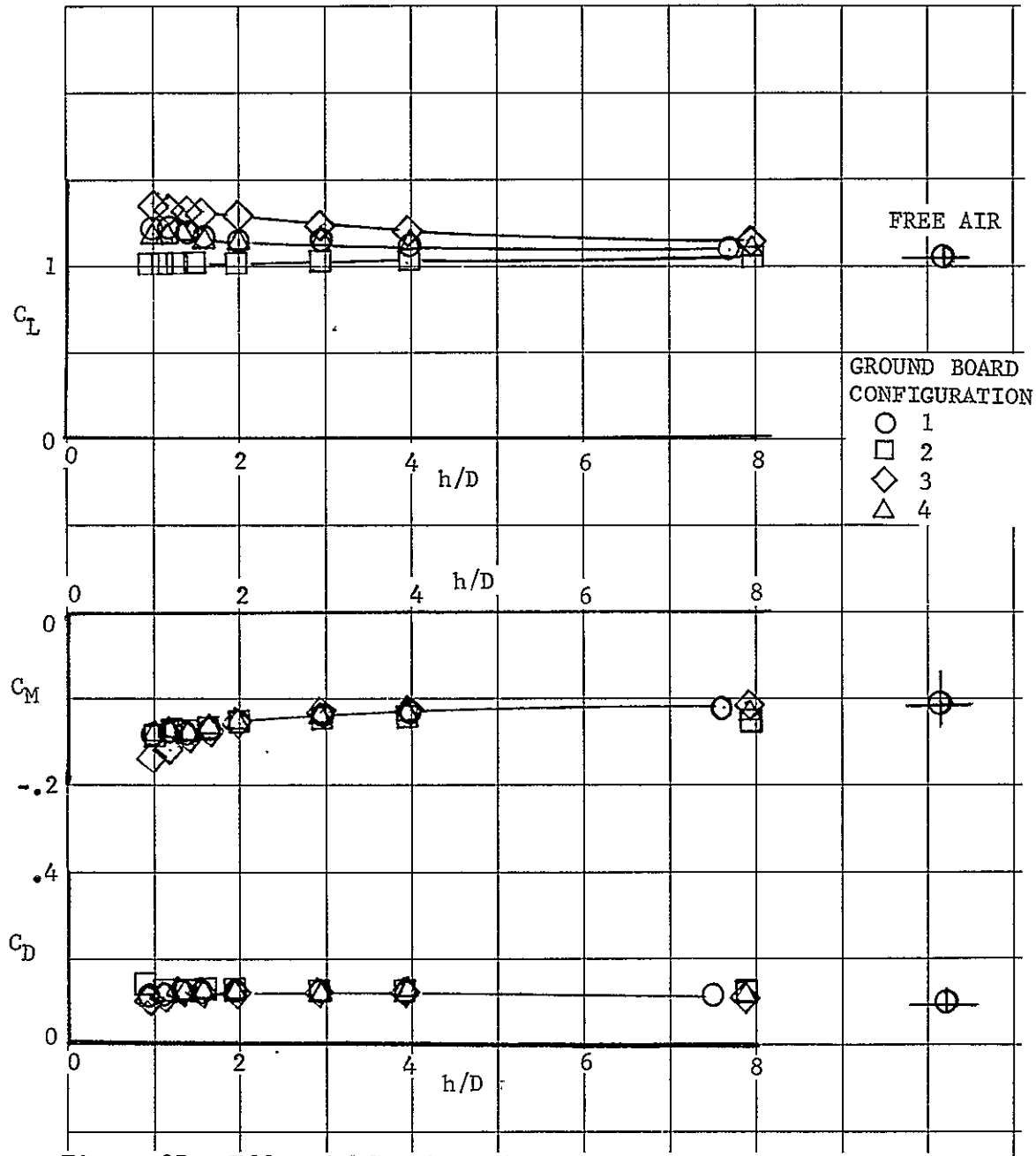

Figure 27. Effect of Height and Ground Board Configuration on Longitudinal Characteristics - Power off, $\alpha = 0^{\circ}$, $\emptyset = 0^{\circ}$

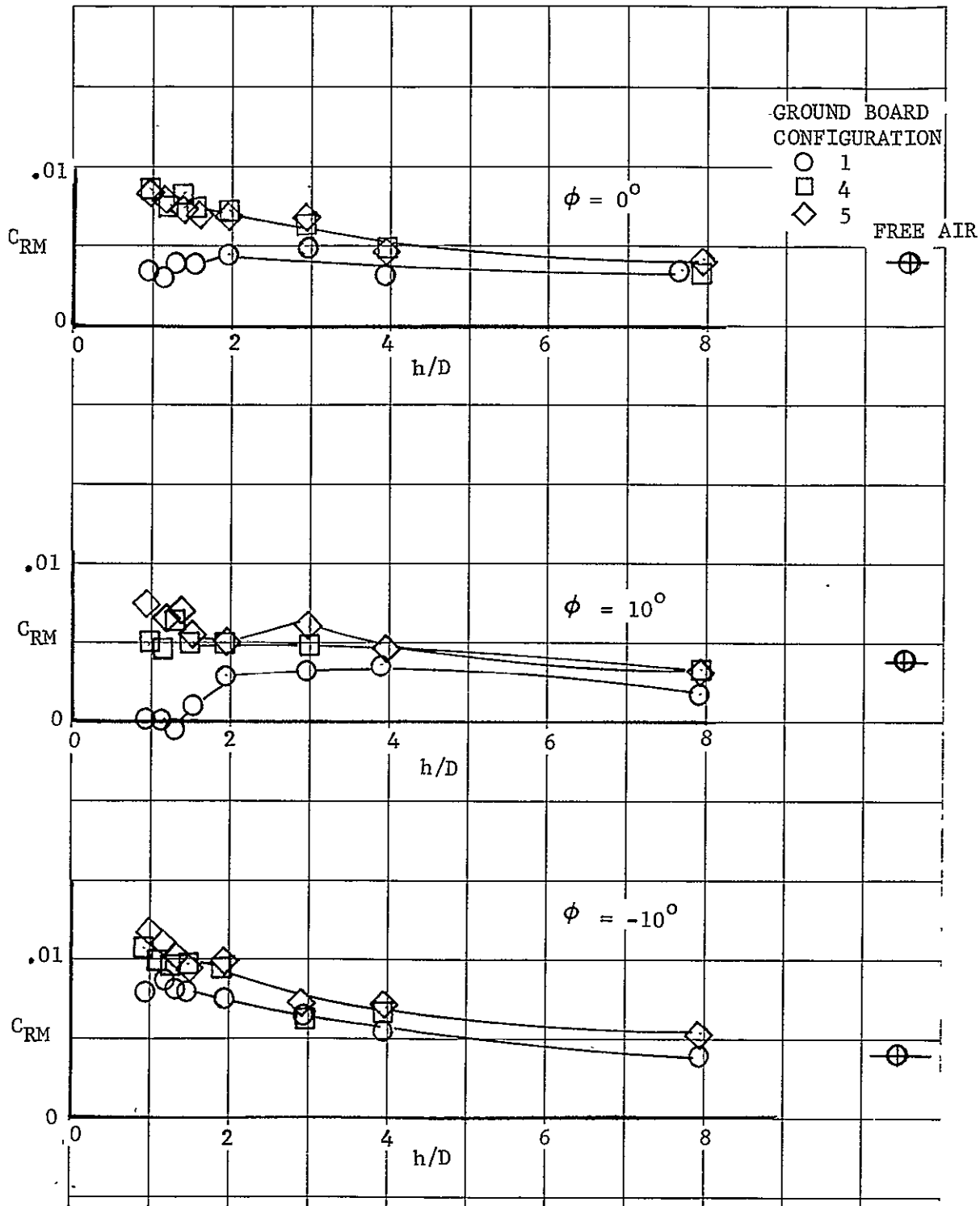

Figure 28. Effect of Height and Ground Board Configuration on Rolling Moment Coefficient - Power off, $\alpha = 0^{\circ}$

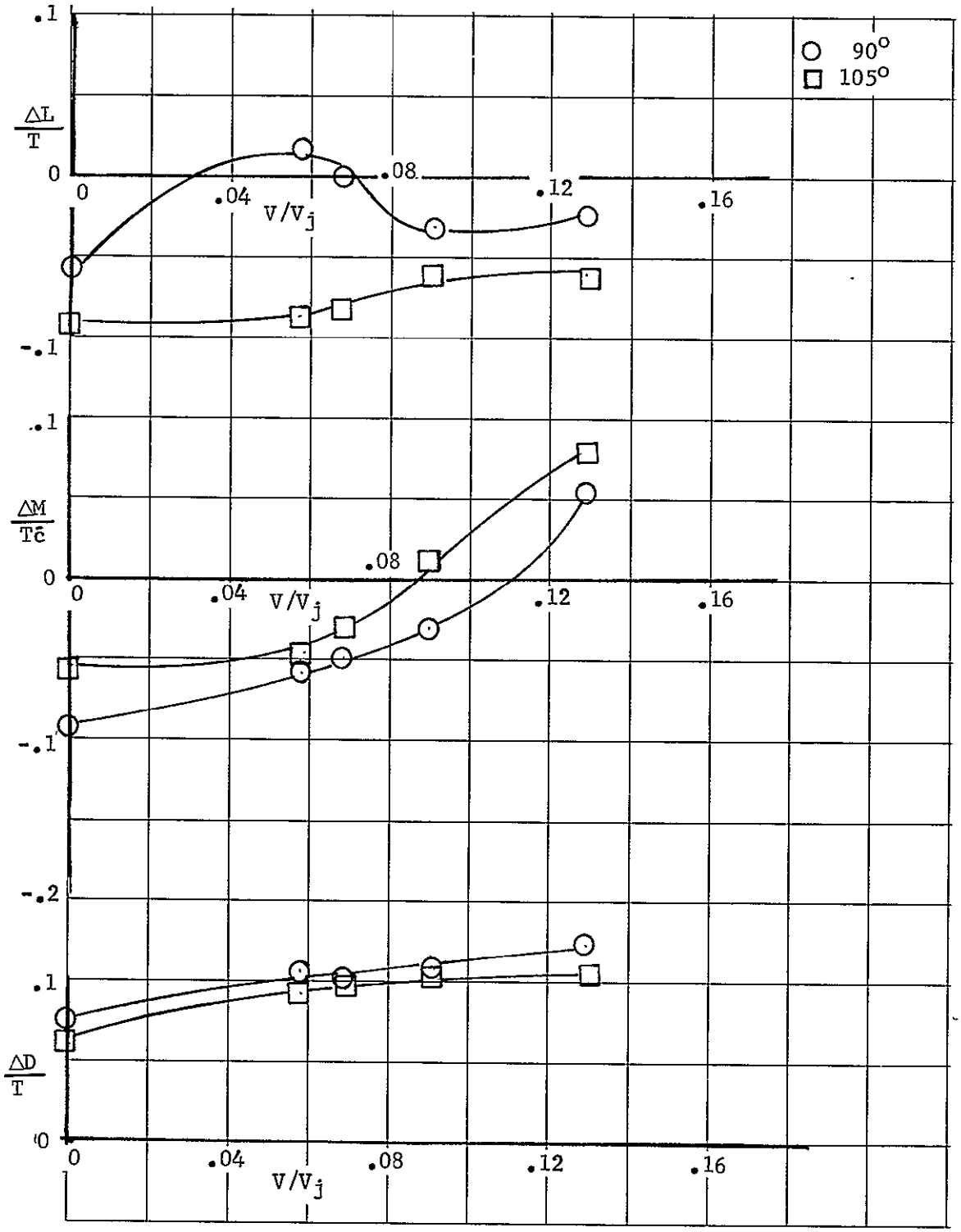

Figure 29. Effect of Velocity Ratio on the Thrust Induced Longitudinal Characteristics - Free Air, $\alpha = 0^{\circ}$, $\phi = 0^{\circ}$

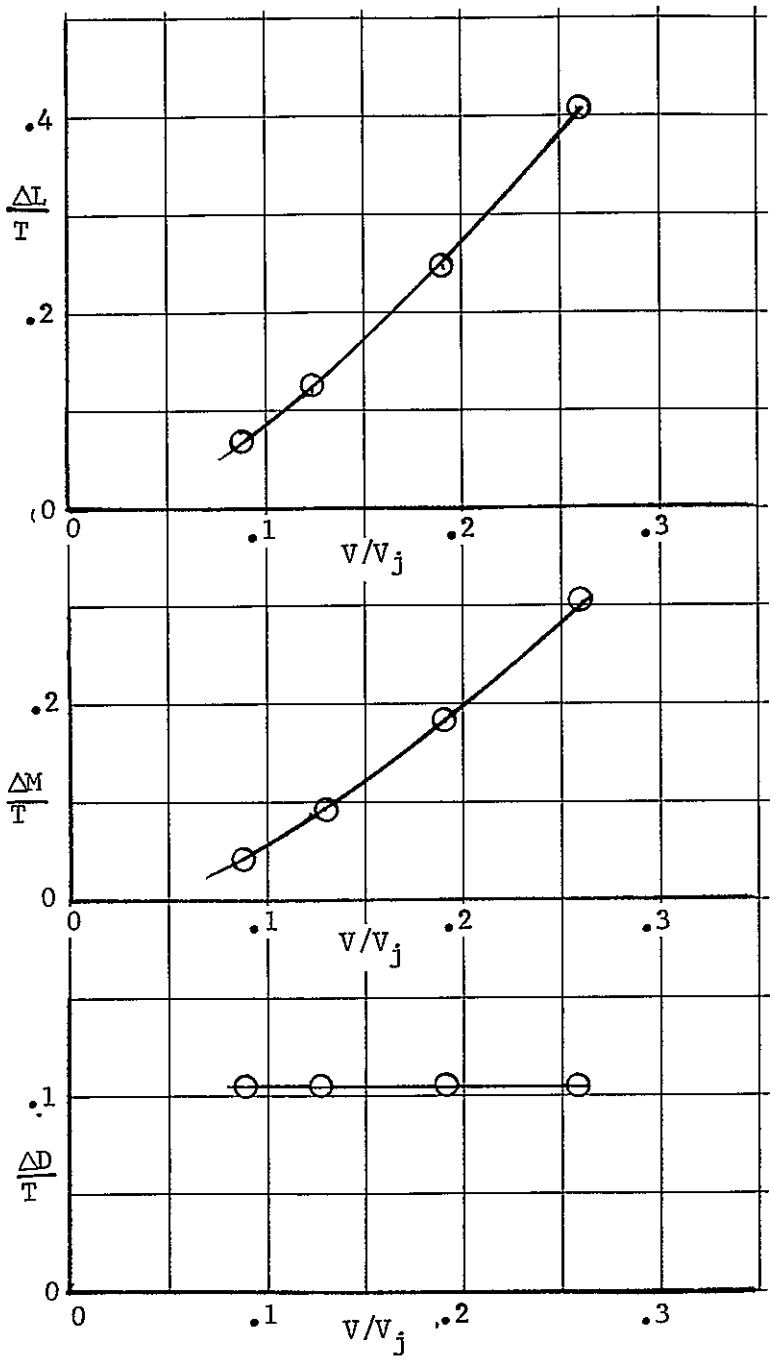

Figure 30. Effect of Velocity Ratio on the Thrust Induced Longitudinal Characteristics in Free Air - $\delta_{N_{Fwd}} = 30^{o}$, $\delta_{N_{Aft}} = 60^{o}$, $\alpha = 0^{o}$, $\emptyset = 0^{o}$,

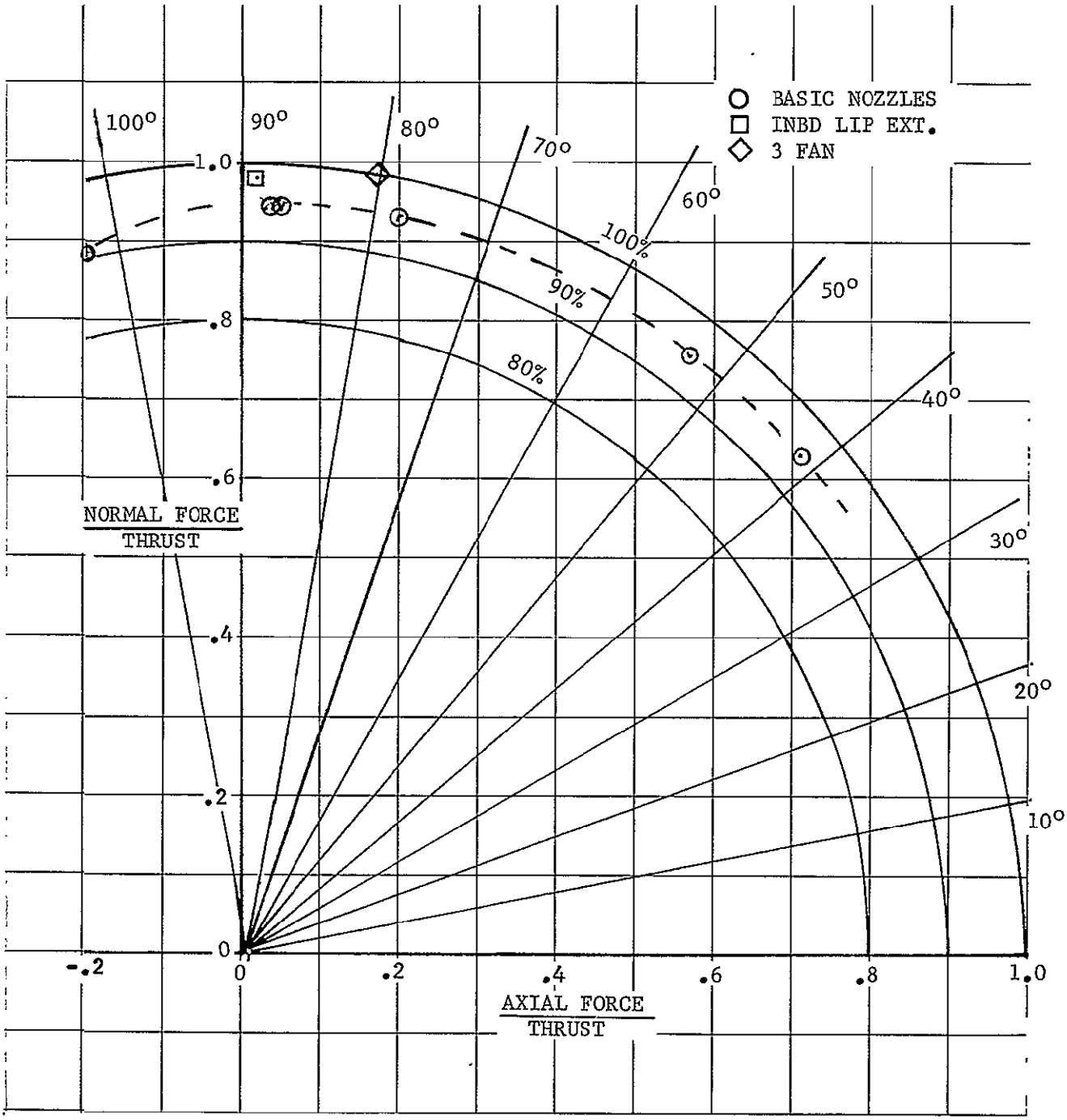

Figure 31. Normal Force vs Axial Force - Free Air $V/V_j = 0$, $\alpha = 0^o$, $\phi = 0^o$

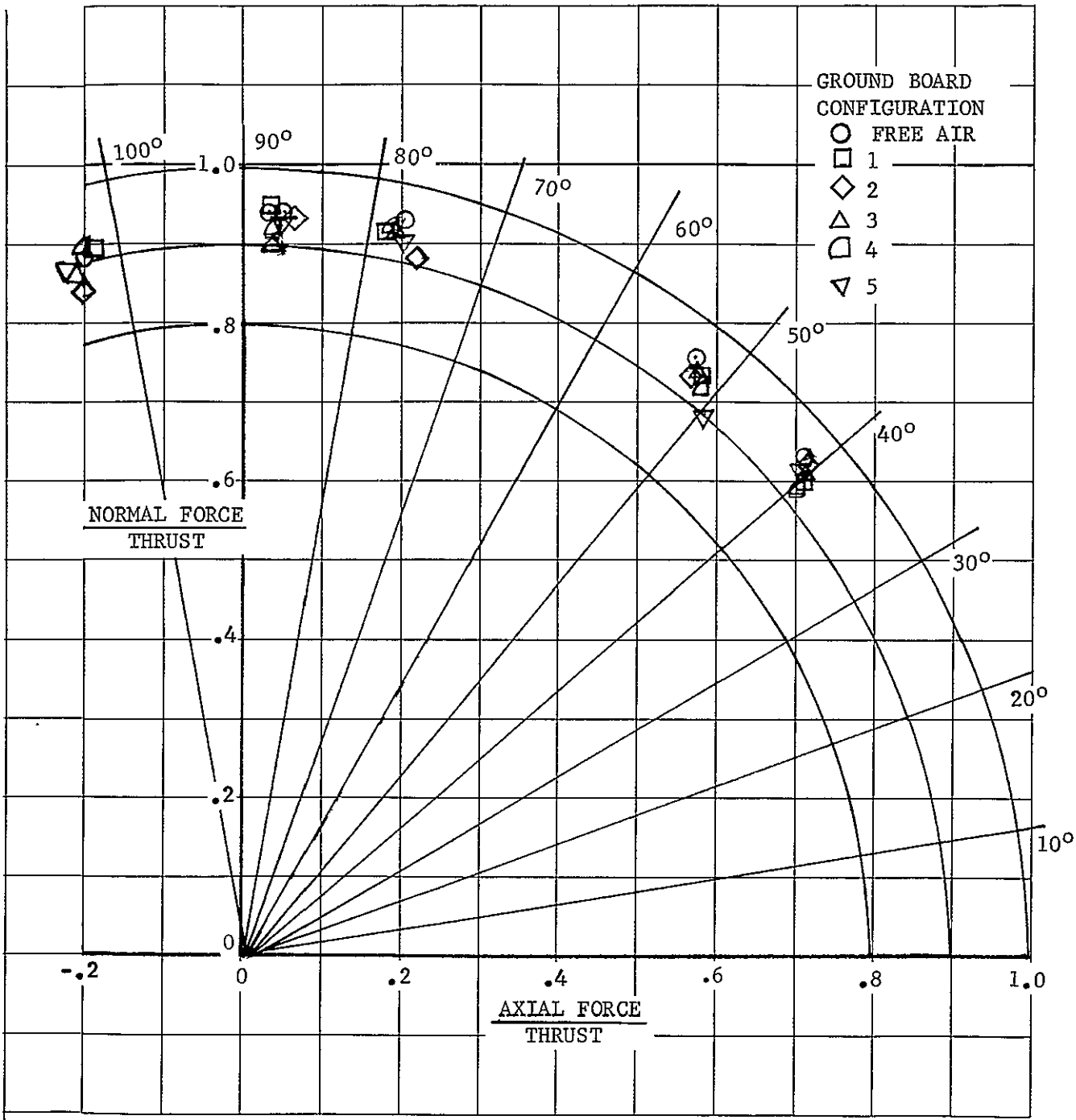

Figure 32. Normal Force vs Axial Force - Ground Board in $V/V_j = 0$, $\alpha = 0^\circ$, $\emptyset = 0^\circ$, $h/D = 4$

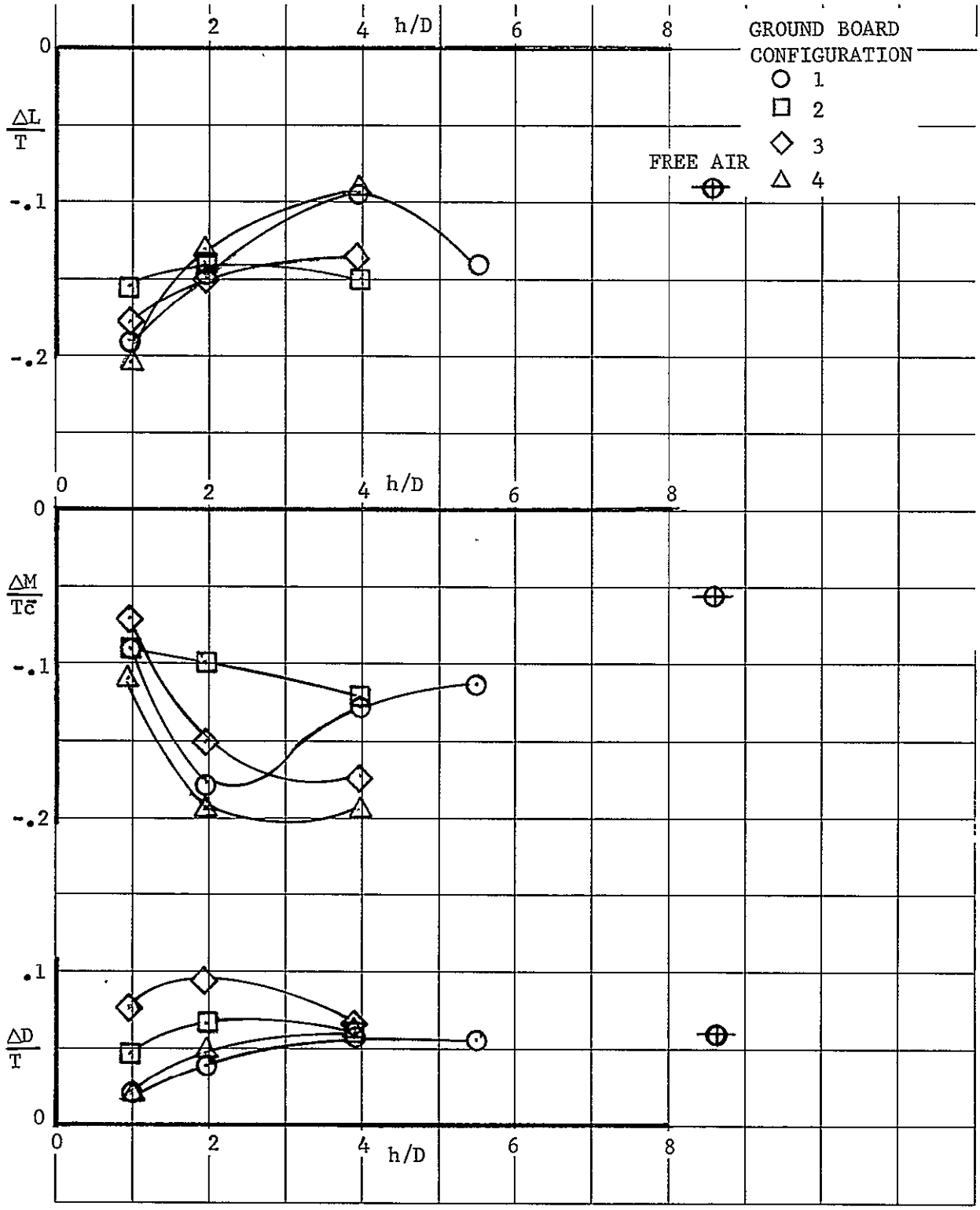

Figure 33. Effect of Height on the Thrust Induced Characteristics with Various Ground Board Configurations - $\delta_N = 105^o$, $V/V_j = 0$, $\alpha = 0^o$, $\phi = 0^o$

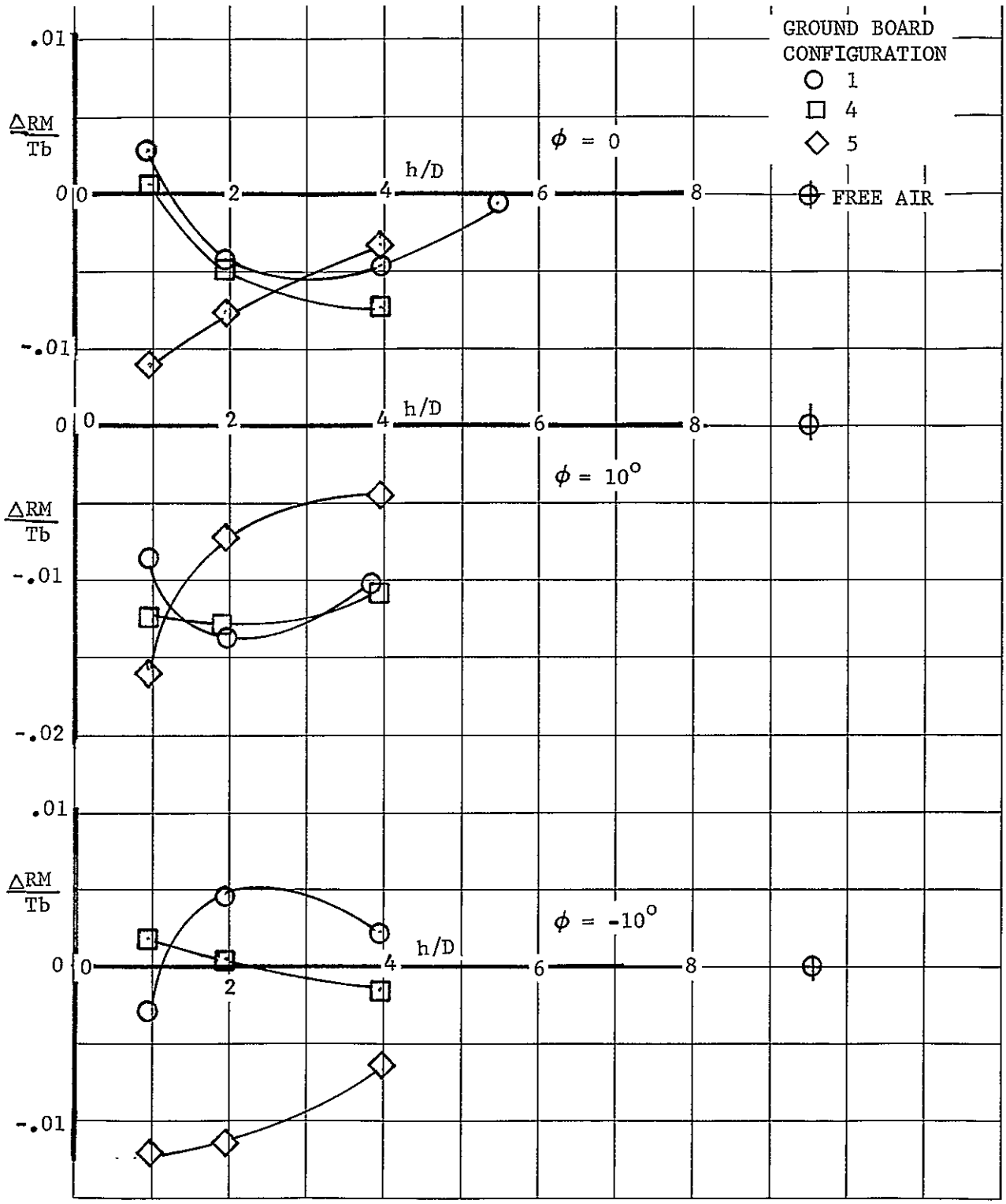

Figure 34. Effect of Height on the Thrust Induced Rolling Moment with Various Ground Board Configurations - $\delta_N = 105^\circ$, $V/V_j = 0$, $\alpha = 0^\circ$, $\emptyset = 0^\circ$

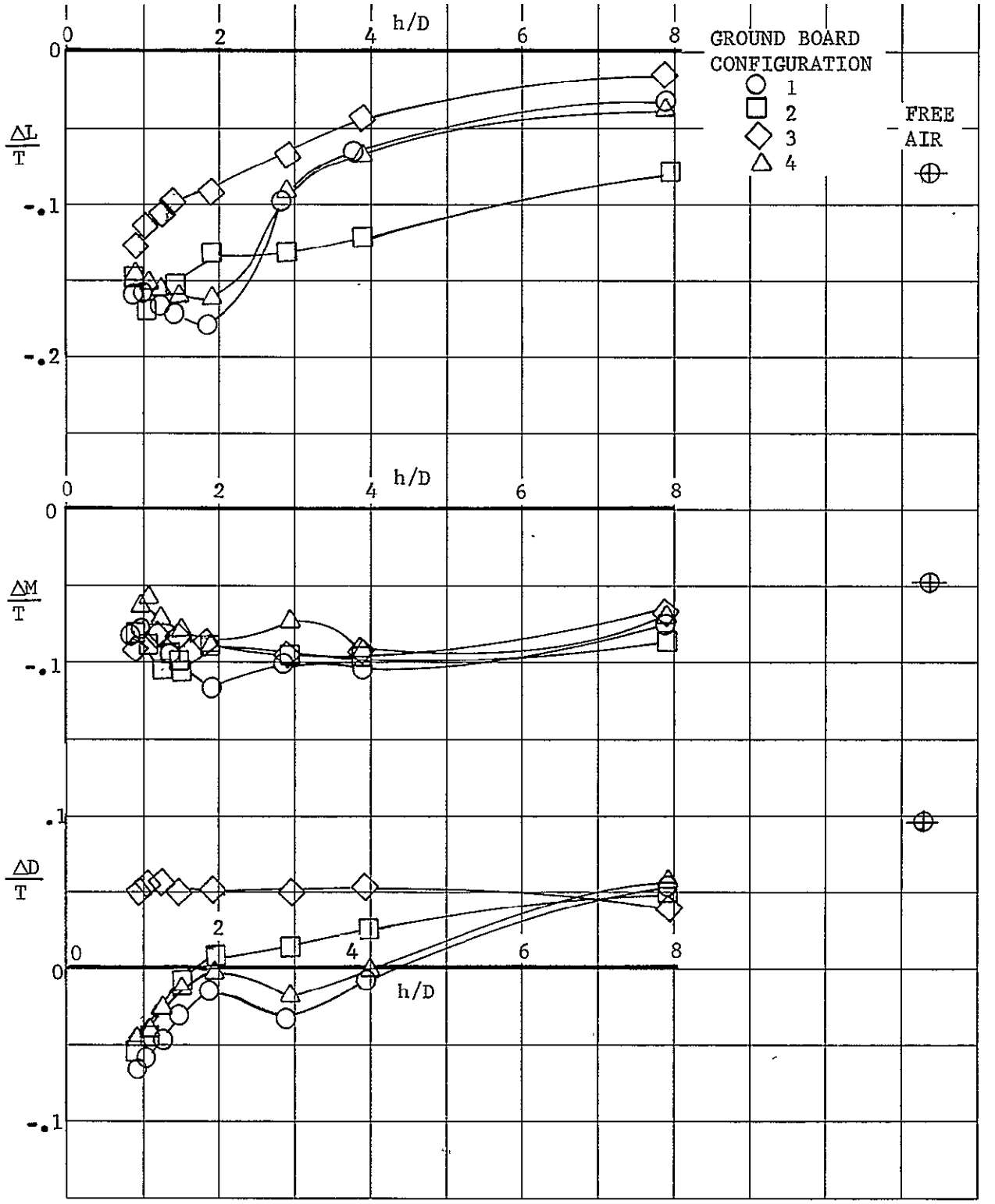

Figure 35. Effect of Height on the Thrust Induced Longitudinal Characteristics with Various Ground Board Configurations - $\delta_N = 105^o$, $V/V_j = 0.058$, $\alpha = 0^o, \emptyset = 0^o$

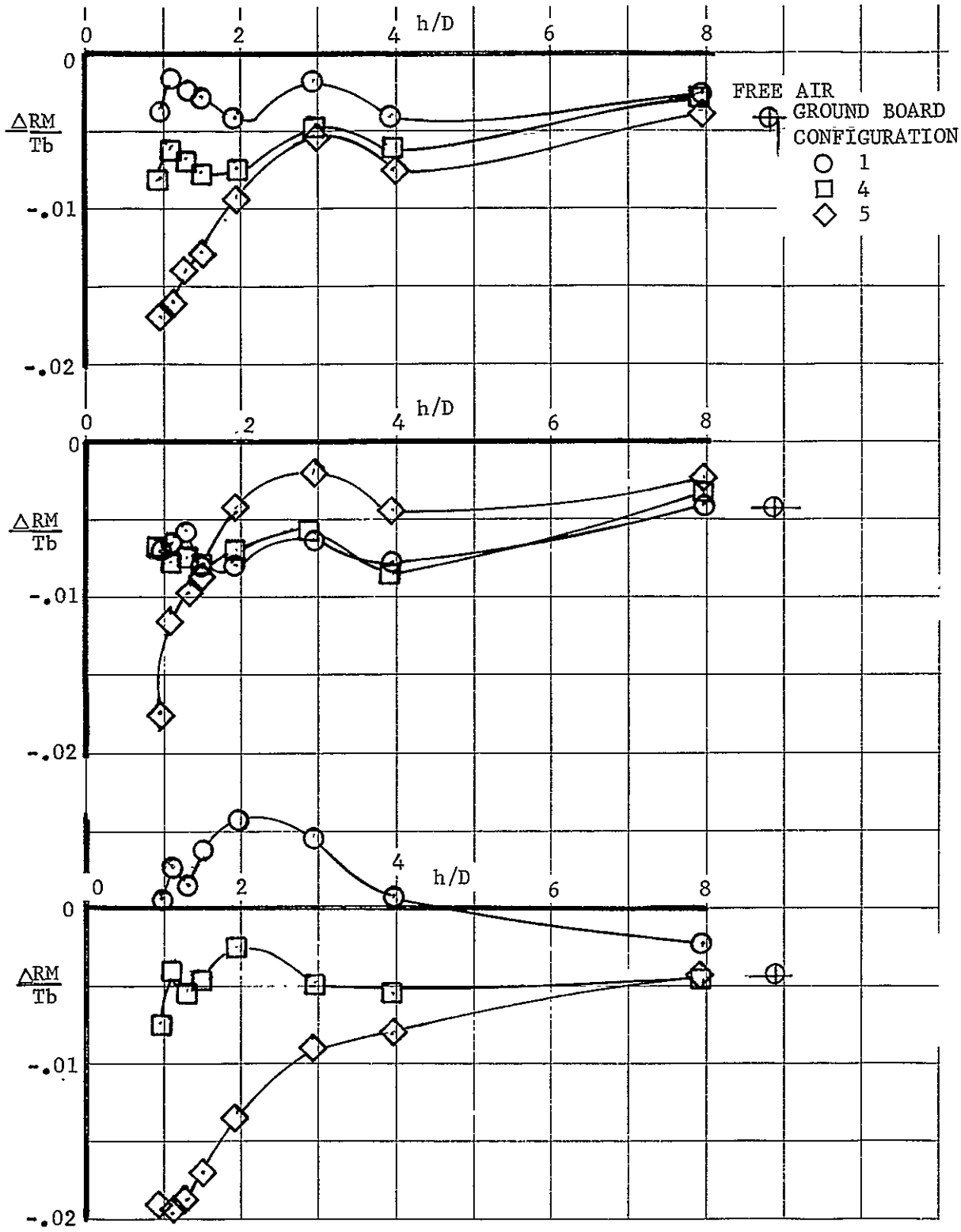

Figure 36. Effect of Height on the Thrust Induced Rolling Moment with Various Ground Board Configurations - $\delta_N = 105^o$, $V/V_j = .058$, $\alpha = 0^o$

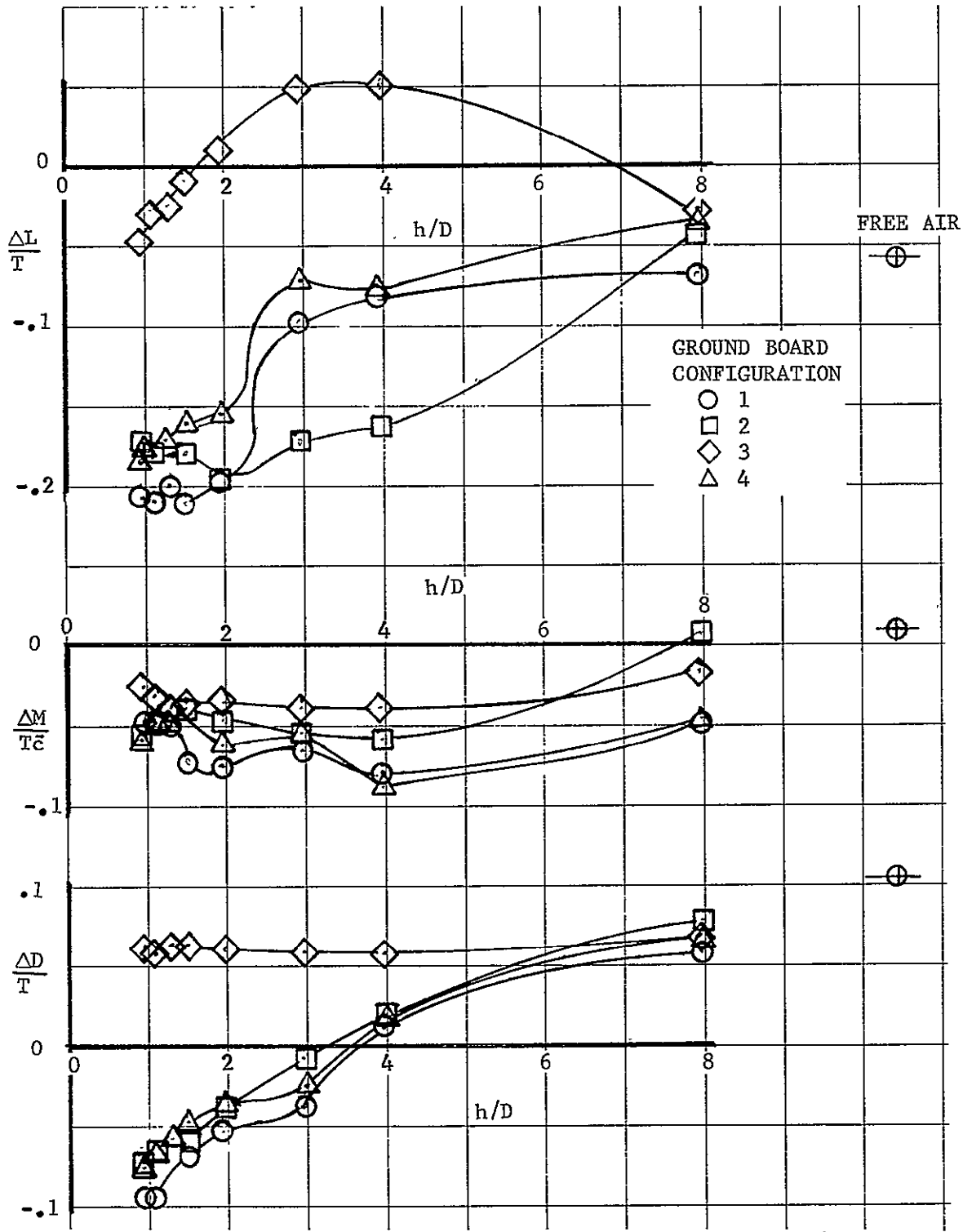

Figure 37. Effect of Height on the Thrust Induced Longitudinal Characteristics with Various Ground Board Configurations - $\delta_N = 105^o$, $V/V_j = .09$, $\alpha = 0^o$, $\emptyset = 0^o$

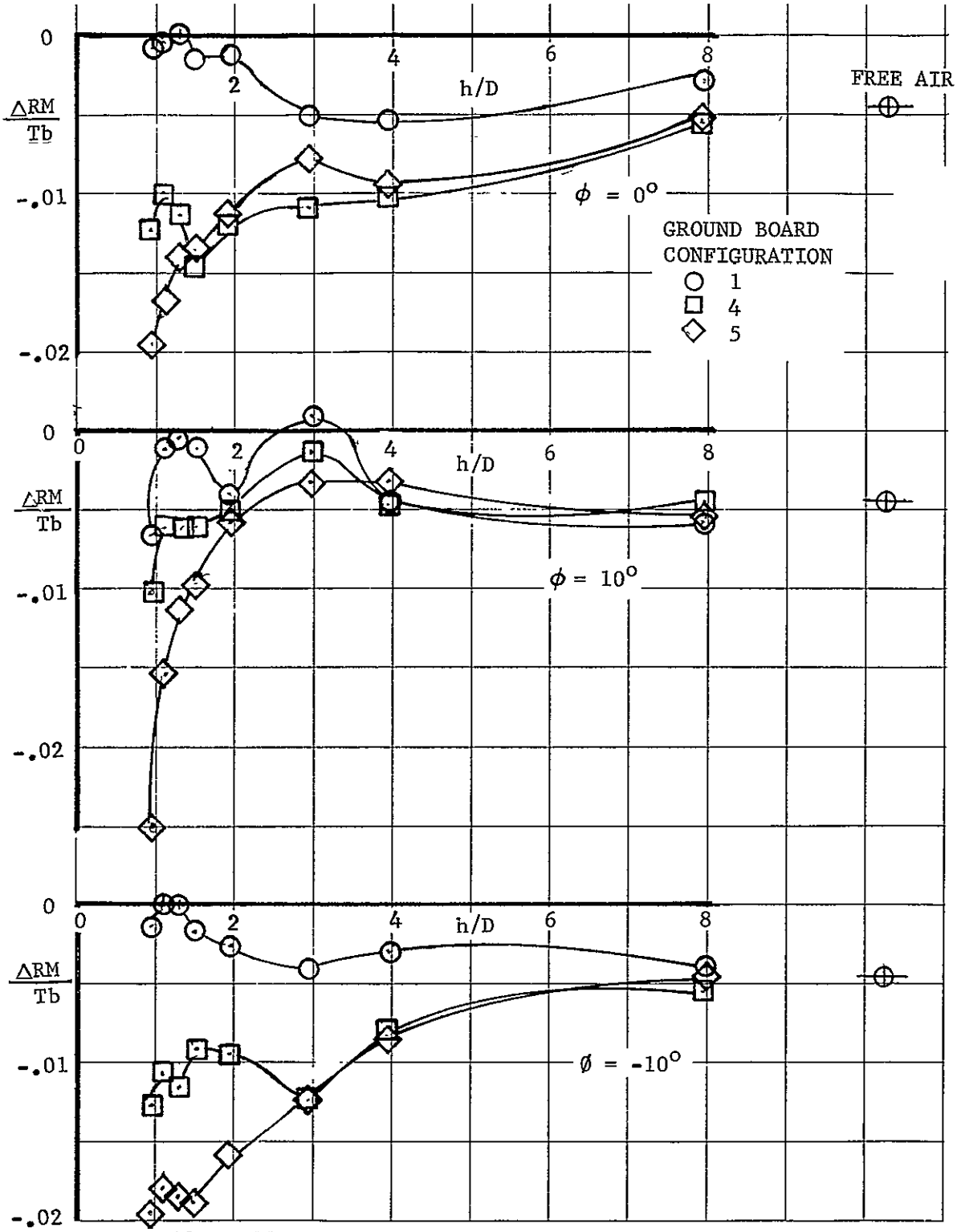

Figure 38. Effect of Height on the Thrust Induced Rolling Moment with Various Ground Board Configurations - $\delta_N = 105^\circ$, $V/V_j = .09$, $\alpha = 0^\circ$

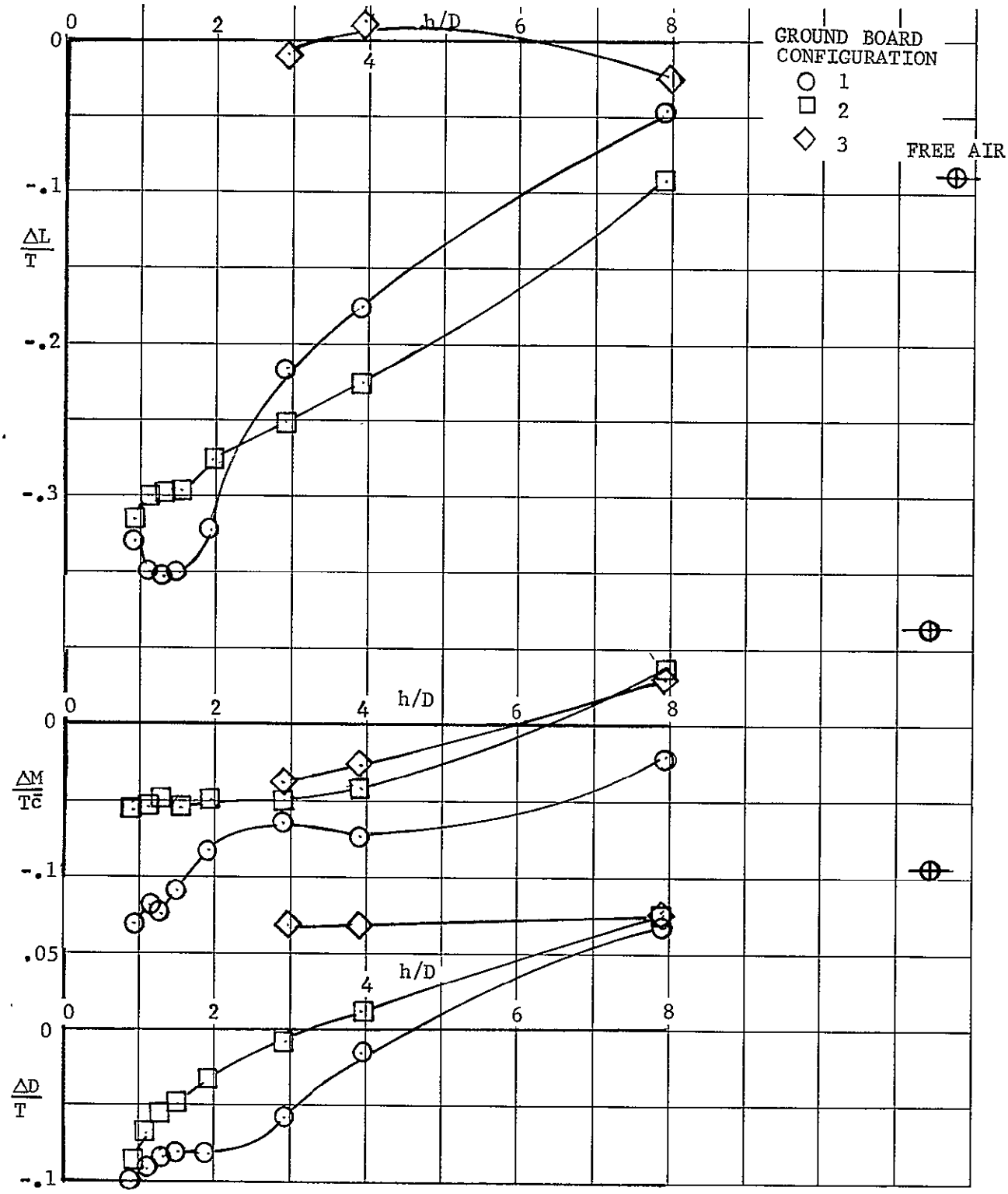

Figure 39. Effect of Height on the Thrust Induced Longitudinal Characteristics with Various Ground Board Configurations - $\delta_N = 105^\circ$, $\alpha = 8^\circ$, $V/V_j = .09$, $\emptyset \approx 0^\circ$

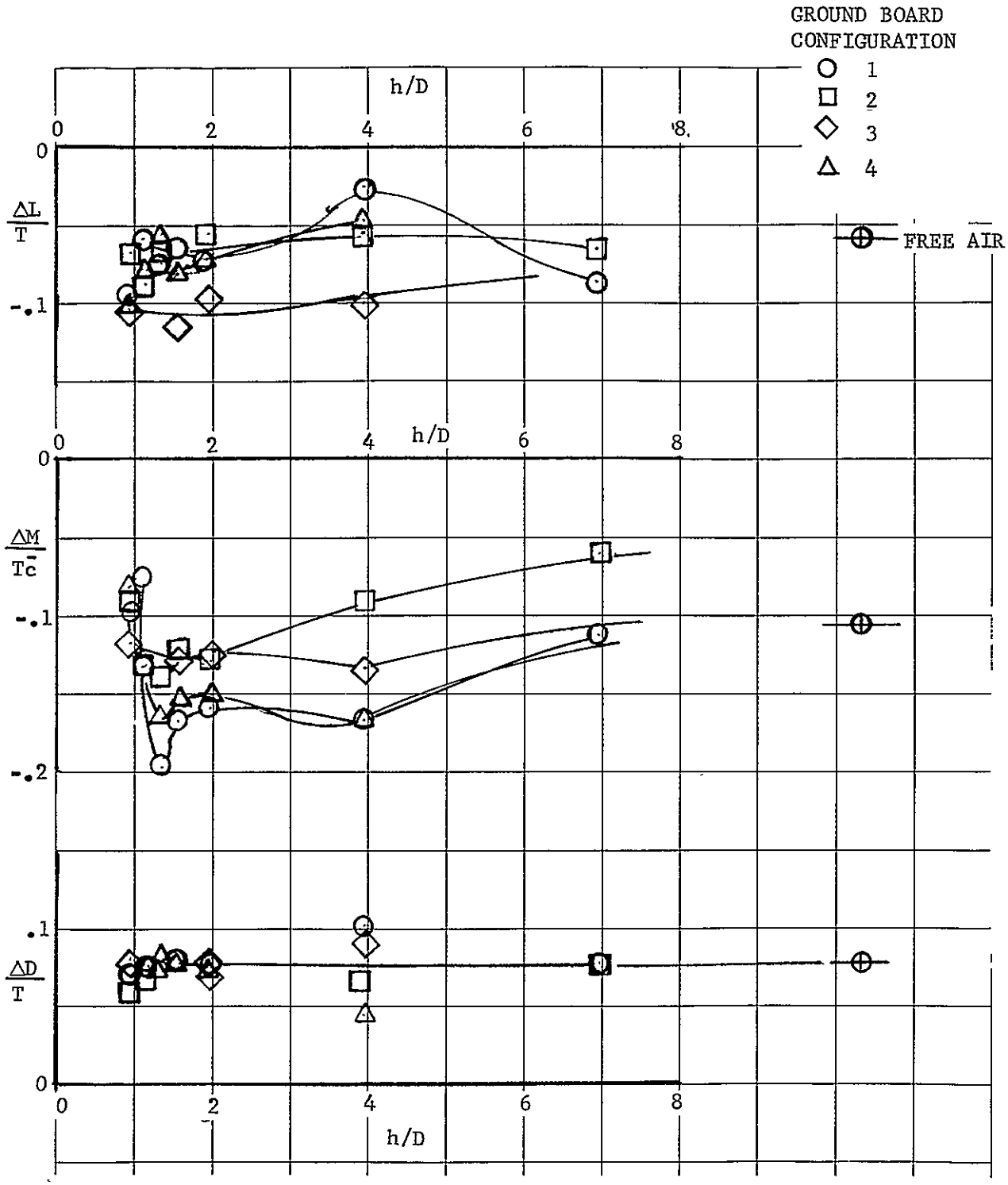

Figure 40. Effect of Height on the Thrust Induced Longitudinal Characteristics with Various Ground Board Configurations - $\delta_N = 90^o$, $V/V_j = 0$ $\alpha = 0^o$, $\emptyset = 0^o$

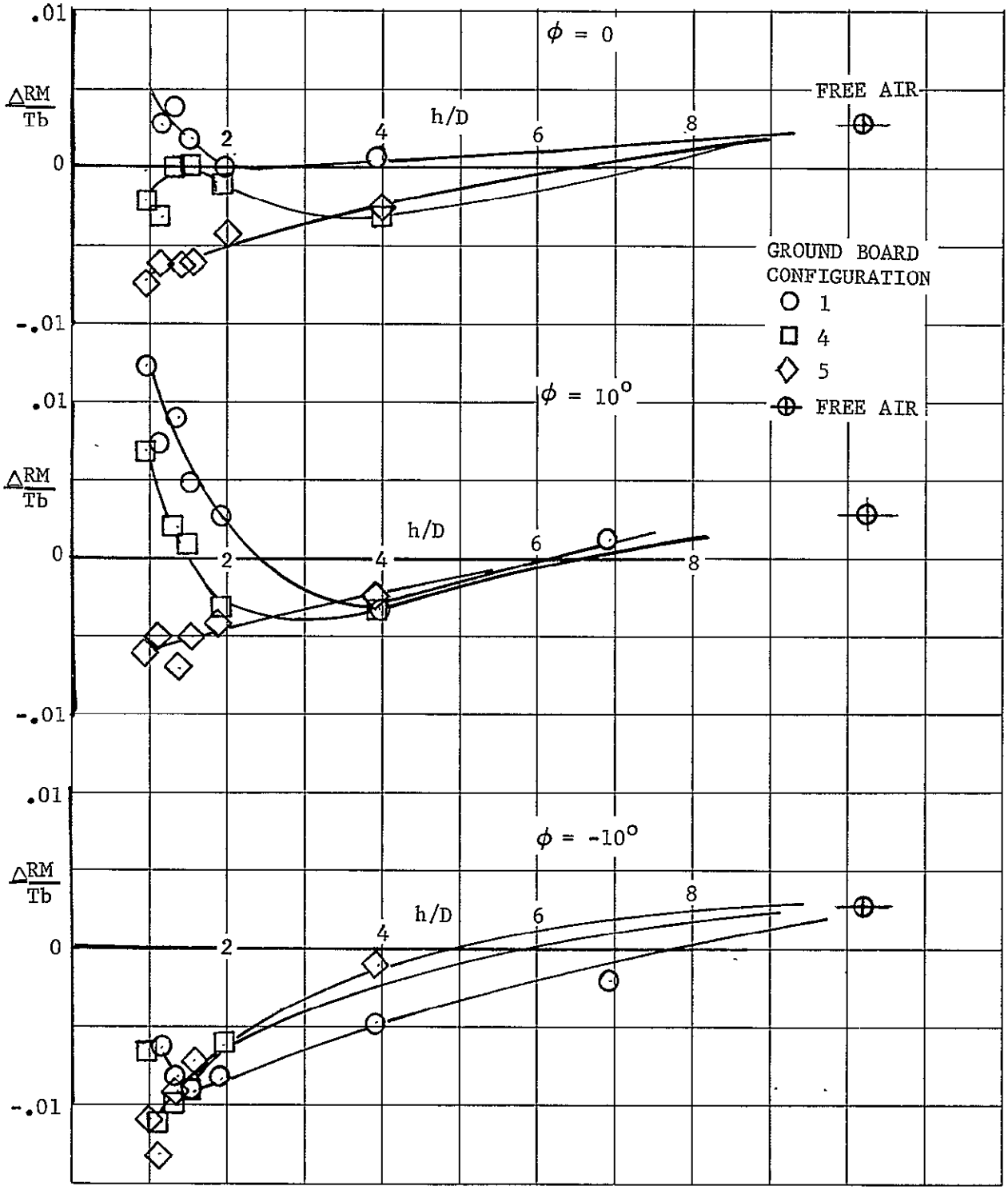

Figure 41. Effect of Height on the Thrust Induced Rolling Moment with Various Ground Board Configurations - $\delta_N = 90^\circ$, $V/V_j = 0$, $\alpha = 0^\circ$

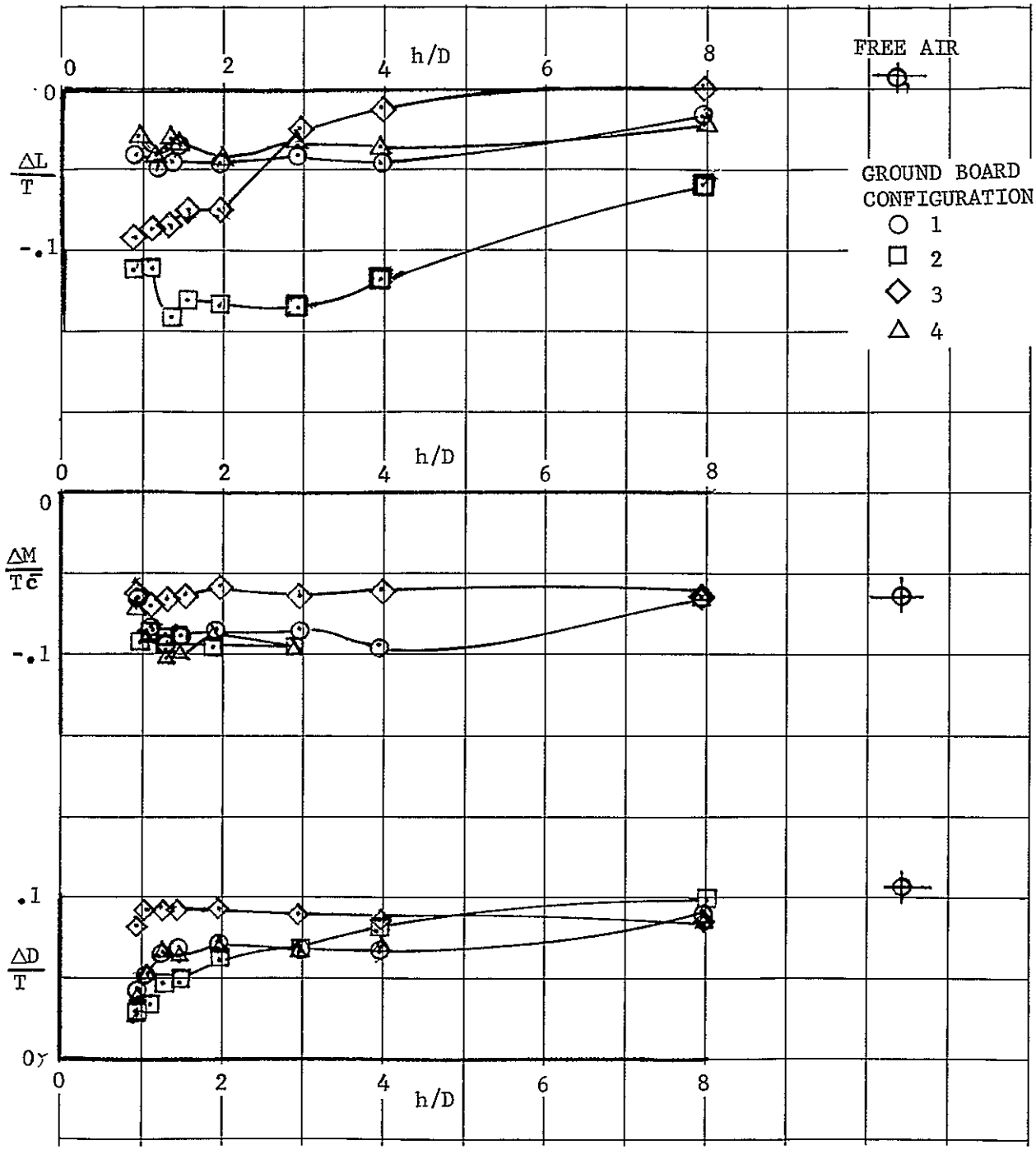

Figure 42. Effect of Height on the Thrust Induced Longitudinal Characteristics with Various Ground Board Configurations - $\delta_N = 90^o$, $V/V_j = .058$, $\alpha = 0^o$, $\emptyset = 0^o$

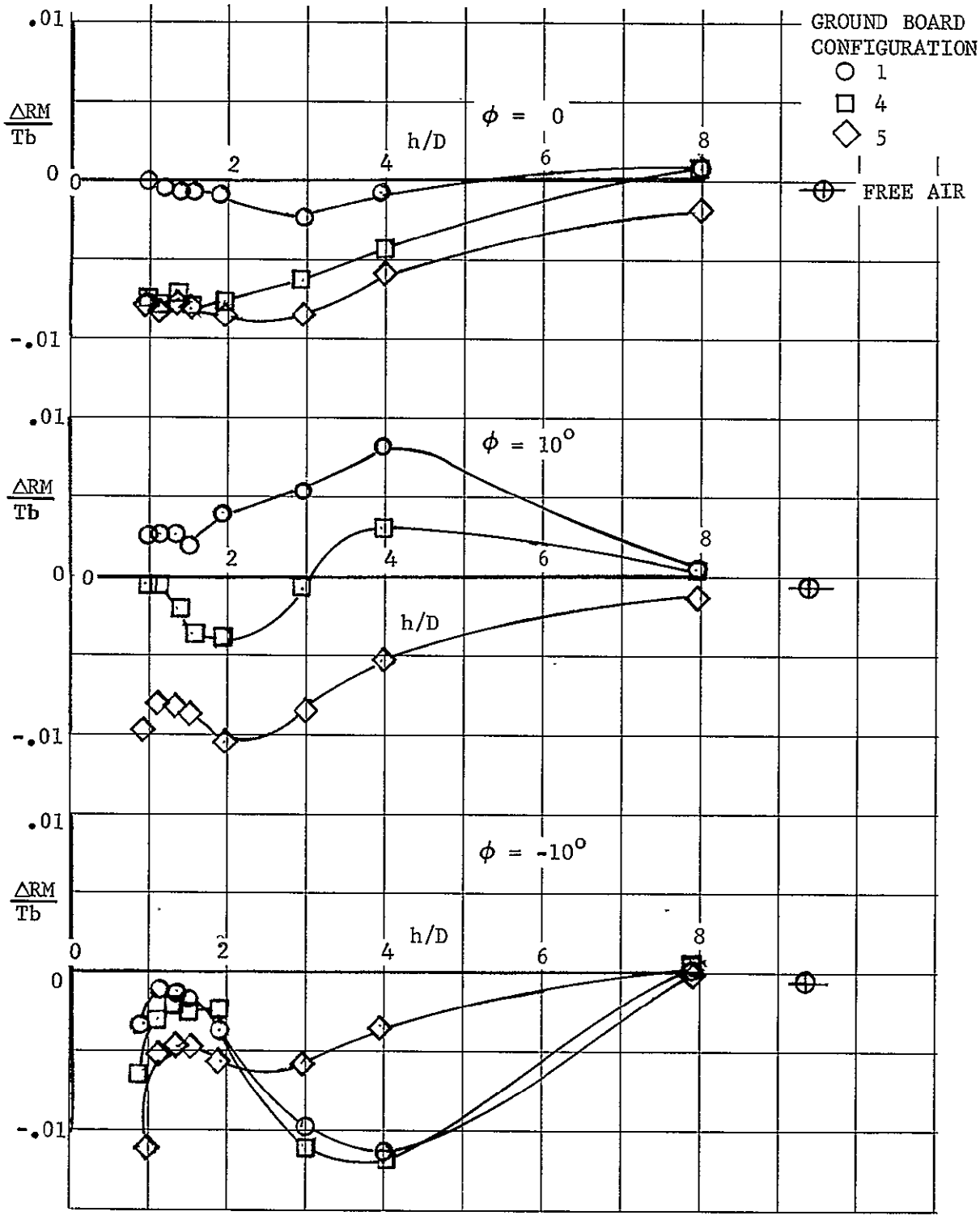

Figure 43. Effect of Height on the Thrust Induced Rolling Moment with Various Ground Board Configurations - $\delta_N = 90^o$, $V/V_j = .058$, $\alpha = 0^o$

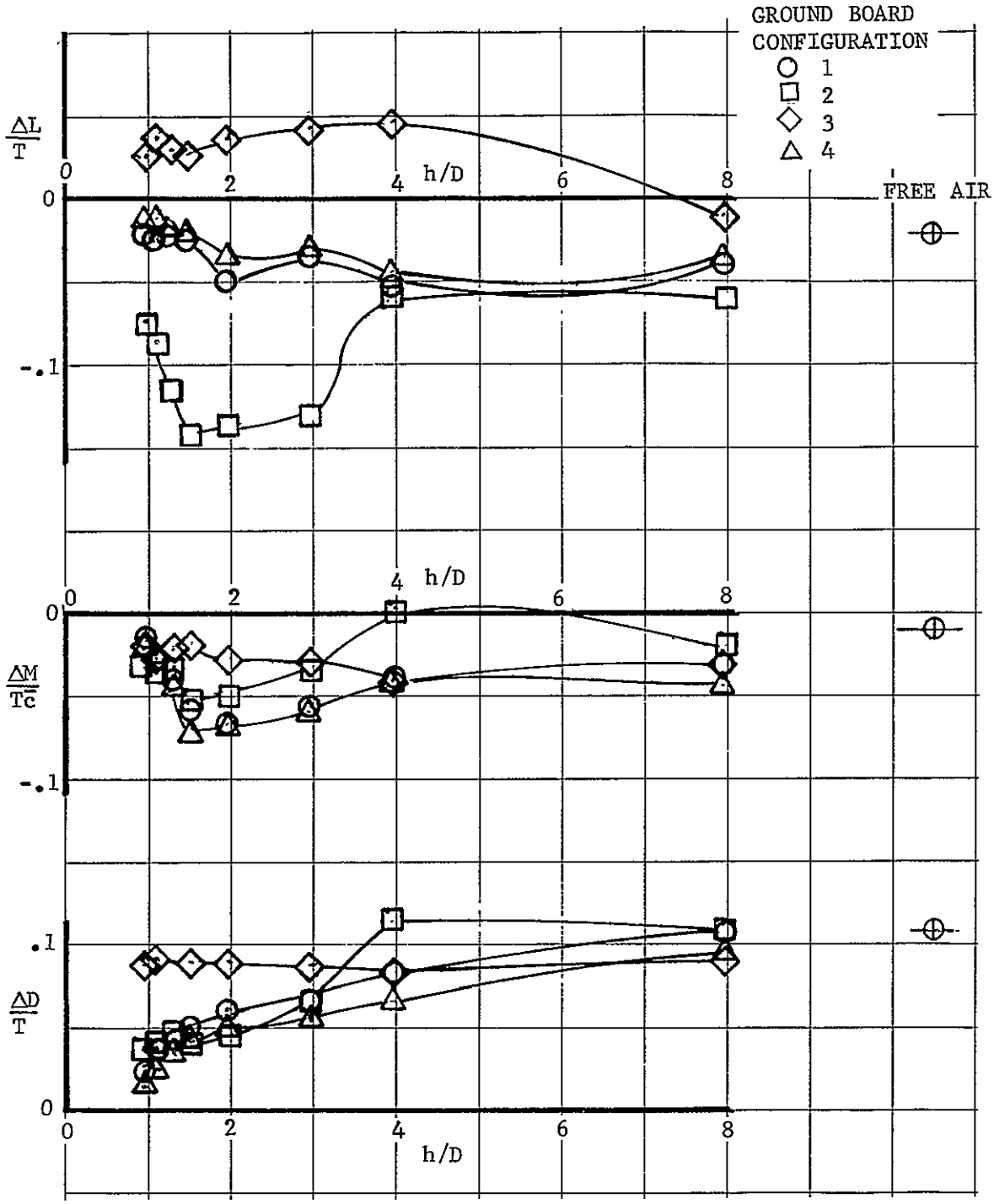

Figure 44. Effect of Height on the Thrust Induced Longitudinal Characteristics with Various Ground Board Configurations - $\delta_N = 90^o$, $V/V_j = .09$, $\alpha = 0^o$, $\emptyset = 0^o$

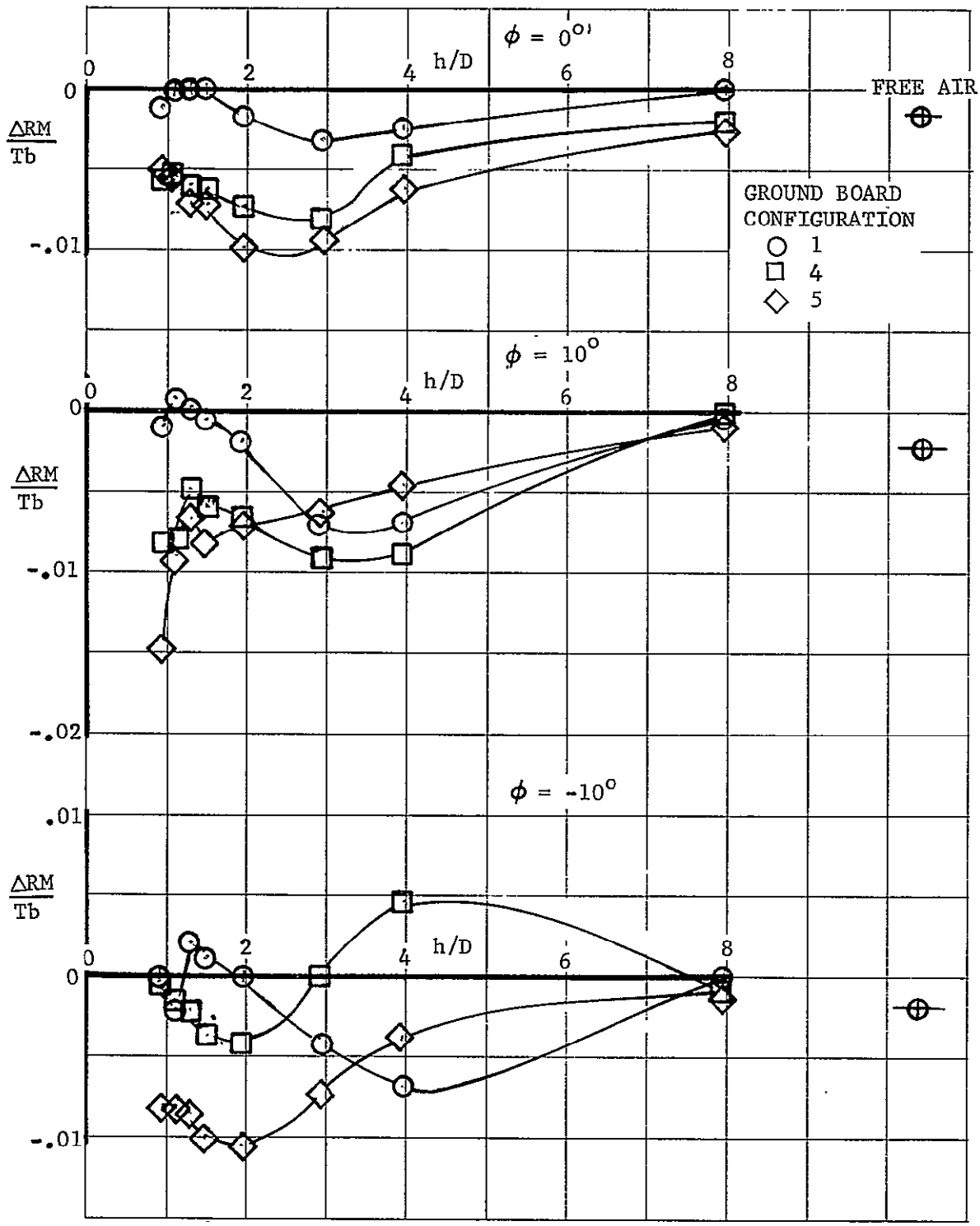

Figure 45. Effect of Height on the Thrust Induced Rolling Moment with Various Ground Board Configurations - $\delta_N = 90^o$, $V/V_j = .09$, $\alpha = 0^o$

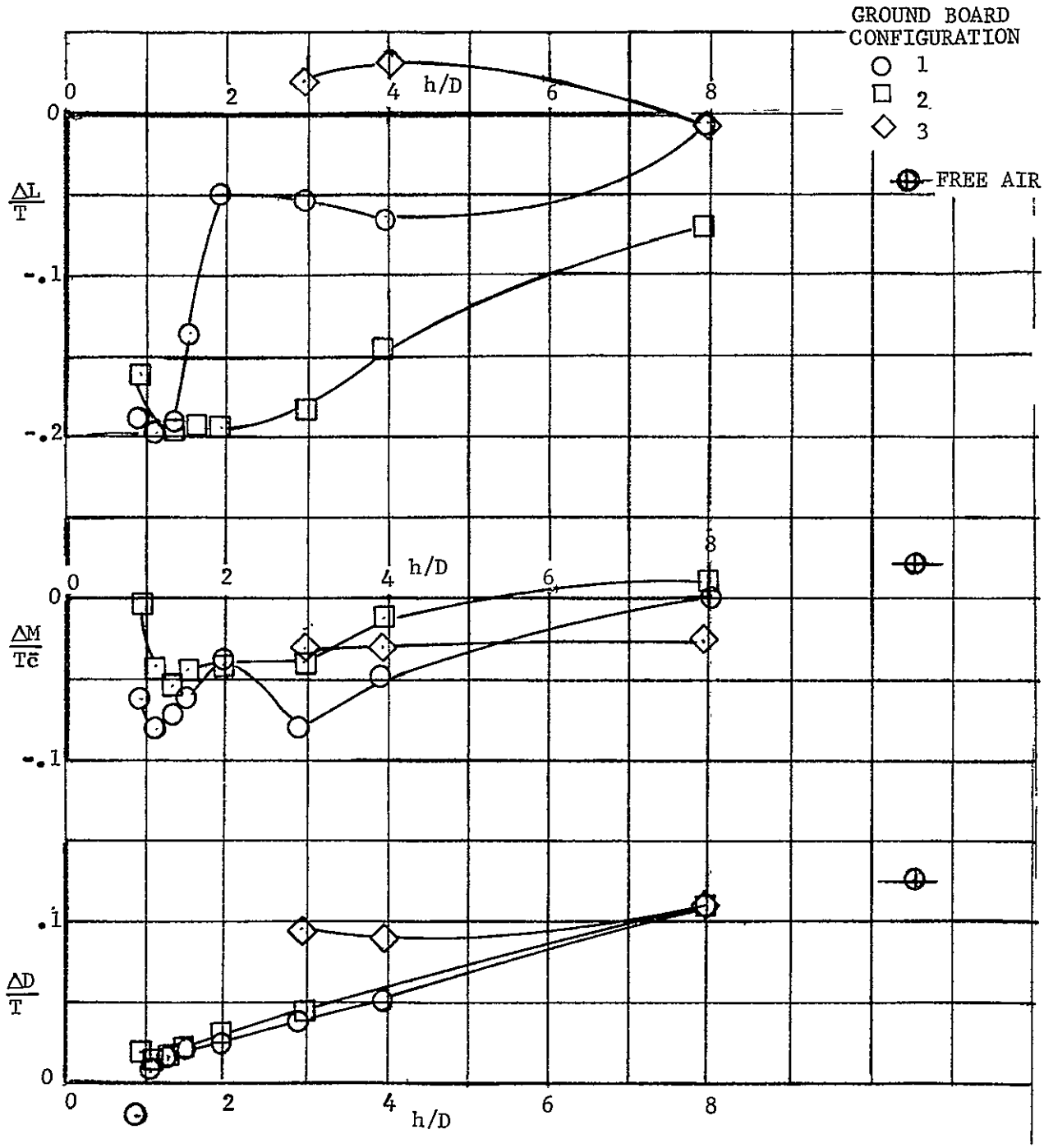

Figure 46. Effect of Height on the Thrust Induced Longitudinal Characteristics with Various Ground Board Configurations - $\delta_N = 90^o$, $\alpha = 8^o$, $V/V_j = .09$, $\emptyset = 0^o$

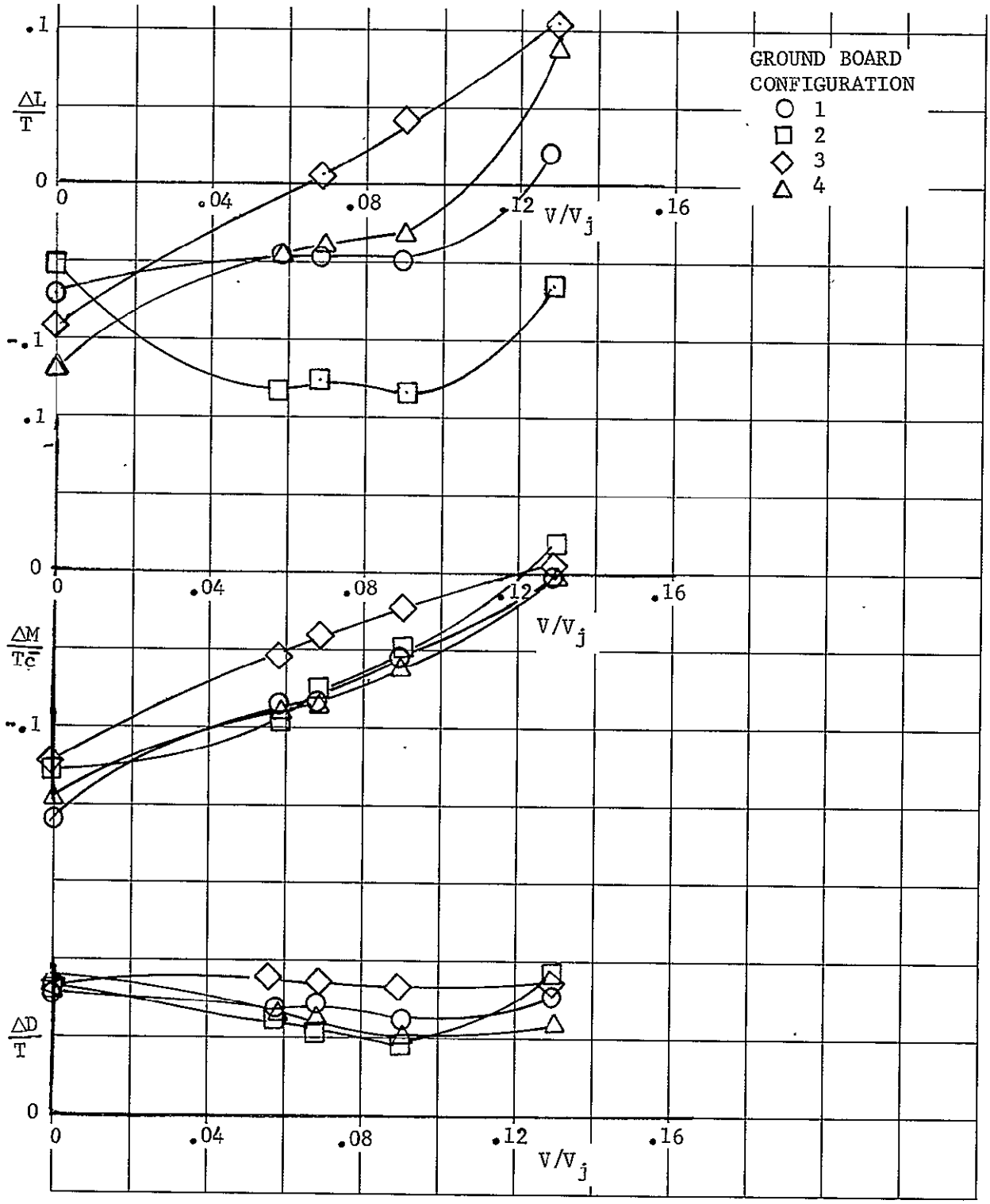

Figure 47. Effect of Velocity Ratio on the Thrust Induced Longitudinal Characteristics with Various Ground Board Configurations - $\delta_N = 90^o$, h/D = 2, $\alpha = 0^o$, $\phi = 0^o$

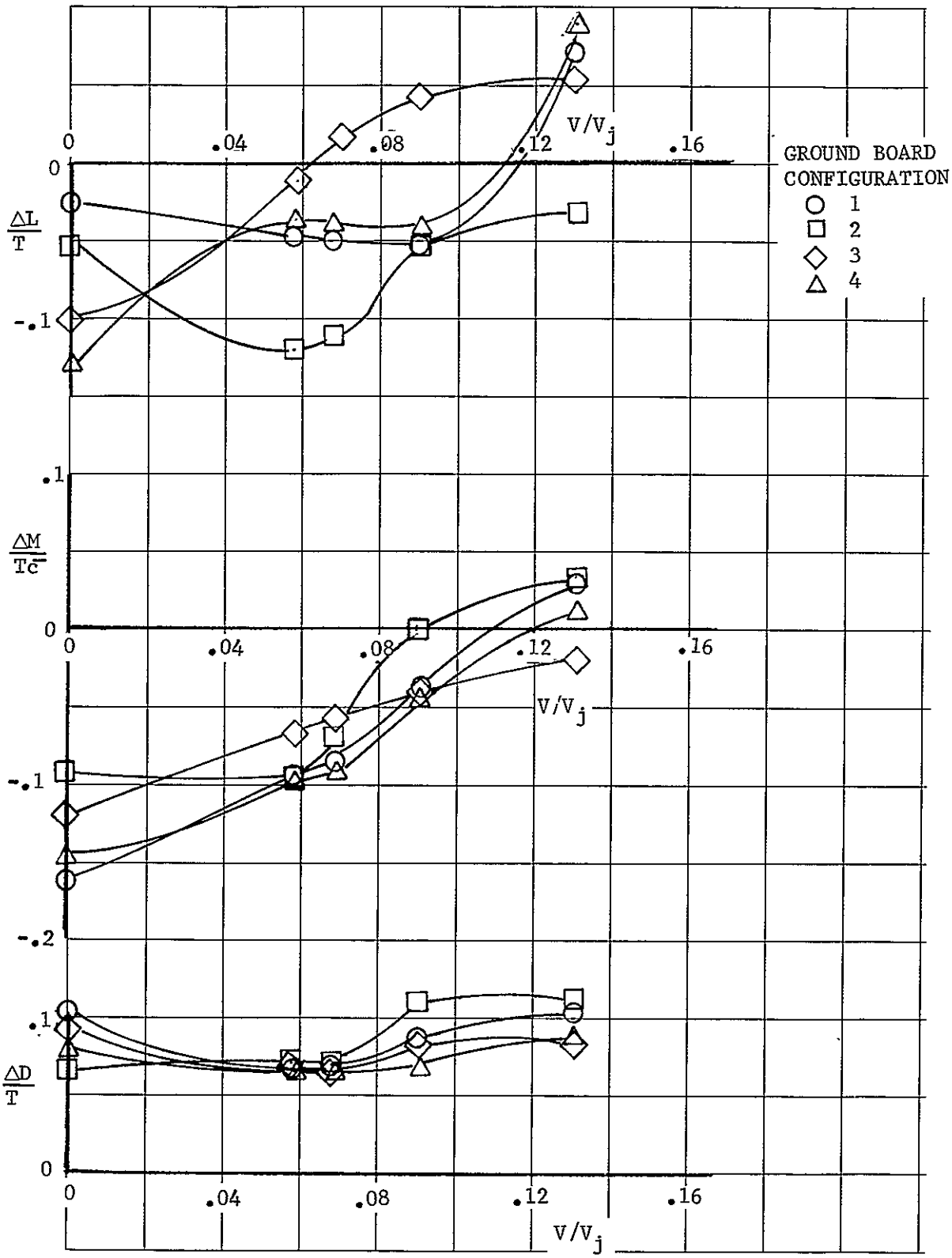

Figure 48. Effect of Velocity Ratio on the Thrust Induced Longitudinal Characteristics with Various Ground Board Configurations - $\delta_N = 90^o$, h/D = 4, $\alpha = 0^o$, $\emptyset = 0^o$

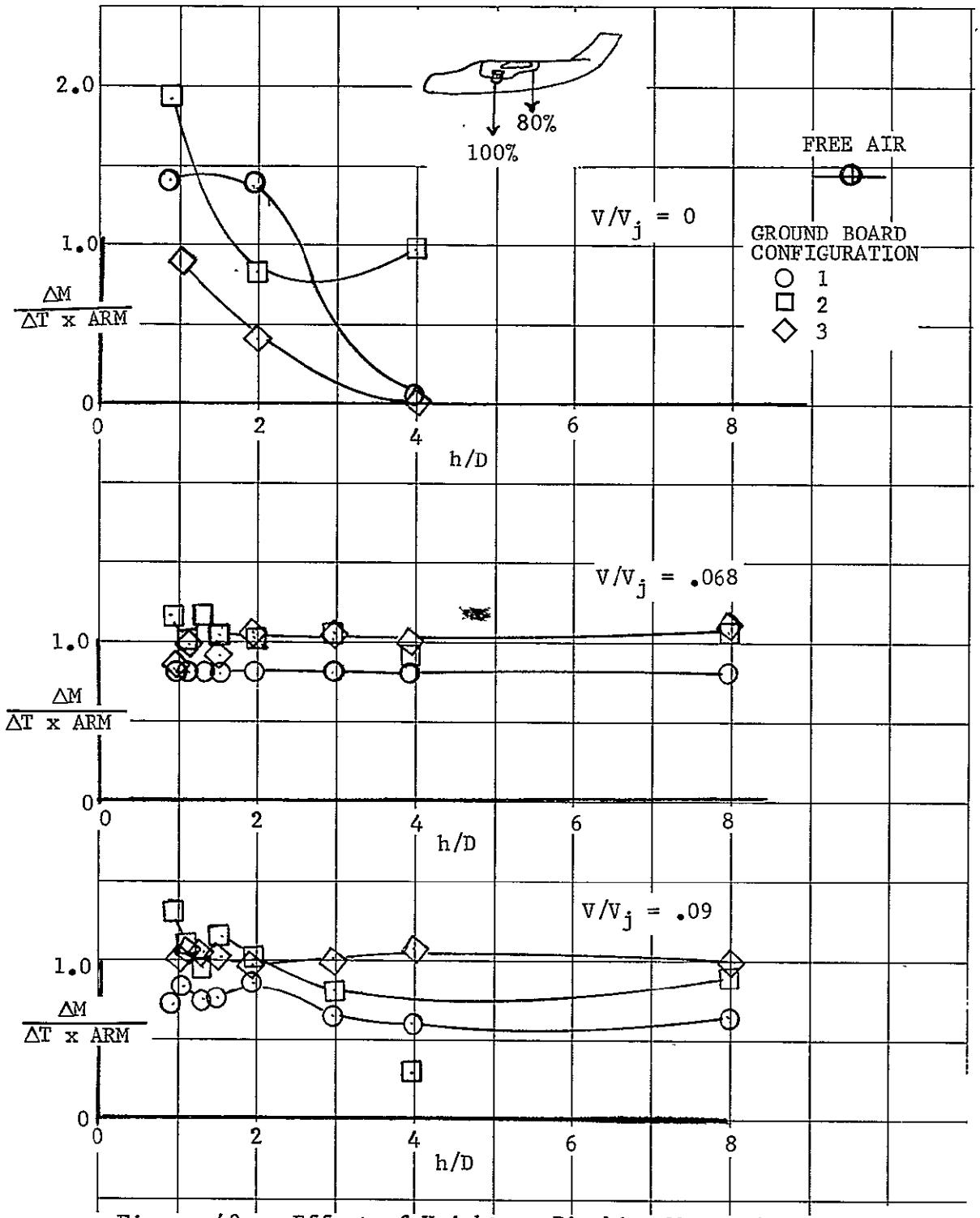

Figure 49. Effect of Height on Pitching Moment Due to Asymmetric Thrust Changes ~ $\delta_N = 90^o$; $\alpha = 0^o$, $\phi = 0^o$

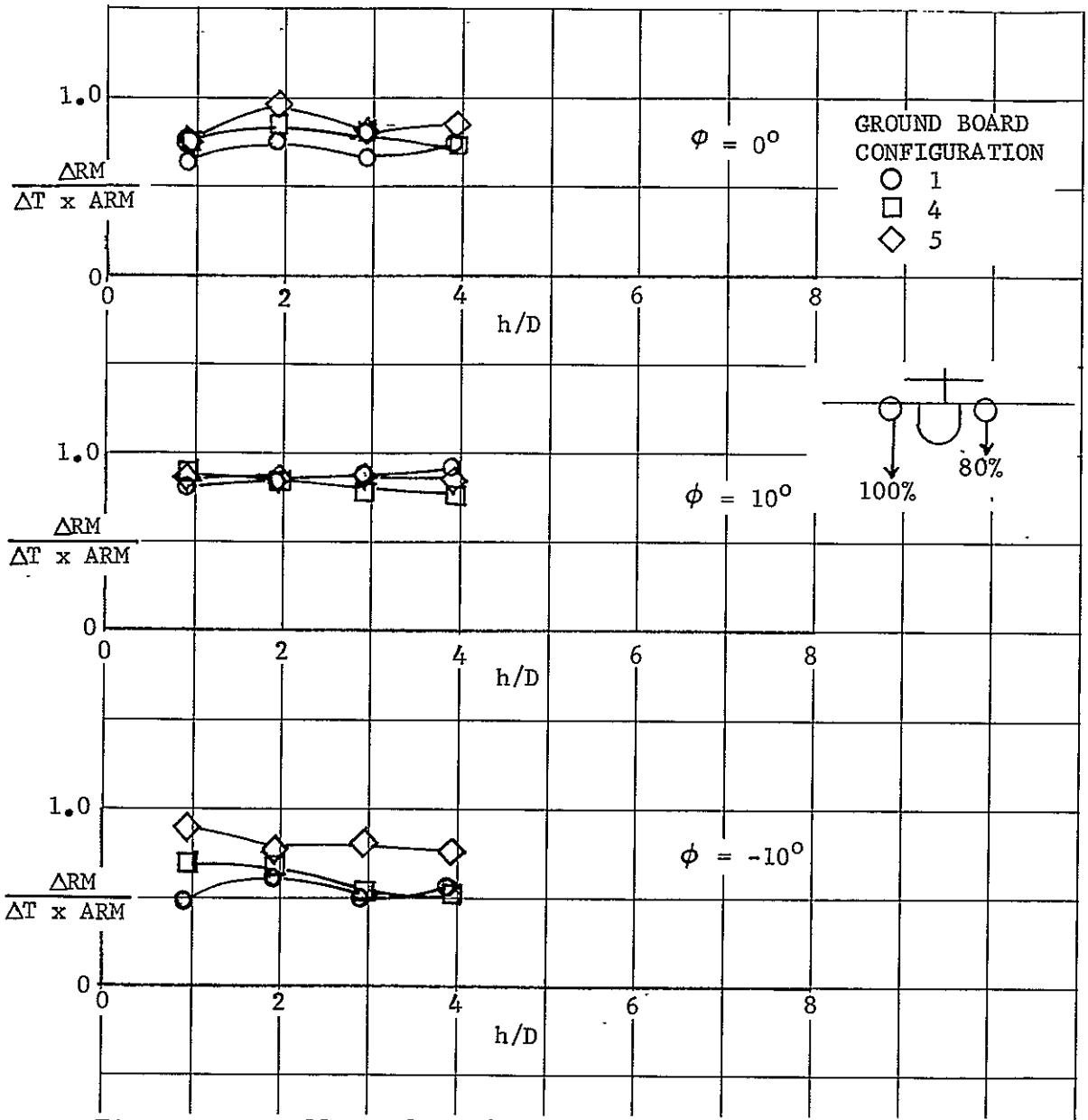

Figure 50. Effect of Height on Rolling Moment Due to Asymmetric Thrust Changes ~ $\delta_N = 90°$, $V/V_j = .09$, $\alpha = 0°$

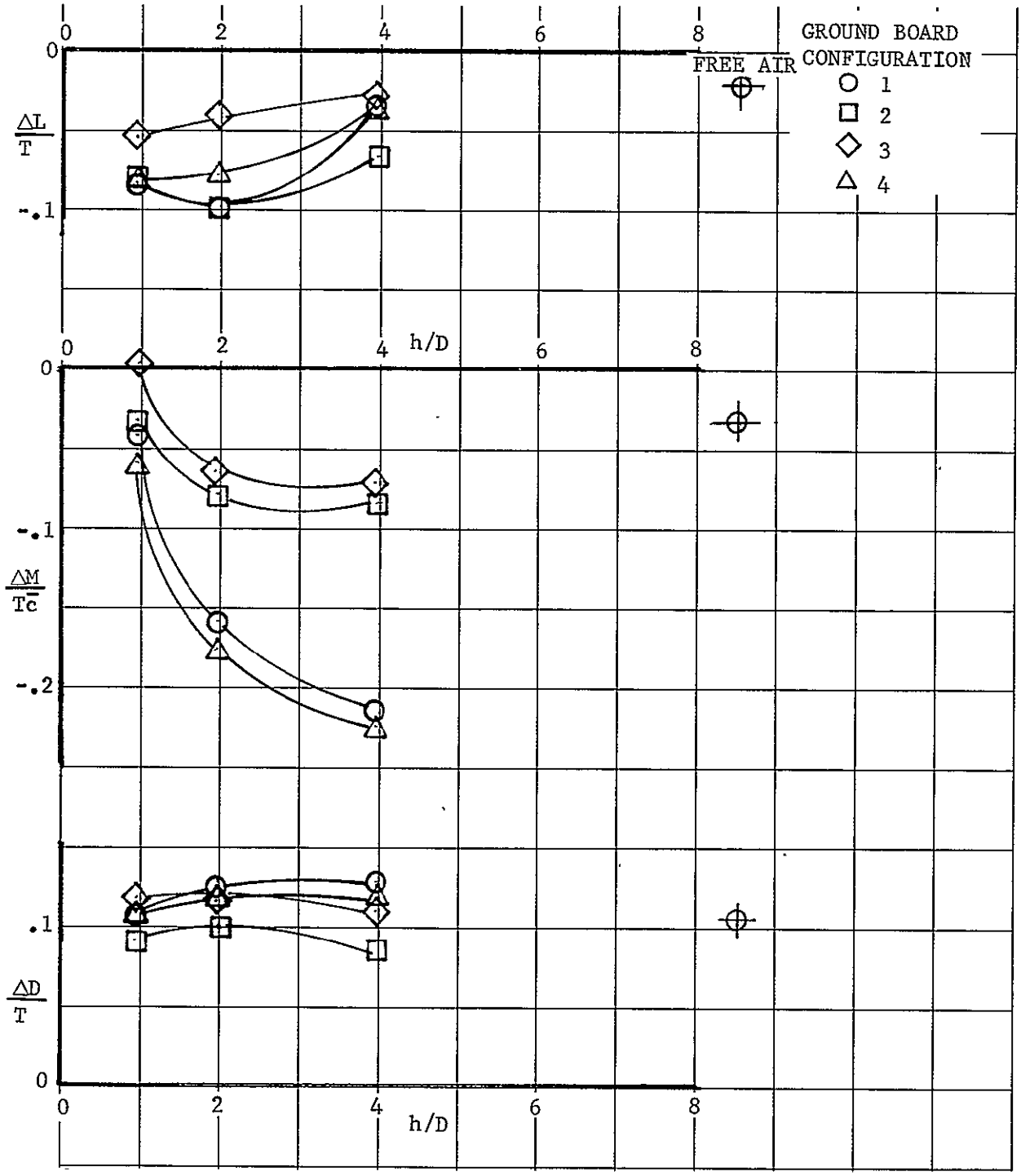

Figure 51. Effect of Height on the Thrust Induced Longitudinal Characteristics with Various Ground Board Configurations - $\delta_N = 80^\circ$, $V/V_j = 0$, $\alpha = 0^\circ$, $\phi = 0^\circ$

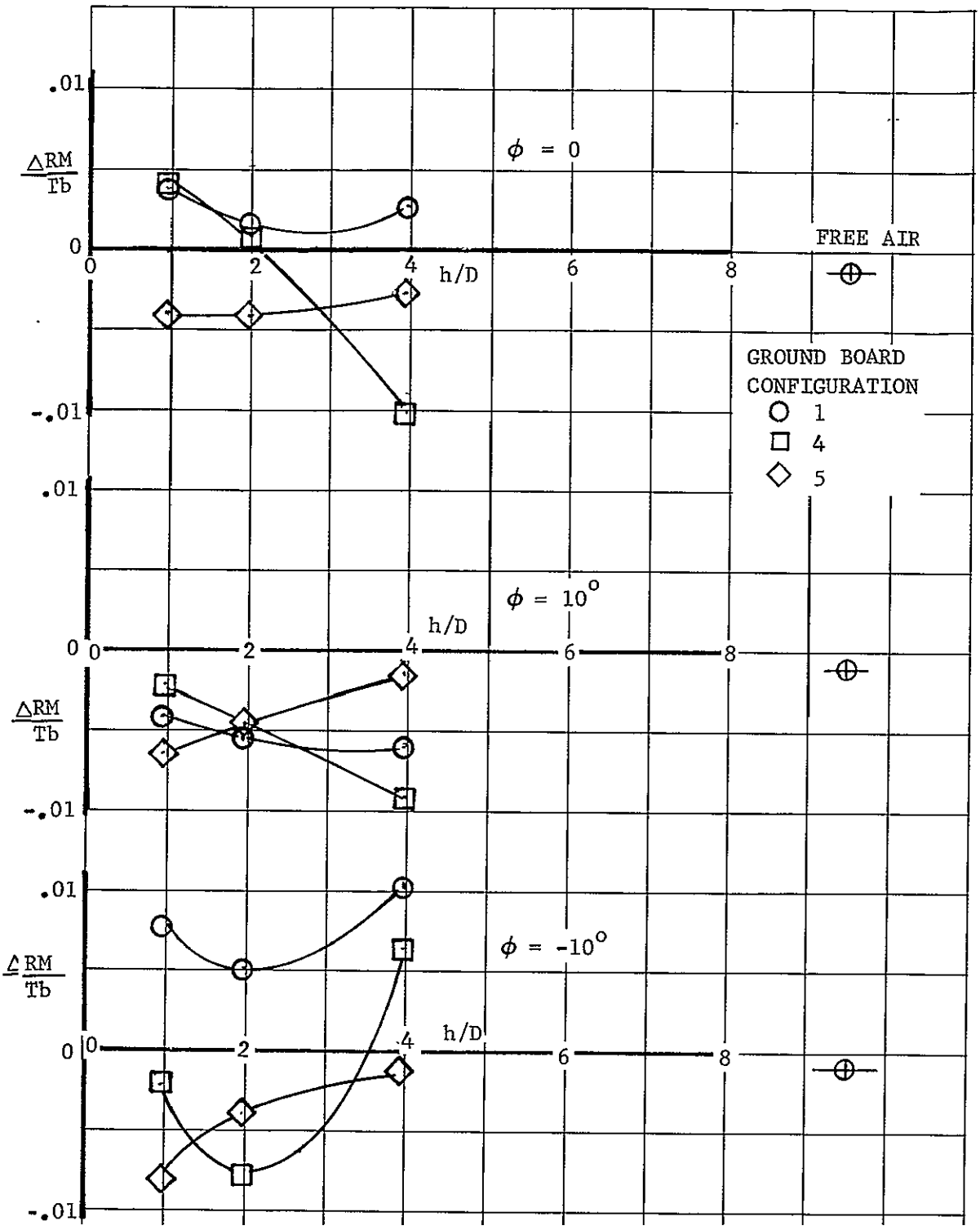

Figure 52. Effect of Height on the Thrust Induced Rolling Moment with Various Ground Board Configurations - $\delta_N = 80^\circ$, $V/V_j = 0$, $\alpha = 0^\circ$

C-2

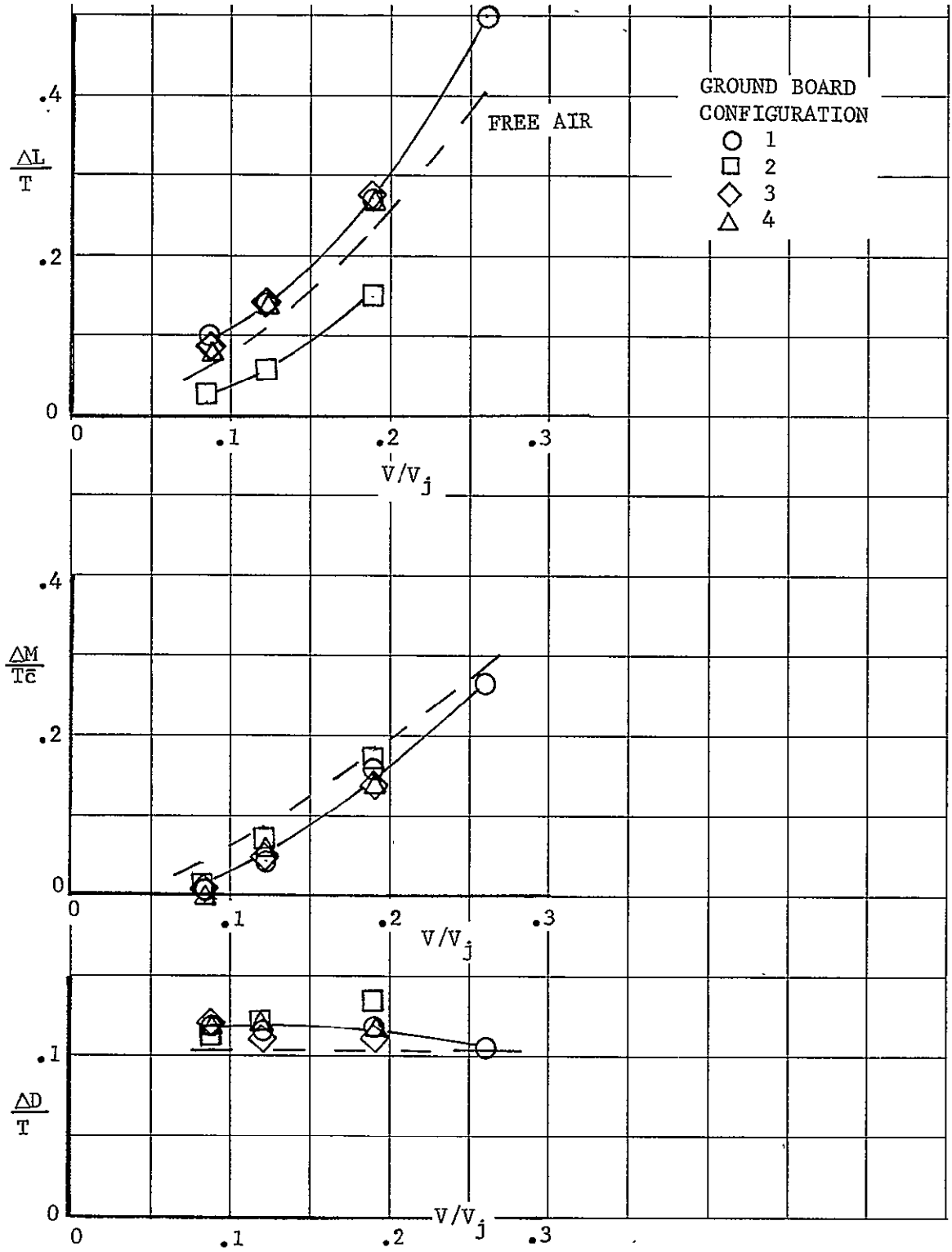

Figure 53. Effect of Velocity Ratio on the Thrust Induced Longitudinal Characteristics with Various Ground Board Configurations - $\delta_{N_{Fwd}} = 30^{\circ}$, $\delta_{N_{Aft}} = 60^{\circ}$, $h/D = 1$, $\alpha = 0^{\circ}$, $\emptyset = 0^{\circ}$

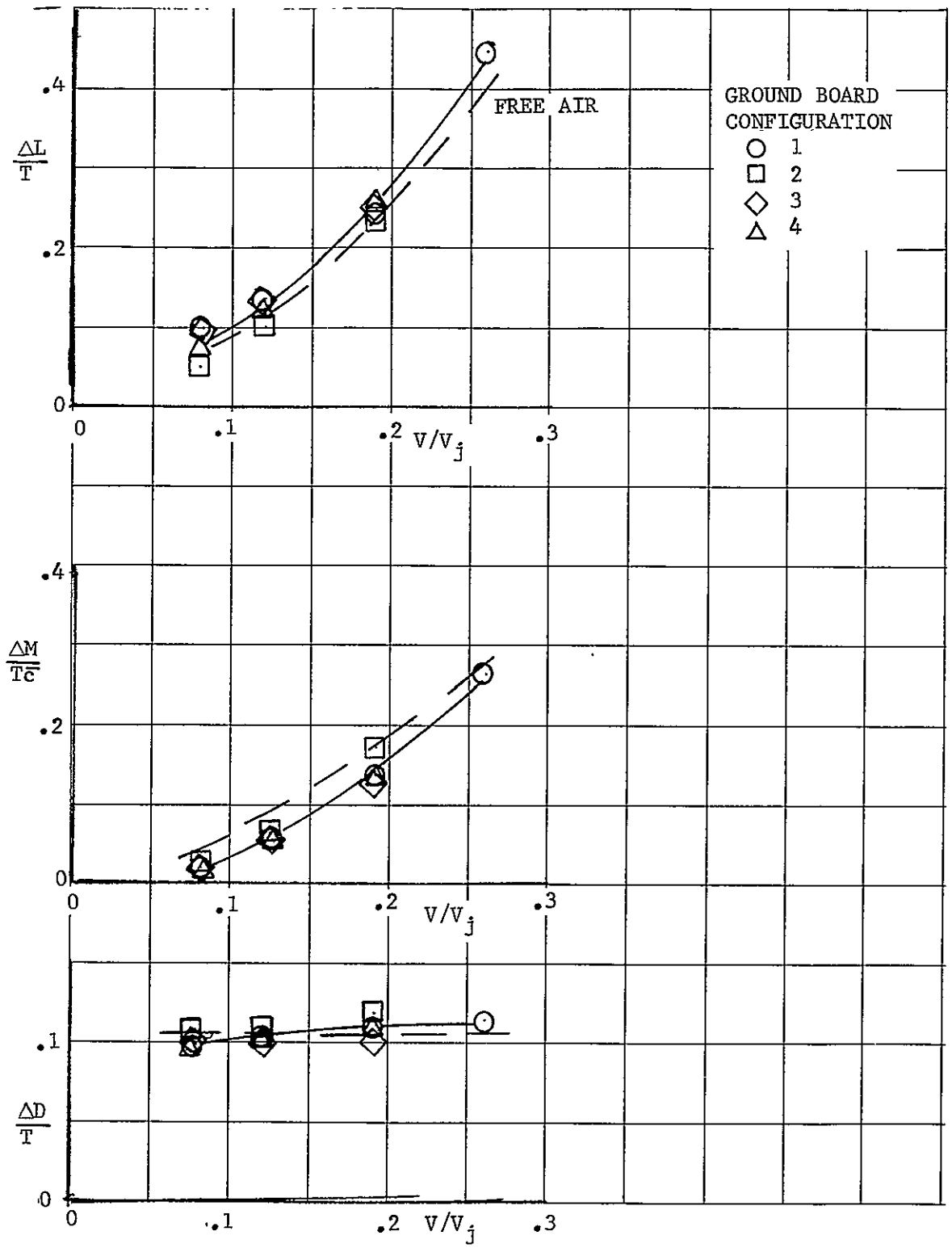

Figure 54. Effect of Velocity on the Thrust Induced Longitudinal Characteristics with Various Ground Board Configurations - $\delta_{N_{Fwd}} = 30^{o}$, $\delta_{N_{Aft}} = 60^{o}$, h/D = 4, $\alpha = 0^{o}$, $\emptyset = 0^{o}$

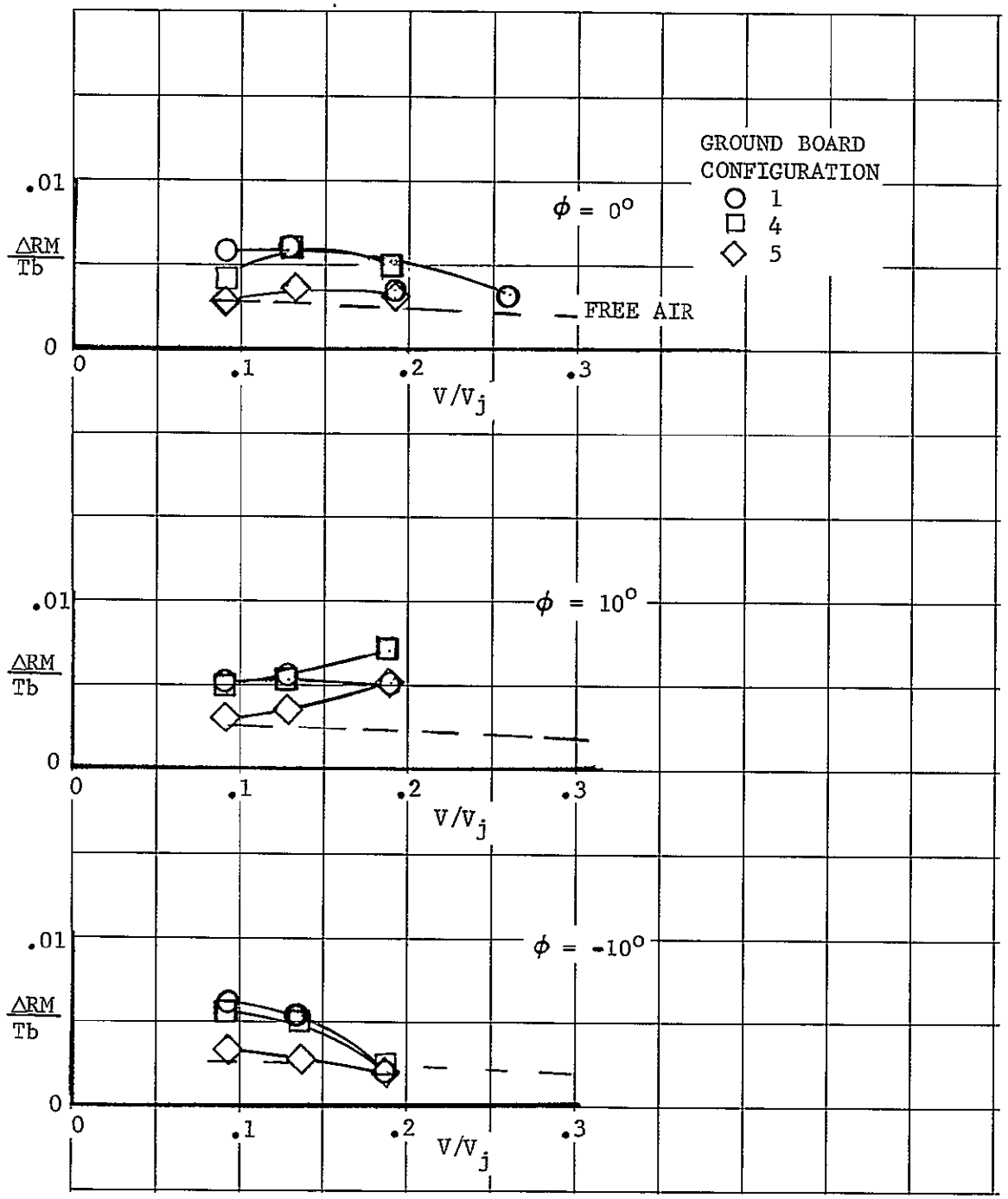

Figure 55. Effect of Velocity Ratio on the Thrust Induced Rolling Moment with Various Ground Board Configurations - δ_N = 30°/60°, h/D = 1.0, α = 0°

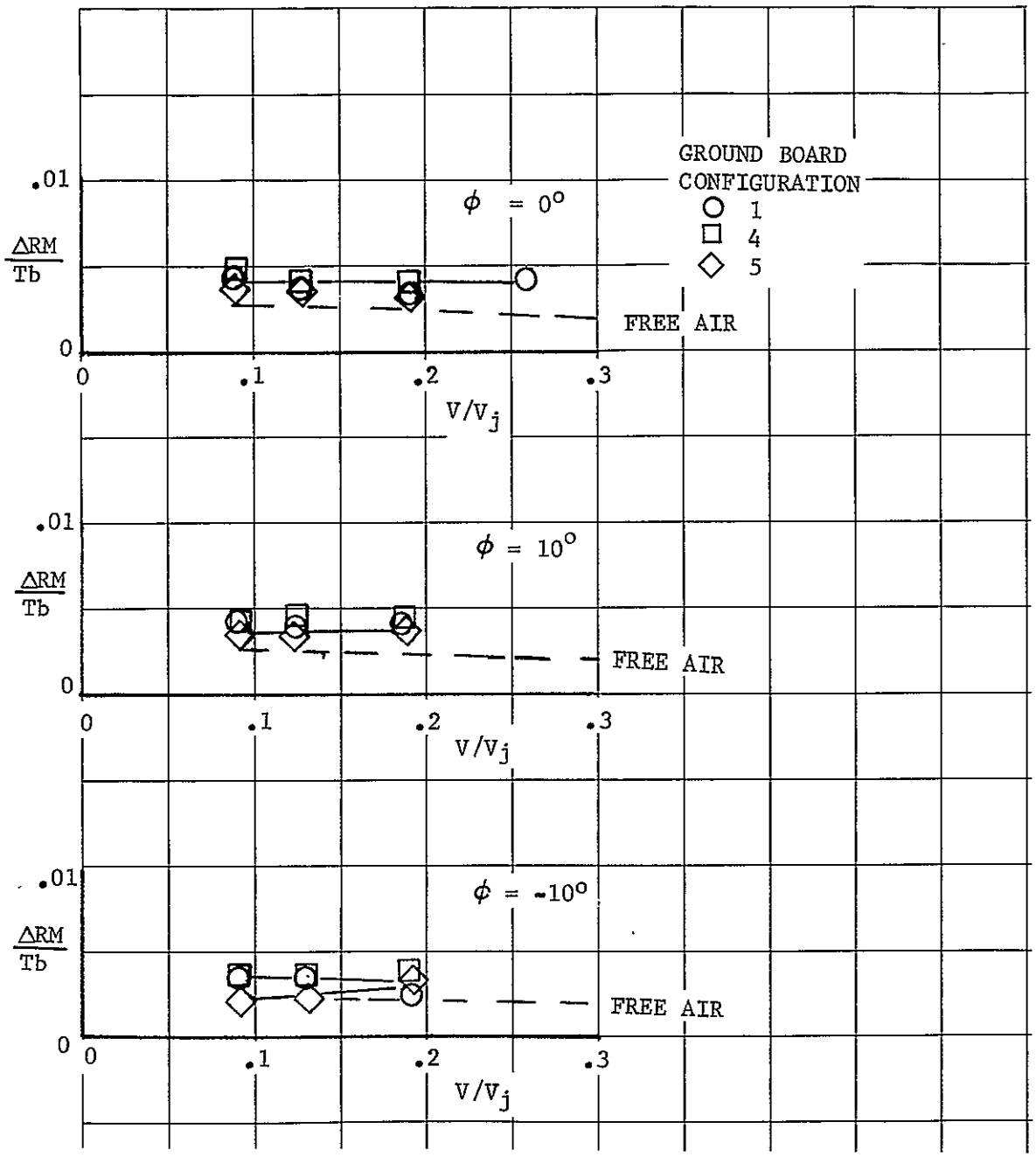

Figure 56. Effect of Velocity Ratio on the Thrust Induced Rolling Moment with Various Ground Board Configurations - $\delta_N = 30^\circ/60^\circ$, h/D = 4.0, $\alpha = 0^\circ$

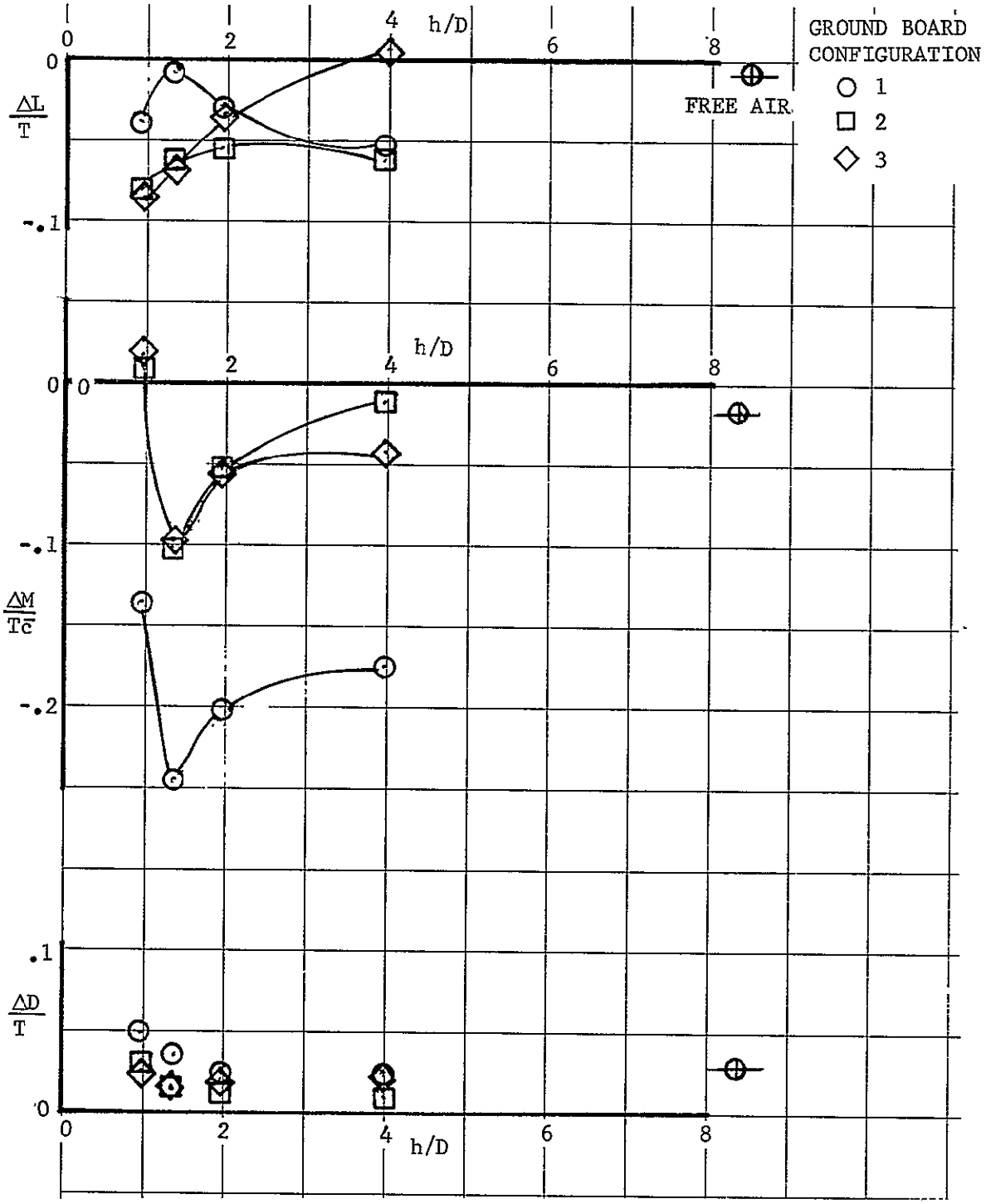

Figure 57. Effect of Height on the Thrust Induced Longitudinal Characteristics with Various Ground Board Configurations, Three Fan - $\delta_{N_{Nose}} = 80^{o}$, $\delta_{N_{Aft}} = 90^{o}$, $V/V_j = 0$, $\alpha = 0^{o}$ $\emptyset = 0^{o}$

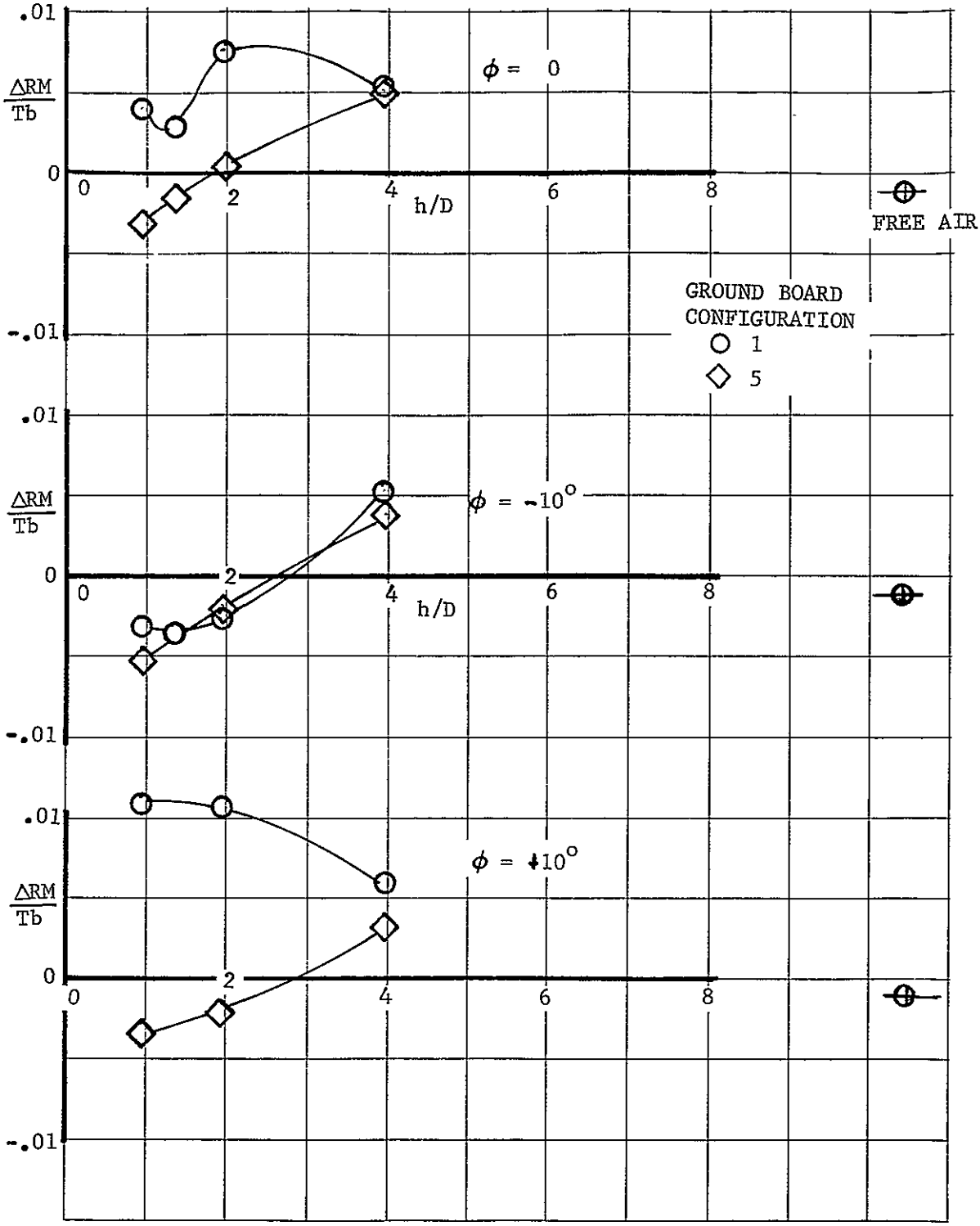

Figure 58. Effect of Height on the Thrust Induced Rolling Moment with Various Ground Board Configurations - $\delta_{N_{Nose}} = 80^{o}$, $\delta_{N_{Aft}} = 90^{o}$, $V/V_j = 0$, $\alpha = 0^{o}$

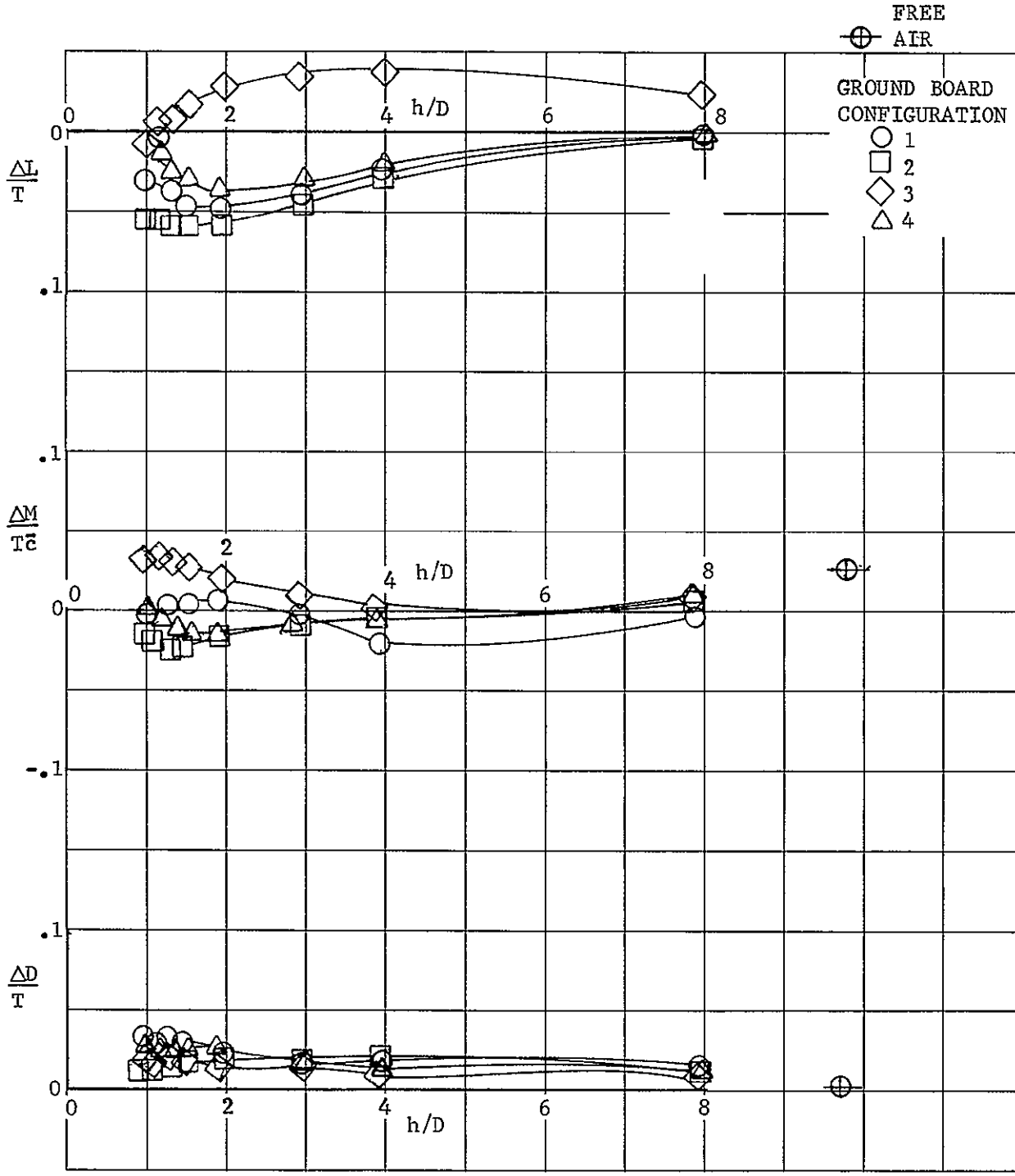

Figure 59. Effect of Height on the Thrust Induced Longitudinal Characteristics with Various Ground Board Configurations, Three Fan - $\delta_{N_{Nose}} = 80^{\circ}$, $\delta_{N_{Aft}} = 90^{\circ}$, $V/V_j = .068$, $\alpha = 0^{\circ}$, $\phi = 0^{\circ}$

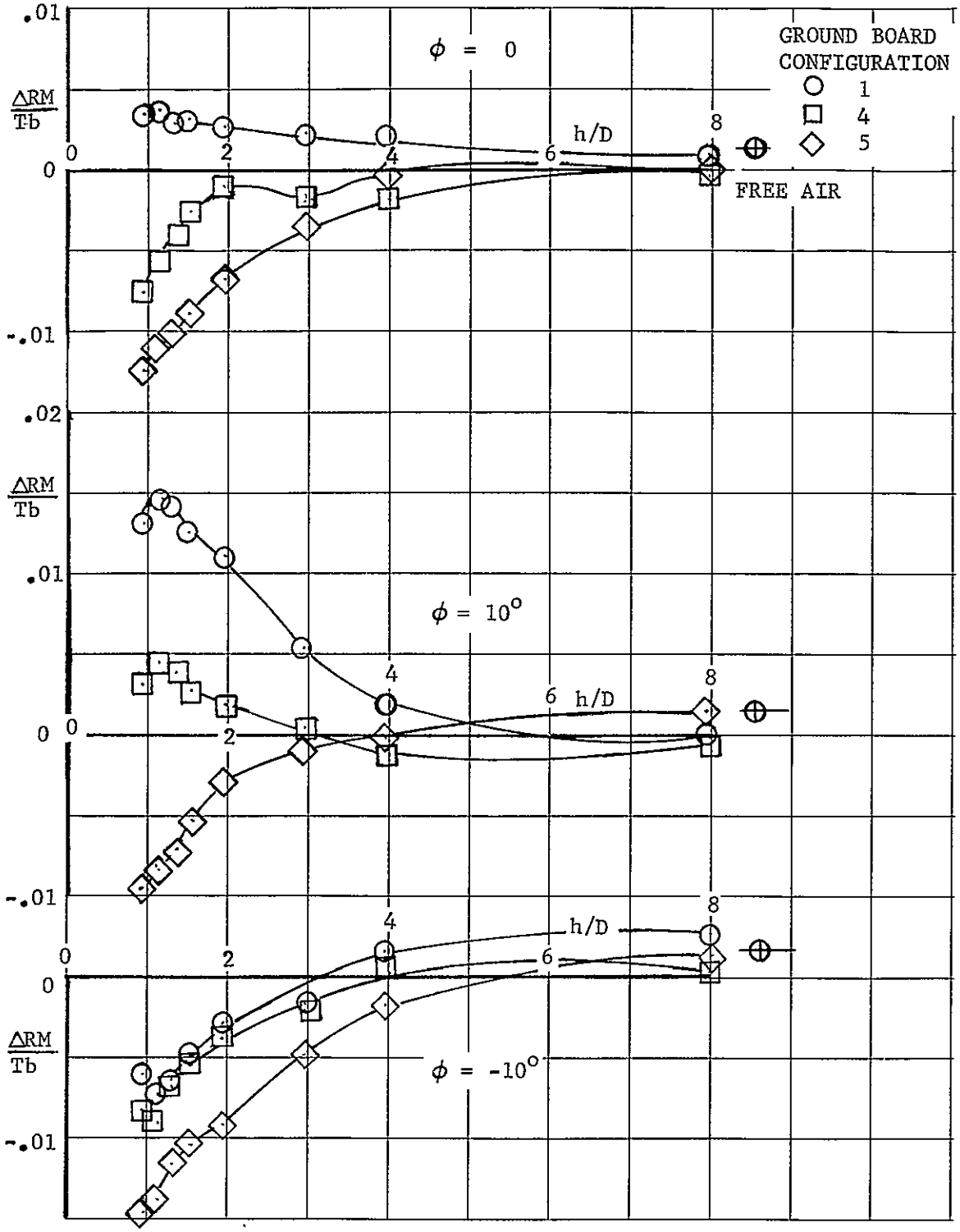

Figure 60. Effect of Height on the Thrust Induced Rolling Moment with Various Ground Board Configurations, Three Fan - $\delta_{N_{Nose}} = 80$, $\delta_{N_{Aft}} = 90^{o}$, $V/V_j = .068$, $\alpha = 0^{o}$

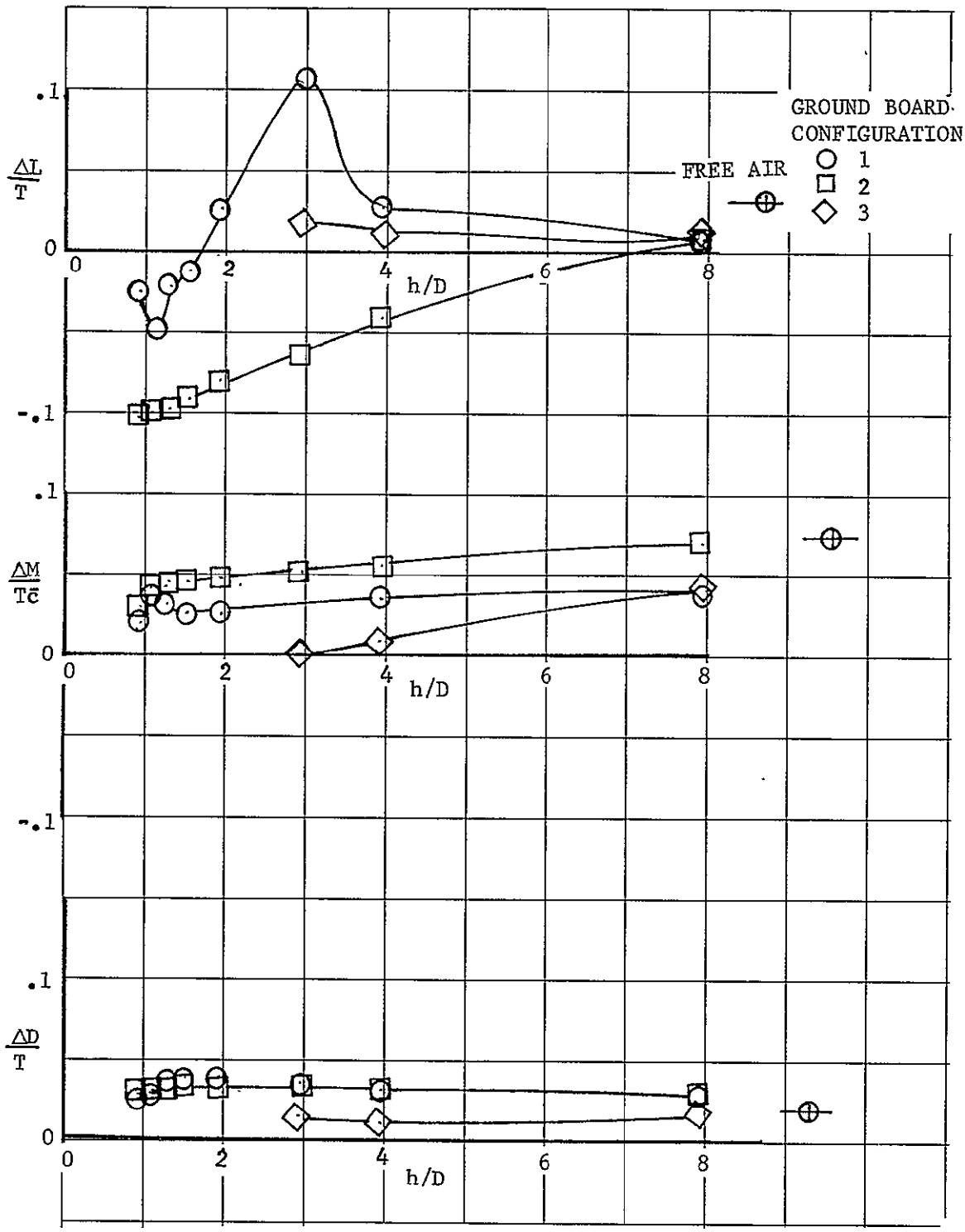

Figure 61. Effect of Height on the Thrust Induced Longitudinal Characteristics with Various Ground Board Configurations, Three-Fan - $\delta_{N_{Nose}} = 80^{o}$, $\delta_{N_{Aft}} = 90^{o}$, $V/V_j = .09$, $\emptyset = 0^{o}$

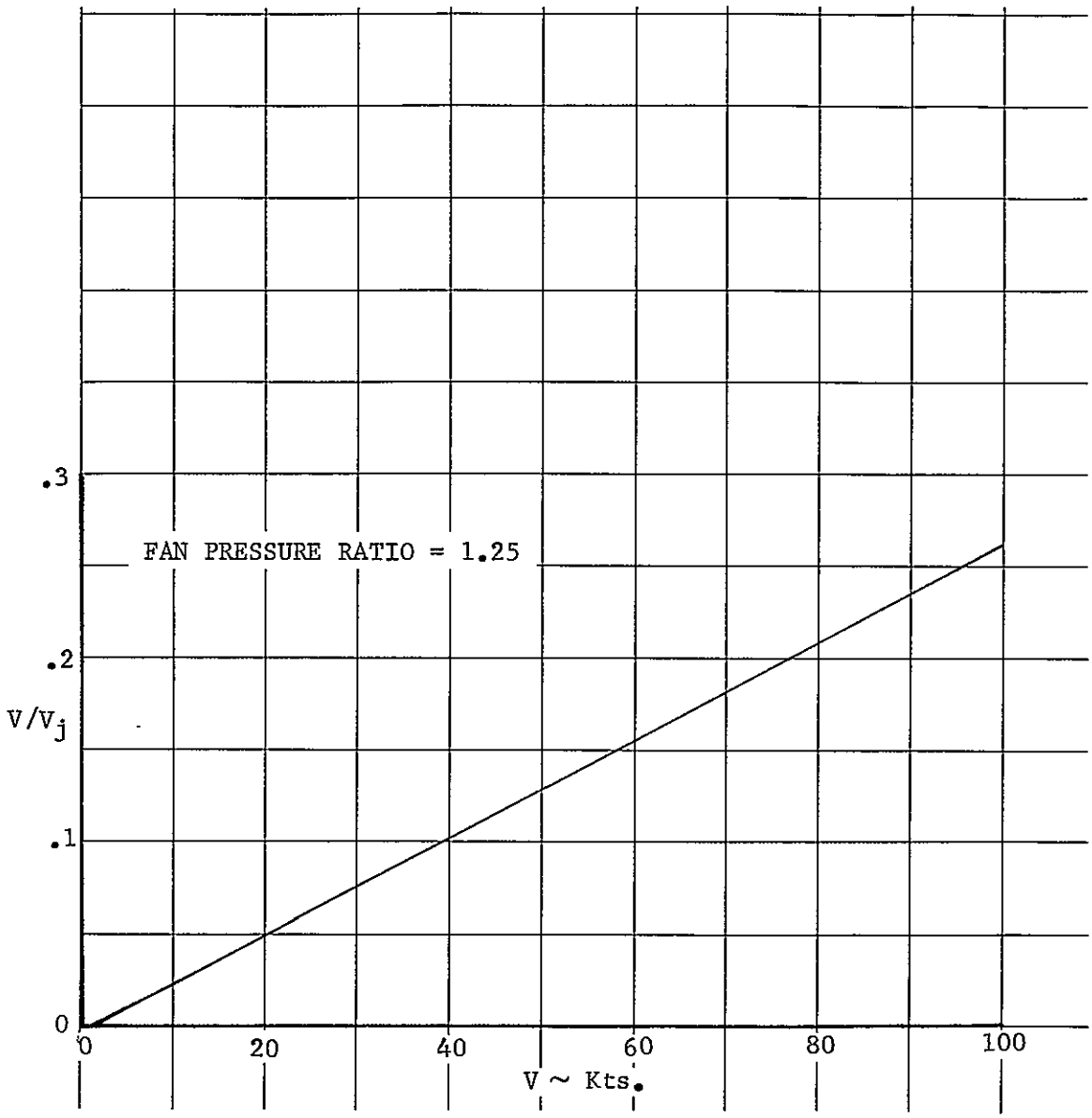

Figure 62. Variation of Velocity Ratio with Airspeed - Full Scale Airplane, Sea Level, Standard Day

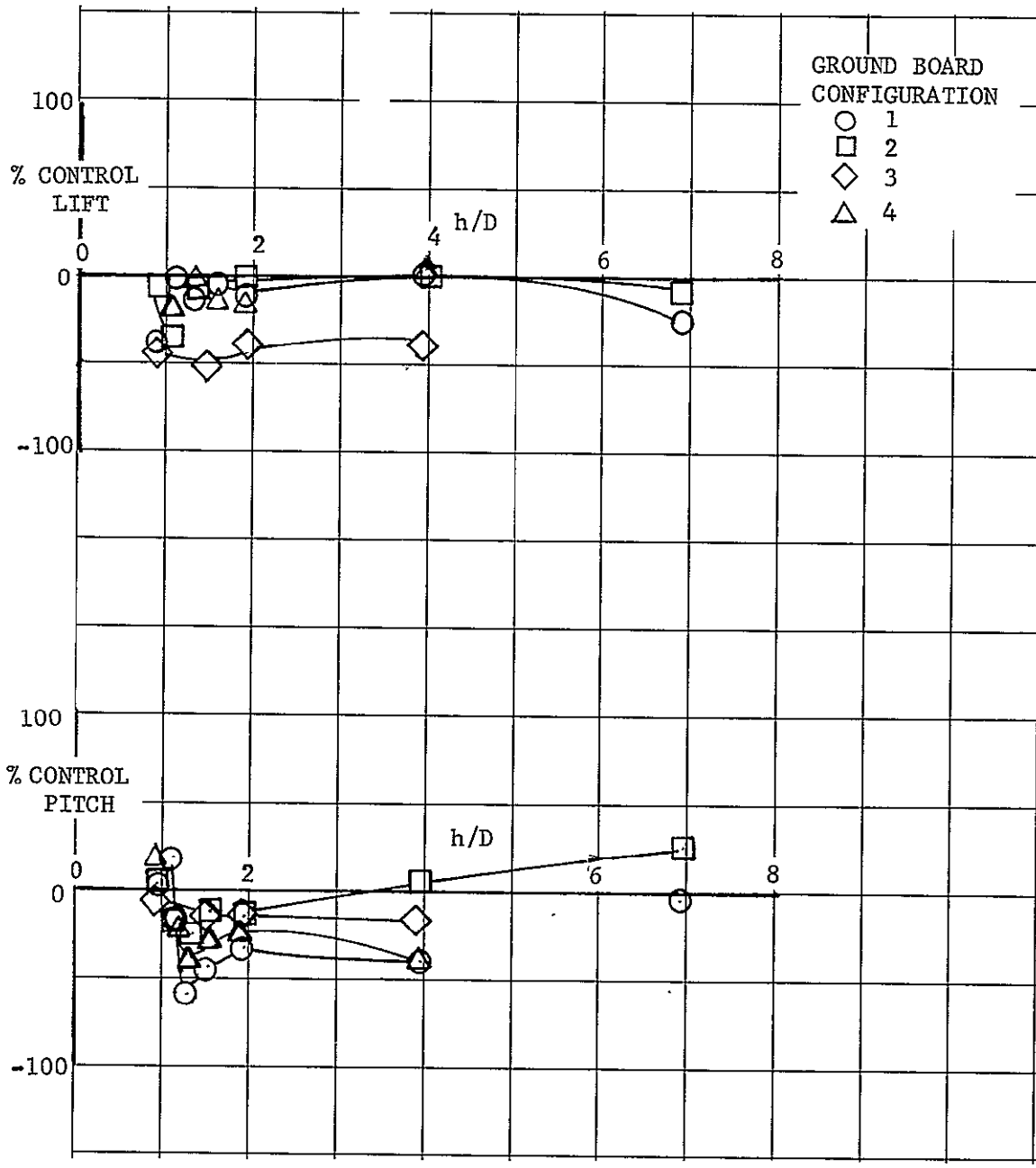

Figure 63. Percent of Available Longitudinal Control Required to Trim the Full Scale Airplane with Various Ground Board Configurations, Airplane Initially Trimmed in Free Air - $\delta_N = 90^o$, $V/V_j = 0$, $\alpha = 0^o$, $\phi = 0^o$

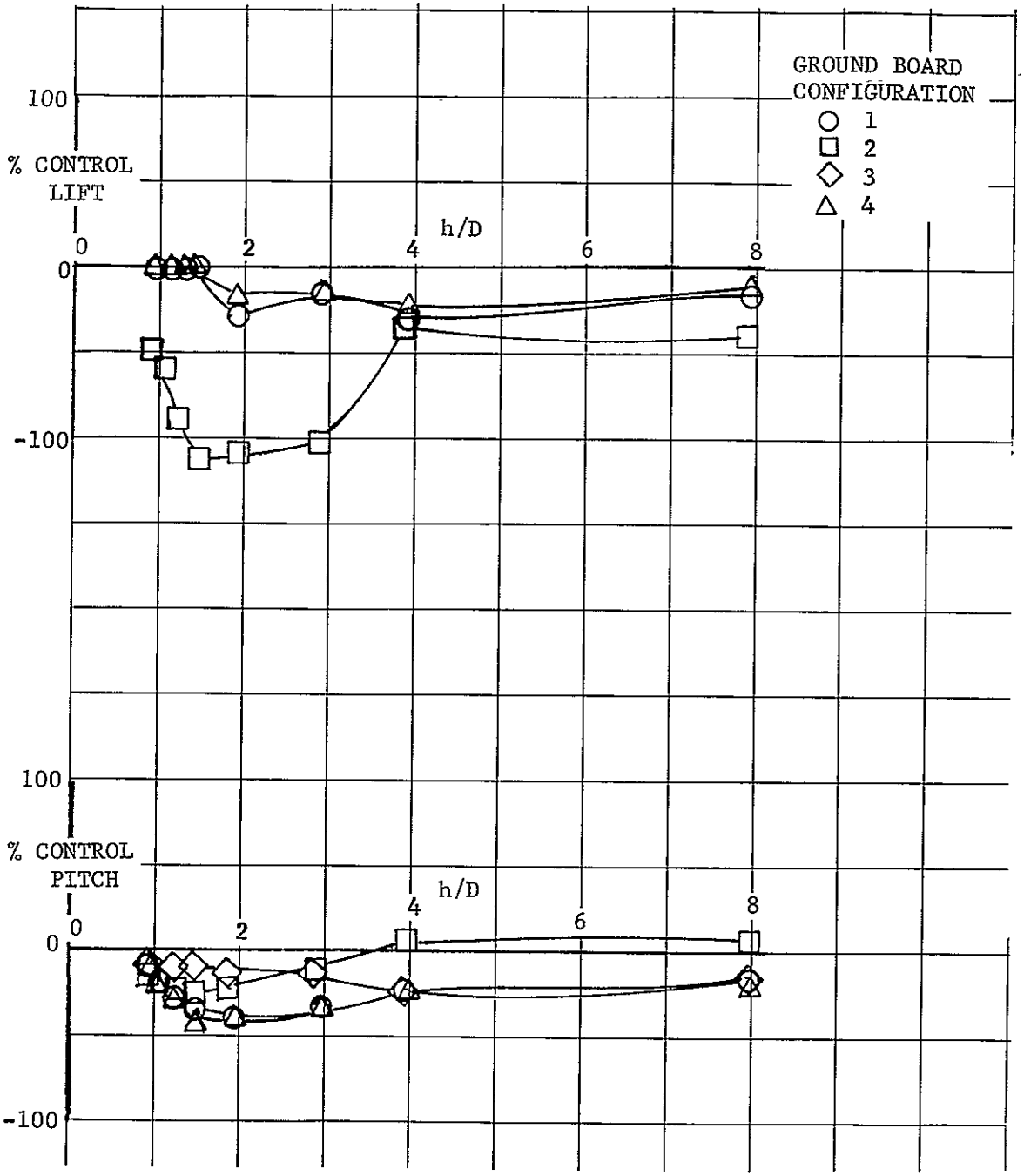

Figure 64. Percent of Available Longitudinal Control Required to Trim Full Scale Airplane with Various Ground Board Configurations, Airplane Initially Trimmed in Free Air - $\delta_N = 90^\circ$, $V/V_j = .09$, $\alpha = 0^\circ$, $\emptyset = 0^\circ$

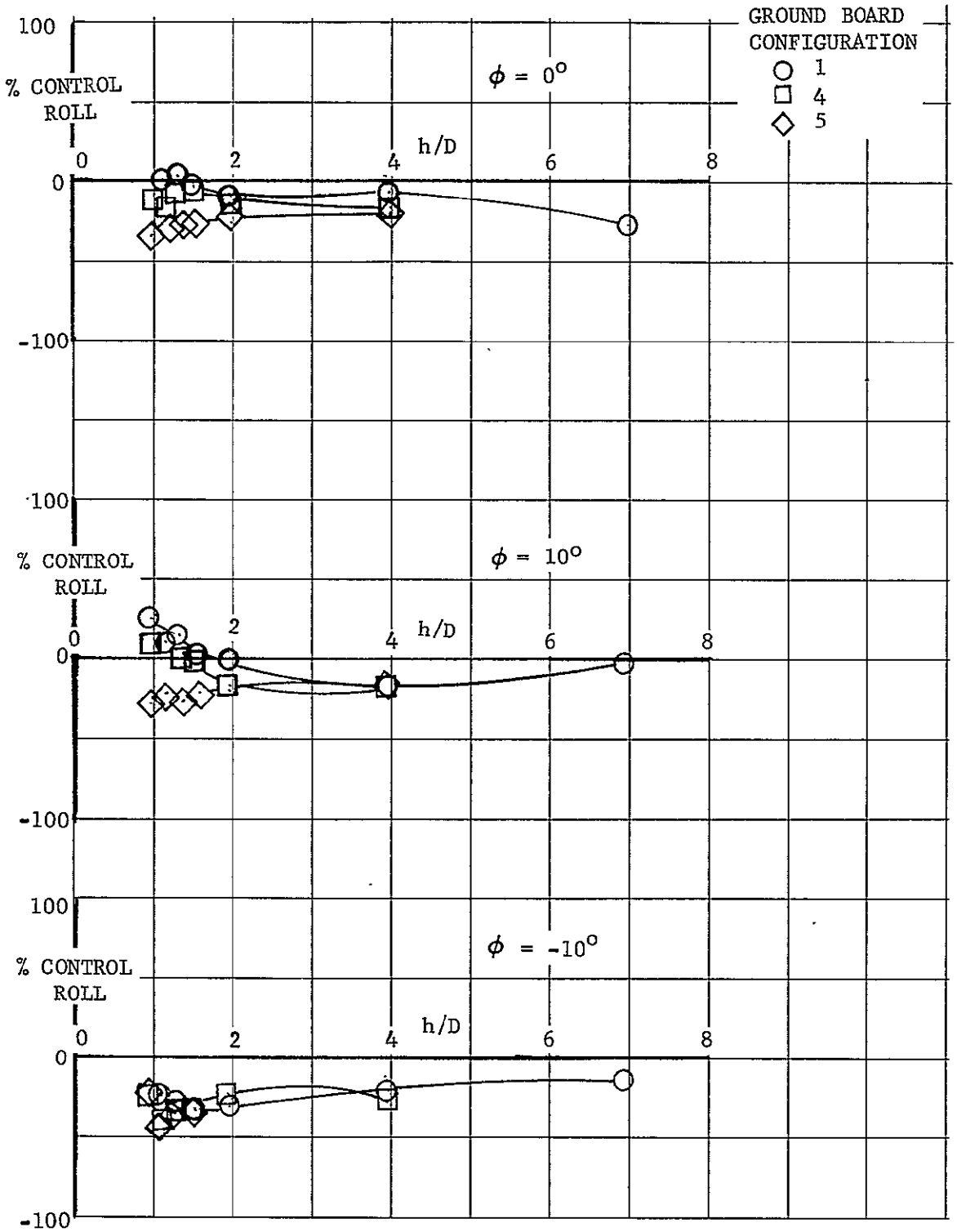

Figure 65. Percent of Available Roll Control Required to Trim Full Scale Airplane with Various Ground Board Configurations, Airplane Initially Trimmed in Free Air - $\delta_N = 90^o$, $V/V_j = 0$, $\alpha = 0^o$

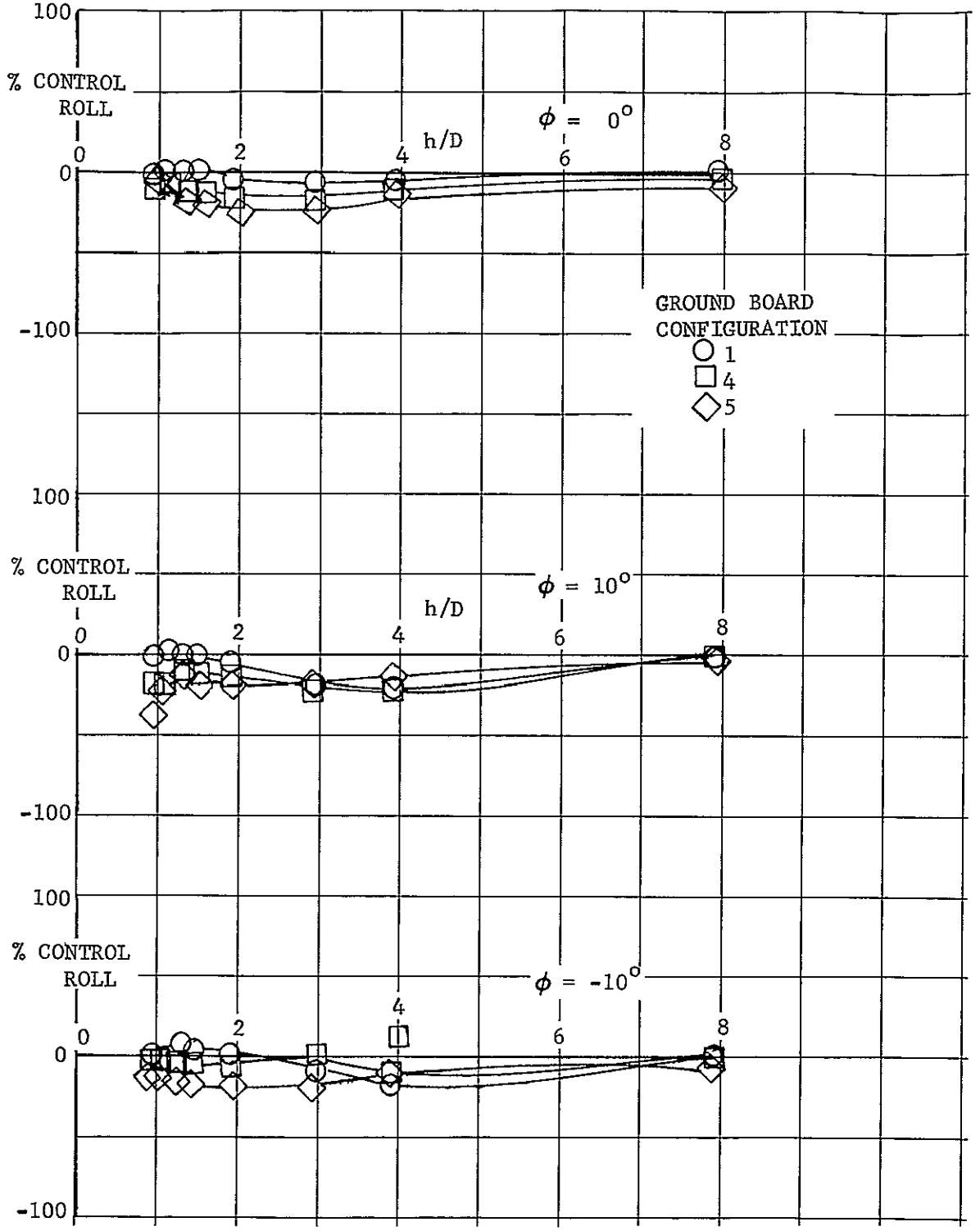

Figure 66. Percent of Available Roll Control Required to Trim Full Scale Airplane with Various Ground Board Configurations, Airplane Initially Trimmed in Free Air - δ_N = 90°, V/V_j = .09, α = 0°

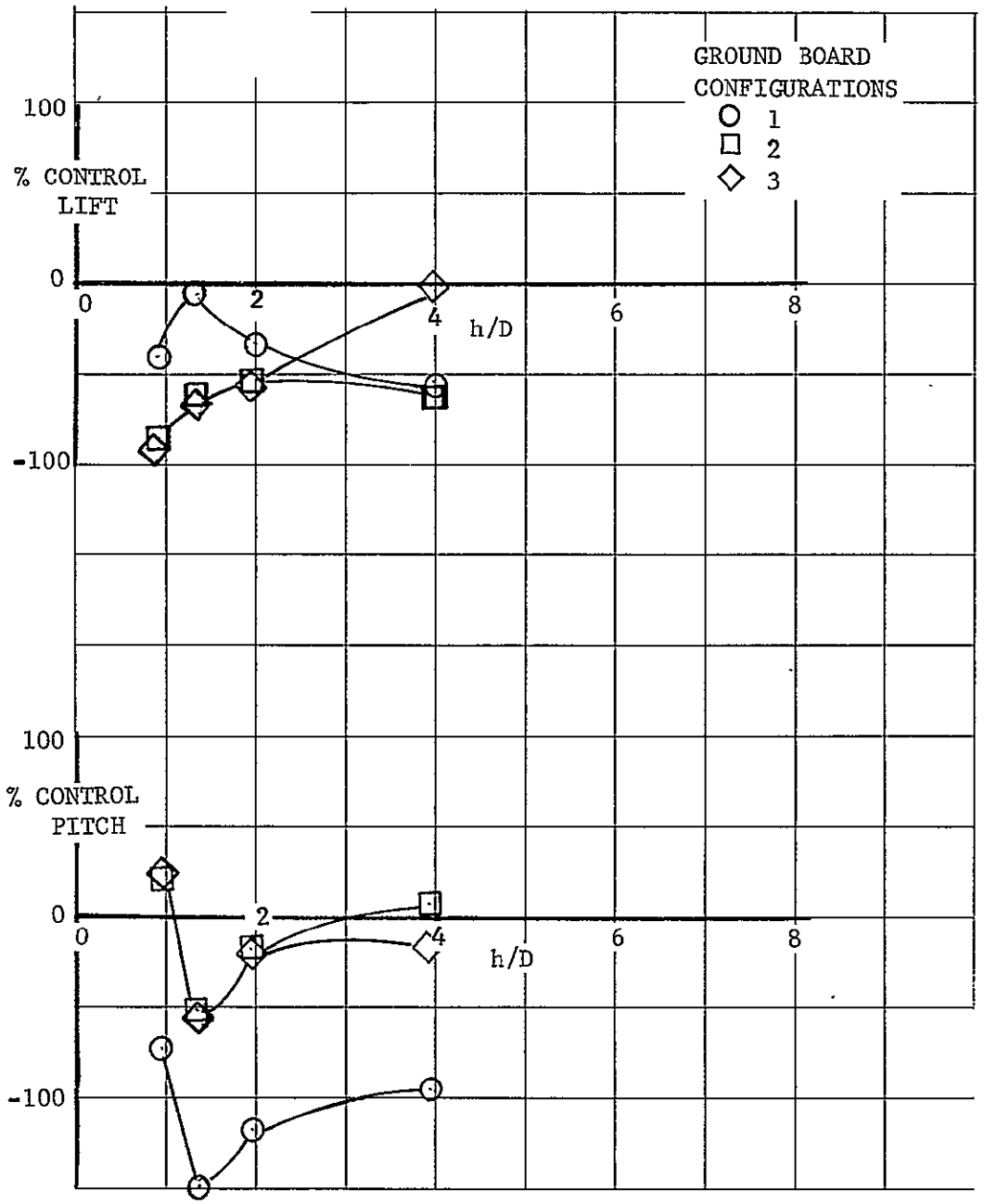

Figure 67. Percent of Available Longitudinal Control Required to Trim Full Scale Airplane with Various Ground Board Configurations, Airplane Initially Trimmed in Free Air, 3-Fan - $\delta_{N_{Nose}} = 80^{o}$, $\delta_{N_{Aft}} = 90^{o}$ $V/V_j = 0$, $\alpha = 0^{o}$, $\emptyset = 0^{o}$

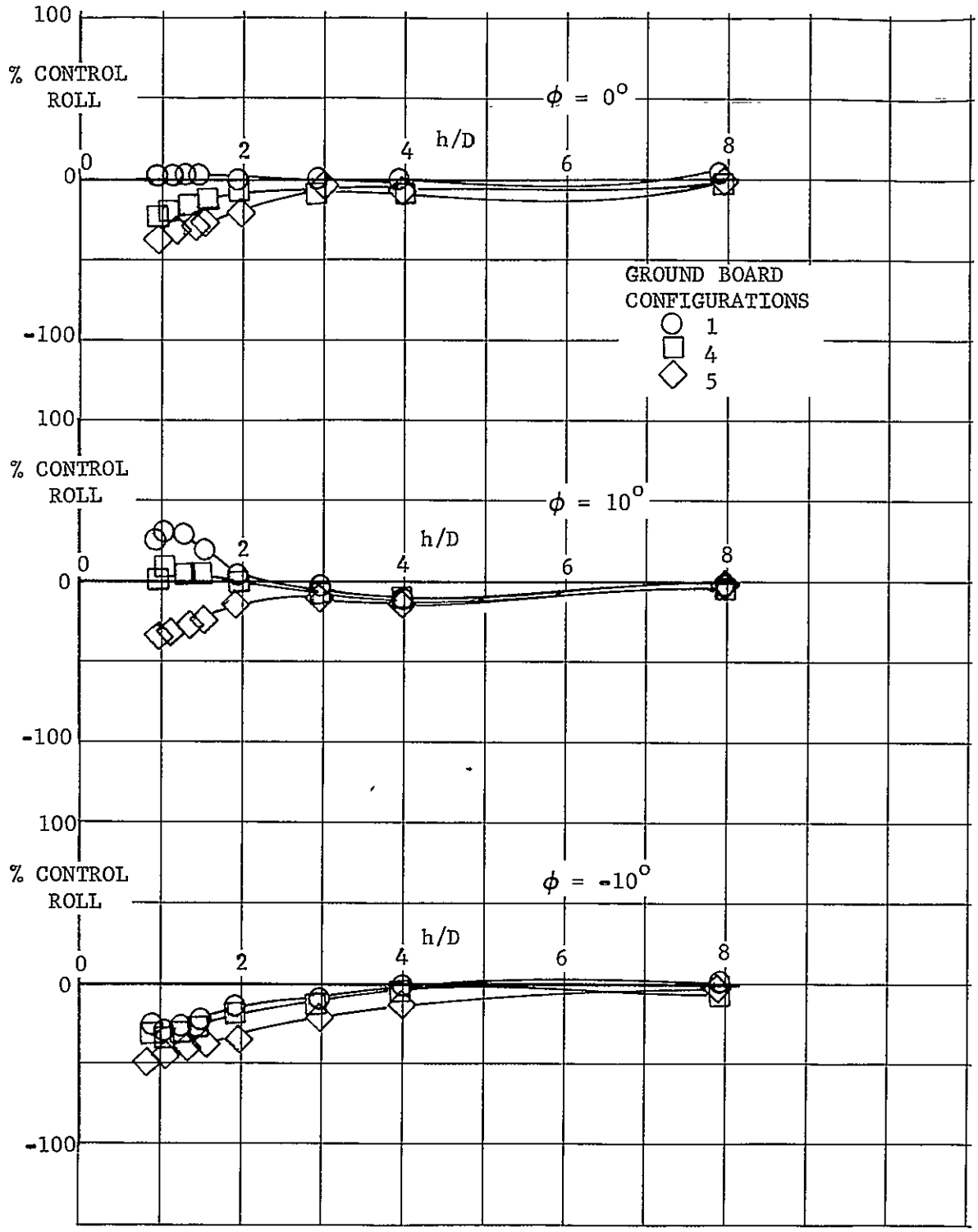

Figure 68. Percent of Available Roll Control Required to Trim Full Scale Airplane with Various Ground Board Configurations, Airplane Initially Trimmed in Free Air, 3-Fan - $\delta_{N_{Nose}} = 80^{\circ}$, $\delta_{N_{Aft}} = 90^{\circ}$, $V/V_j = .068$, $\alpha = 0^{\circ}$

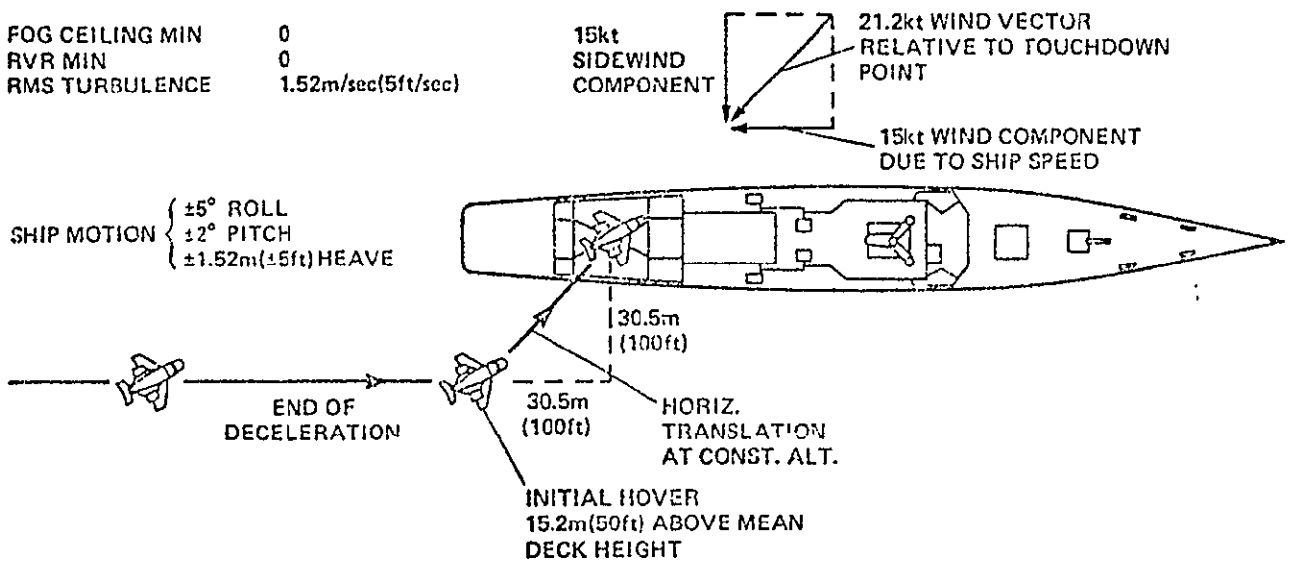

Vernon K. Merrick and Ronald M. Gerdes
NASA Ames Research Center, Moffett Field, Calif.

Figure 69. Design and Piloted Simulation of a VTOL Flight-Control System

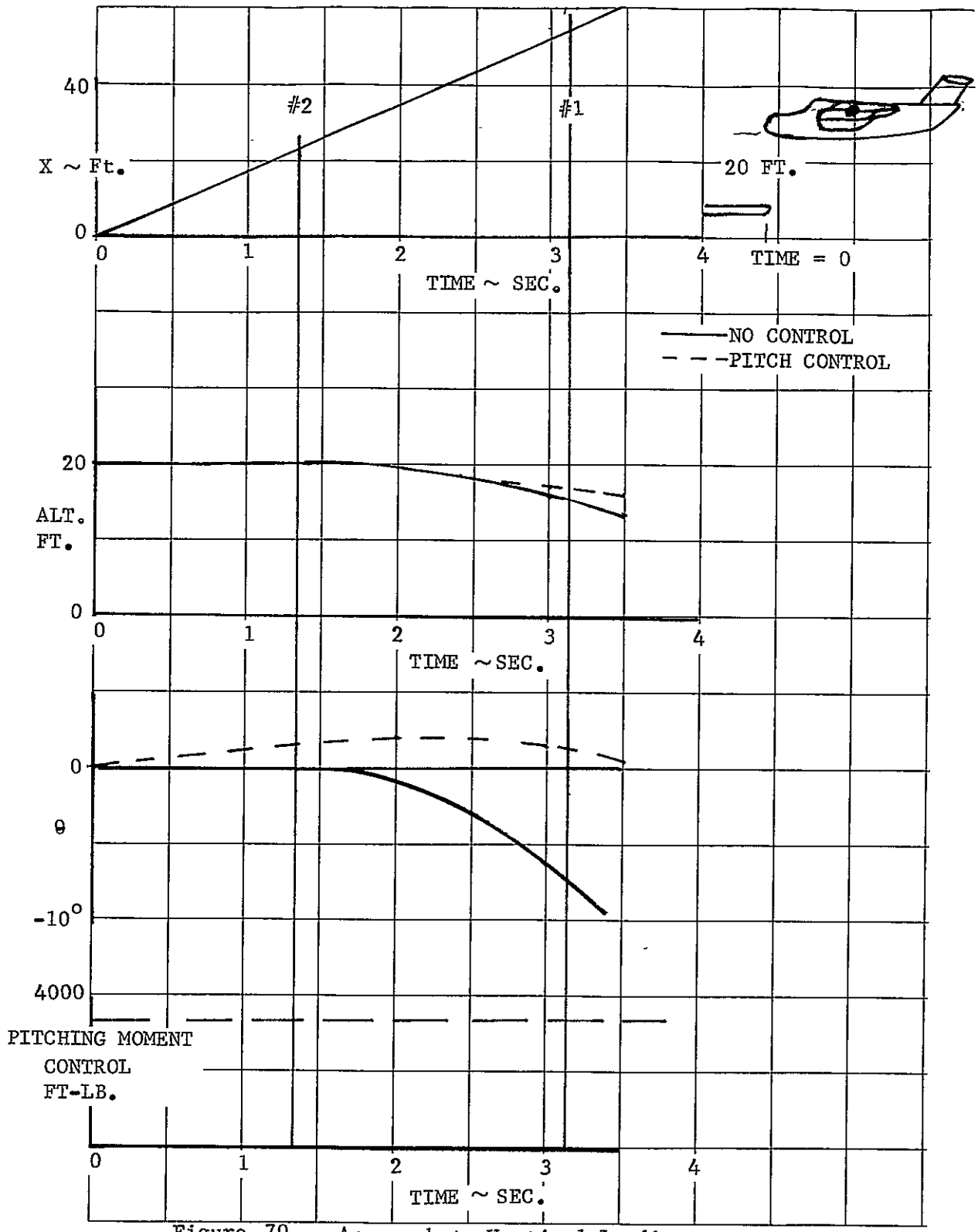

Figure 70. Approach to Vertical Landing

REFERENCES

1. V/STOL Handling-Qualities Criteria, AGARD R-577, 1970.
2. Renselaer, D. J.: Low Speed Aerodynamic Characteristics of a Vectored Thrust V/STOL Transport with Two Lift/Cruise Fans, NASA CR 152029, July 1977.
3. Hunt, D., Clingan, J., Saleman, V., and Omar, E.: Wind Tunnel and Static Tests of a 0.094 Scale Powered Model of a Modified T-39 Lift/Cruise Fan V/STOL Research Airplane, NASA CR 151923, Jan. 1977.
4. Wind Tunnel and Ground Static Investigation of a Large Scale Model of A Lift/Cruise Fan V/STOL Aircraft, NASA CR 137916, Aug. 1976.
5. Heyson, Harry H.: Linearized Theory of Wind Tunnel Jet Boundary Corrections and Ground Effect for VTOL-STOL Aircraft, NASA TR R-124, 1962.
6. Static and Forward Speed Thrust Calibration of the 5.5 Inch Tip Turbine Fans of the Rockwell-NASA .1 Scale V/STOL Lift/Cruise Fan Model, Rockwell Report NR77H-43, 10 March 1977.
7. Merrick, V. K., and Gerdes, R. M.: Design and Piloted Simulation of a VTOL Flight-Control System, Ames Research Center, Unpublished